POST CRITICAL HEAT TRANSFER TO FLOWING LIQUID IN A VERTICAL TUBE

David N. Plummer
Onwuamaeze C. Iloeje
Warren M. Rohsenow
Peter Griffith
Ejup Ganic

Report No. 72718-91
Contract No. NSF GK-17745

Department of Mechanical Engineering
Massachusetts Institute of Technology
Cambridge, Massachusetts 02139

September 1974

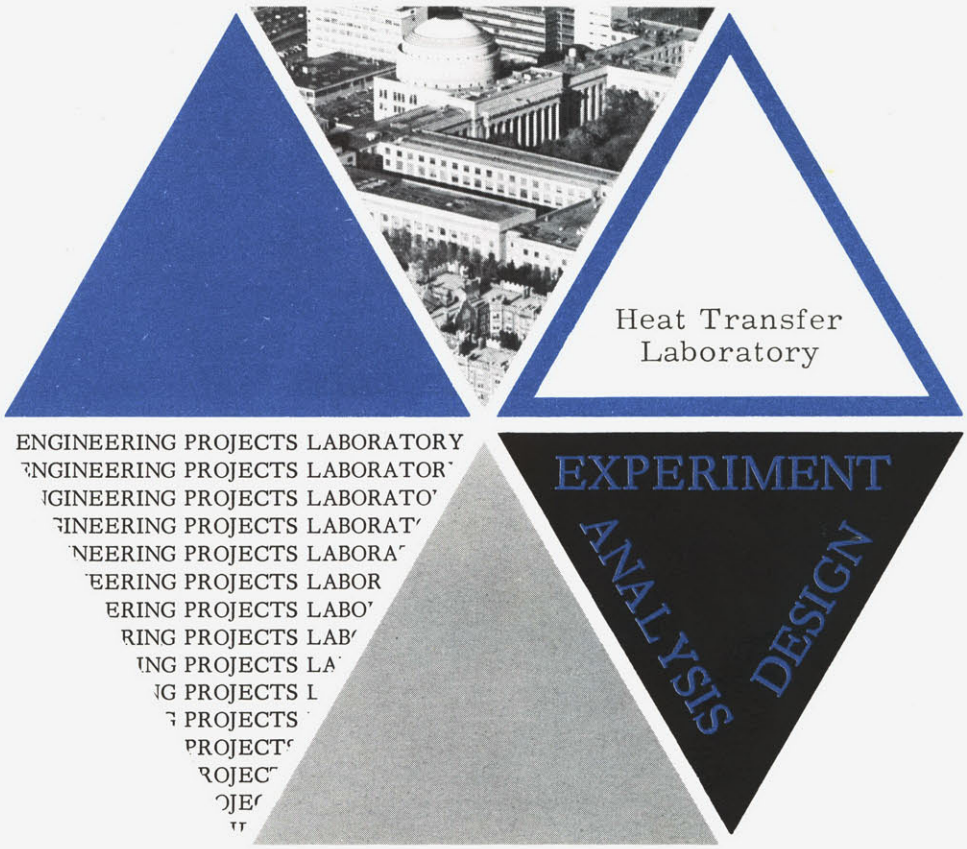

TECHNICAL REPORT NO. 72718-91

POST CRITICAL HEAT TRANSFER TO FLOWING LIQUID IN A VERTICAL TUBE

by

D. N. PLUMMER
O. C. ILOEJE
W. M. ROHSENOW
P. GRIFFITH
E. GANIC

Sponsored by
National Science Foundation
Contract No. NSF GK-17745
D. S. R. Project No. 72718

September 1974

Department of Mechanical Engineering
Massachusetts Institute of Technology
Cambridge, Massachusetts 02139

ABSTRACT

The heat transfer characteristics of a liquid in vertical upflow in a tube in which the critical heat flux has been exceeded is investigated. Using a novel transient experimental technique the entire forced convection boiling curve for liquid nitrogen was obtained for a given mass flux-quality combination from which parametric effects of heater material, surface roughness and oxide scale, and dryout length on the dry wall film boiling region were determined.

The results show that both increased roughness and oxide scale increase the post critical heat transfer. Increasing the dryout length decreases the heat transfer at a given mass flux-quality combination due to thermal nonequilibrium effects. No material effects were noted. Post critical heat transfer data is presented for a 0.4 inch I.D. tube at mass velocities of 30,000 to 220,000 lbm/hr-ft^2 for a quality range of 5 to 90 percent. Heat fluxes of 1,000 to 25,000 btu/hr-ft^2 at wall superheats, $(T_{wall} - T_{sat})$, from 50 to 550°F were obtained.

A post critical heat transfer prediction scheme has been developed from the simplification of an existing dispersed flow film boiling model which predicts the transient nitrogen data within approximately 10%. The scheme gives the correct functional dependence of mass flux, dryout quality, dryout length, and wall superheat, $(T_{wall} - T_{sat})$, due to the implicit inclusion of thermal nonequilibrium effects.

A preliminary comparison of the post critical heat transfer prediction scheme with post dryout water and Freon 12 data indicates similar results.

Procedures are also presented that allow one to obtain the upper and lower bounds to the post critical heat transfer.

ACKNOWLEDGEMENTS

The financial support for the project was provided for by the National Science Foundation.

The authors wish to express their gratitude to Professors Neil Todreas and Borivoje Mikic for their assistance in and review of the work.

TABLE OF CONTENTS

LIST OF FIGURES

LIST OF TABLES

NOMENCLATURE

A	area	ft^2
A, B	correlating coefficients to Equation (4.	-
C_D	drag coefficient	-
C	specific heat	Btu/lbm-^oF
C_p	specific heat at constant pressure	Btu/lbm-^oF
C_v	specific heat at constant volume	Btu/lbm-^oF
D_T	tube diameter	ft
D	diameter	ft
f	friction factor	-
F	force	lbf
g	acceleration due to gravity (4.17×10^8)	ft/hr^2
G	mass flux or mass velocity	$lbm/hr\text{-}ft^2$
h_{fg}	latent heat of evaporation	Btu/lbm
h_{fg}^*	latent heat of evaporation (corrected by Baumeister and defined in Equation (3.22))	Btu/lbm
h, $\bar{h}$	heat transfer coefficient	Btu/hr-ft^2-^oF
k, K_s	thermal conductivity	Btu/hr-ft-^oF
$K_1 K_2$	Correlating constant for the Forslund wall-to-drop heat transfer coefficient (Equation (3.22))	-
L, Z	length	ft
N_d	droplet flux	droplets/ft^2 -hr
N	time scale on analog computer	-
Nu	Nusselt number	hD/k
P	pressure	psia
P1, P2	potentiometer settings on analog computer	-

Pr	Prandtl number	$\mu C_p/k$
q/A	surface heat flux	Btu/hr-ft^2
q	heat flow	Btu/hr
r, R	radius	ft
R	gas constant	Btu/lbm-^oR
Re	Reynolds number	$\rho VD/\mu$
S	slip ratio	V_g/V_ℓ
Sc	Schmidt number	-
t	thichness	ft
t	time	hr
T	temperature	^oF or ^oR
T_{cb}	contact boundary temperature at the liquid-wall interface	^oF
T_{wo}	initial wall temperature	^oF
T_{Lo}	intial liquid temperature	^oF
V	velocity	ft/hr
V	volume	ft^3
V_g	saturated and superheated vapor velocity	ft/hr
We	Weber number	$\rho(V_g - V_\ell)^2 D/\sigma$
X	quality	

Greek

α	void fraction	-
γ	C_p/C_v	-
δ	drop diameter	ft
δ_{film}	correlating constant for the Groeneveld wall-to-drop heat transfer coefficient (Equation (3.23))	-

κ	slope of linear approximation to X_A vs X_E curve in post dryout (Equation (4.1))	-
ρ	density	lbm/ft^3
μ	dynamic viscosity	lbm/hr-ft
σ	surface tension	lbm/hr^2
Π	$G\sqrt{D_T/\rho_v\sigma}(1 - X_{DO})^5$	-
ΔT_s, ΔT	$(T_{wall} - T_{sat})$	^oF
Δt	incremental time	hr
ΔX	incremental length	ft

Subscripts

A	actual	
crit	critical	
d	drag	
E	equilibrium	
f	film temperature	$(T_v + T_w)/2$ --- wall-to-vapor terms $(T_w + T_{sat})/2$ - wall-to-drop terms
g	gravity	
g	saturated vapor	
DO	dryout	
CHF	critical heat flux	
ℓ	liquid	
min	minimum	
o	initial, at last shatter	
sat, s	saturated value	
v	vapor	
wall, w	heated wall	

w,v	wall to saturated or superheated vapor
w,δ	wall to drop
δ, drop	refers to droplet
i	insulation
cu	copper
a	air
m	micarta
r	rubber O-ring
cold spot	defined in Fig A2

1. Introduction

1.1 General Description of Problem:

For centuries man has known that a liquid can be converted to vapor by a suitable application of heat and with his seemingly unlimited ingenuity has expanded this knowledge to the point where he is now capable of converting, with giant nuclear reactors, tremendous amounts of energy for performing useful work. But in sharp contrast to this high level of technical competence in energy conversion, the knowledge and understanding of its basic underlying principles, specifically that of boiling heat transfer and two phase flow phenomena, is still at an unexceptable low level.

Qualitatively, the physics of boiling heat transfer in a convective system is quite well understood. When a heated surface is in contact with a fluid, the general heat transfer behavior of the heater can be described on what is commonly referred to as a boiling curve. The boiling curve for a convective system which is similar to that given in a pool boiling situation is plotted in terms of the heater wall superheat defined as $(T_{wall} - T_{sat})$ on the abscissa and heat flux from the heater surface on the ordinate. Figure 1 gives a qualitative representation of a boiling curve in forced convection. As most forced convection boiling systems consist of a conduit (tube annulus,

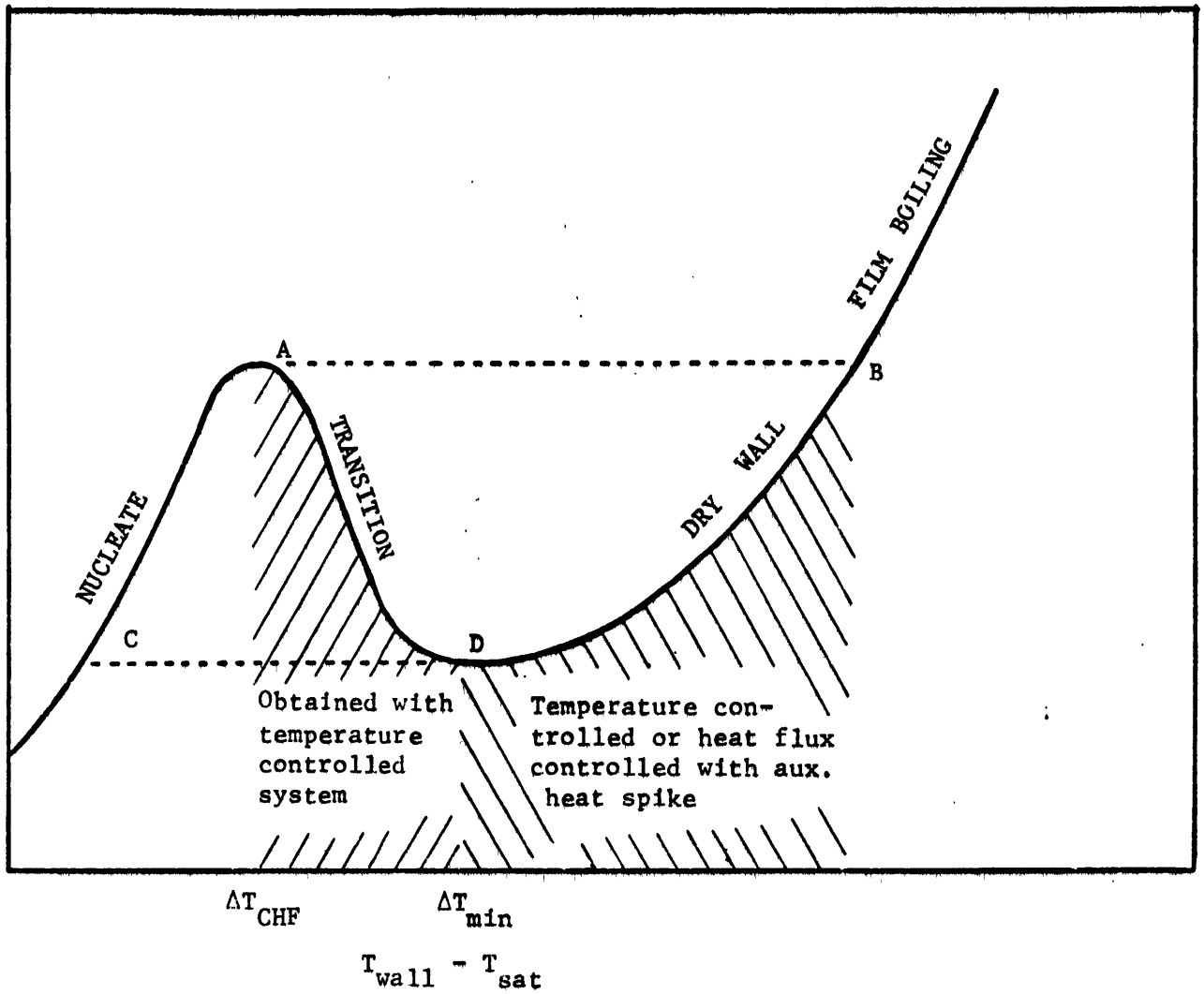

FIGURE 1 QUALITATATIVE BOILING CURVE IN FORCED CONVECTION

enclosed rod bundle) of some length through which the fluid is passed, Figure 1 represents the boiling characteristics at a particular axial position in the conduit for a given mass flux.

The peculiar shape of the boiling curve is a result of a change in the relationship of the liquid and generated vapor to the heater surface as the surface heat flux is increased. The nucleate boiling region has the liquid completely attached to the heater surface with the vapor being generated from preferred cavities. This is a very effective heat transfer mode where tremendous amounts of heat can be transferred for low wall superheats. But if the surface heat flux exceeds the critical heat flux value given by point A, the wall becomes dry with the vapor insulating the liquid from the surface causing the wall temperature to rapidly increase to point B*. This region is called the drywall film boiling region or the post critical heat transfer region. The term, post critical heat transfer is actually used to define the entire boiling curve to the right of the maximum nucleate boiling temperature, thereby including the transition region, whereas the term, dry wall film boiling, only includes that part of the boiling curve starting from point D. The two terms

---

*Consideration is made of the possibility of direct liquid wall contact in film boiling which is discussed in section 2.7.4 as a possible explanation of the oxide effects observed in experimental phase of this work.

are used interchangeably for a heat flux controlled system in which the transition region can not be maintained. In this regime the heat transfer rates are two orders of magnitude lower than in the nucleate regime. The vapor is now generated at the vapor liquid interface and is capable of superheating. Further increase in the heat flux to the surface results in the surface temperature moving up along the film boiling curve. Once the heater has achieved a condition of stable film boiling it can return to the wet wall nucleate boiling condition in one of two paths. First it can return along path B-A once the heat flux is reduced to the critical heat flux value which previously forced that particular axial position into the film boiling mode or it can continue down further along the film boiling curve until the minimum heat flux is reached thereby transiting via path D-C. The surface can only reach this lower portion of the film boiling curve under certain conditions. This portion of the curve can be reached in a temperature controlled system such as a quench process, or it can be reached in a heat flux controlled system if there is no liquid reattached somewhere else in the heated conduit. It is the axial conduction inside the body of the heater from the dry area to the wet area of the heated surface that wipes out the hysteresis effect and results in the preferential path being B-A for the

transition back to complete wet wall conditions for the heat flux controlled case.

The region between the minimum film boiling point and maximum nucleate boiling point is the transition region characterized by intermittant liquid attachment to the heating surface and subsequent reevaporation. The frequency of liquid contact increases with decreasing wall superheat until liquid is completely reattached at the maximum nucleate boiling superheat. This region is difficult to define on the boiling curve as one instant, liquid is in contact with the surface providing good heat transfer and the next instant the surface is dry giving poor heat transfer. The transition line drawn on Figure 1 is, therefore, a time average of the two extreme conditions. Only a quench experiment or other types of temperature controlled systems can provide data in this negatively sloping region, and this data is only the average effect of the large temperature and or heat flux oscillations produced at the heating surface.

From this simplified description of the forced convection boiling picture one potentially dangerous aspect stands out for such systems as evaporator tubes in fossil fuel boilers or rod bundles in a water cooled nuclear reactor. That is the rapid temperature rise observed in going from A to B. The temperature at B,

as the critical heat flux is exceeded, could be sufficient to physically damage the heating surface. This transition into the critical heat transfer mode can happen in many types of boiling systems if the systems experience either a flow loss or a power transient. In order to know just what temperature the system will reach and thereby determining just how damaging the transition to post critical heat transfer can be, a quantitative description of the post critical heat transfer regime is necessary.

The nuclear reactor industry is currently placing considerable emphasis, through their safety analysis programs, on the problem of accurately predicting the post critical behavior in a reactor core. Their main concern is to prevent the rod bundle from reaching a temperature sufficient to melt the cladding material containing the fissile material if a post critical situation occurs. Even though there is an extremely low probability of this happening the reactor designer must prove that emergency core cooling systems are capable of cooling the reactor core if it is perturbed out of the design conditions. The worst accident postulated to perturb the reactor is that of a loss-of-coolant accident, Loca[1*], where one of the feed lines to the reactor core is postulated to break. The flow through the core slows down to a final value of zero and due to this flow stoppage the reactor core is tripped into

* Superscripted numbers refer to references at the back of the thesis.

a post critical boiling situation. The situation is brought under control by the initiation of emergency core cooling systems consisting of flooding water from the bottom and spraying water from the top of the core. The conservatism used in estimating the heat transfer rates causes the calculated maximum cladding temperatures in the core to reach the melting point of the metal. This uncertainty factor can force the industry to operate the reactor at a reduced power level as a safety precaution.

1.2 Literature Survey:

Early attempts at understanding the film boiling phenomenon consisted of running experiments in order to observe its fundamental characteristics. The heat transfer data was used to develop empirical film boiling correlations applicable in the range for which the data was taken. The bulk of the film boiling data obtained used such test fluids as water, Freon 113, Freon 12, liquid nitrogen and hydrogen, and some hydrocarbons. The geometries consisted of tube, annular or multi rod, bundles.

Groeneveld in a recent publication[2] does an excellent summary of the entire film boiling investigation of the past fifteen years. He not only lists 16 film boiling correlations developed by various researchers but also presents his own correlations based on the careful study of all available film boiling data. The general form of all the

correlations produced is the same and consists of a single phase forced convection heat transfer coefficient using the Reynolds and Prandtl numbers modified by a two phase flow multiplier to account for quality effects. The Groeneveld correlation for tubes and annuli is presented here for illustration.

$$Nu_g = a[Re_g(X + \frac{\rho_g}{\rho_\ell}(1-X))]^b \, Pr_v^c \, y^d \, (q/A)^e \tag{1.1}$$

$$y = 1 - .1(\frac{\rho_\ell}{\rho_g} - 1)^{.4}(1-X)^{.4}$$

Where the constants are given for either heat flux or no heat flux dependancy as follows

a	b	c	d	e	No. of Points	Rms Error
7.75×10^{-4}	.902	1.47	-1.54	.112	704	11.6%
3.27×10^{-3}	.901	1.32	-1.50	0	704	12.4%

This equation with or without the heat flux dependancy correlates the effects of mass flux, quality and fluid properties on the post critical heat transfer coefficient. As the mass flux increases for a constant quality, the heat transfer coefficient increases. As the quality increases for a constant mass flux, the heat transfer coefficient increases at a decreasing rate until it starts decreasing as the quality reaches 95-100%. The heat transfer coefficient is based on the saturated vapor temperatures

and the quality variable is the equilibrium quality calculated from a thermodynamic heat balance. The limitation of the correlation to the data base is evident as both the vapor temperature and actual quality calculated by weight deviate from the equilibrium values in post dryout. The correlation was developed entirely from post critical water data for the geometry indicated. The mass flux range was .5 - 3.8 x 10^6 lbm/ht-ft^2 and the equilibrium quality ranged from 10-90 percent. By taking these ranges at face value one would assume that the correlation would predict the case where G = .5 x 10^6 and X = 10% . This is not necessarily true, however, as the experimental techniques from which the data for the correlation was obtained links all low quality data with the high mass flux runs. The converse is not always true but one can say that all low mass flux data points had high qualities associated with them. Therefore extrapolating a correlation which correlates a low mass flux, high quality data point within 10% is almost surely going to lead to considerable uncertainties at low mass flux low quality range.

Recently Slaughterback[3] conducted a parametric study and comparison analysis of Groeneveld's correlation for tubes only with four other film boiling correlations. The general conclusion from this study was that significant descrepancies

exist among the different correlations and between the correlations and experimental data. This conclusion led to statistical regression analysis[4] of Groeneveld's collection of data which resulted in a modified form of the Groeneveld correlation including an empirical formulation of the uncertainty bounds. The uncertainty bounds are presented as upper and lower bounds on the heat transfer with a 95% confidence limit. Again the same limitation as discussed for the Groeneveld correlation applies for this one.

Groeneveld as well as this author feels that the answer to the problem of predicting film boiling heat transfer does not lie in statistical manipulation of large amounts of data but instead in the complete understanding of the physical phenomenon involved. Considerable advancement was made in this direction when Forslund[5] of MIT and Bennett[6] of UKAEL independently developed governing differential equations for the so-called dispersed flow film boiling region. Both models have been subsequently revised, the Bennett model by Groeneveld[7] and the Forslund model by Hynek[8]. Both of these models will be extensively compared in Chapter II with the intension of taking the best points of each of the models to give a resulting hybrid model from which the generalized post critical heat transfer correlation presented in this thesis will be derived.

1.3 General Description of Post Dryout Heat Transfer And Flow Regimes:

Experimentally, the post critical heat transfer regime can be obtained in several ways which result in different two phase flow patterns depending on the technique used to generate the dryout condition. Most experimentors including all those using water develop the dry wall condition in the following manner. Flow of a particular mass flux and inlet quality is allowed into the uniformly heated tube whose power is either zero or at a very low value. The power is then increased incrementally until the dryout condition which starts from the exit moves into the tube to the desired position. Figure 2 gives a qualitative picture of this flow regime pattern and wall temperature profile. It consists of an annular liquid film attached to the heater surface with droplets entrained in vapor core upstream of dryout and a dry wall with droplets dispersed in a superheating vapor downstream. Characteristically this is a high quality, high void dryout phenomenon (above 50% void). This is of course dependent on a number of parameters such as inlet quality, heat flux and mass flux as well as the type of fluid used. (There is a possibility of an upstream dryout which will not be treated here but is discussed in some detail in Section 11.3.3 of Groeneveld[7]).

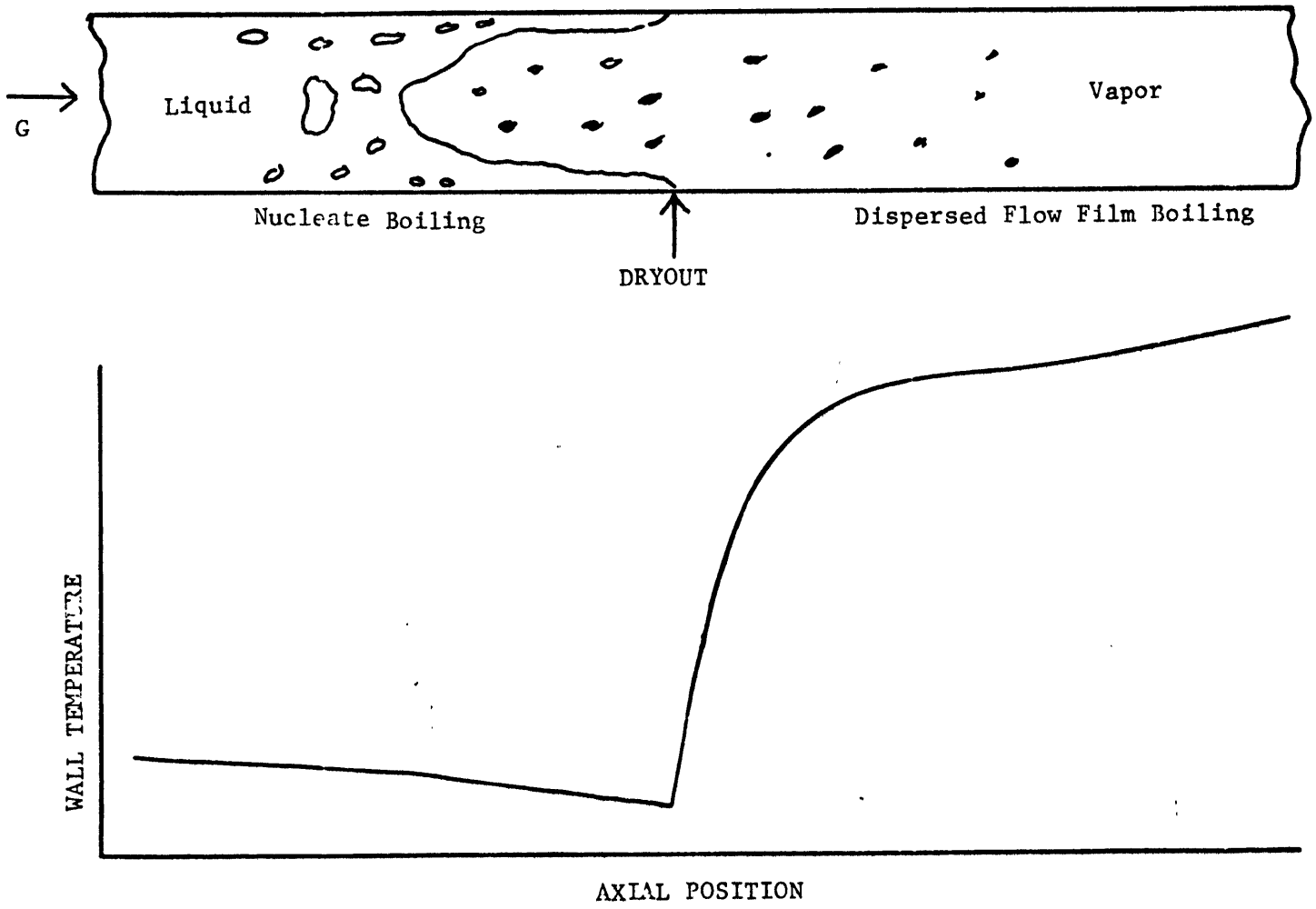

FIGURE 2 FLOW REGIME AND WALL TEMPERATURE PROFILE FOR HIGH VOID DRYOUT

The second technique used extensively by researchers employing liquid nitrogen [5,8,9] consists of raising the tube wall temperature at least above the minimum film boiling temperature as indicated on the boiling curve in Figure 1 before allowing the fluid to enter the tube. When the fluid is finally allowed into the tube, a dryout condition is set up throughout the entire heated tube length. Figure 3 gives a qualitative picture of this flow regime pattern. The flow pattern is initially that of a solid liquid core separated from the heater surface by a vapor film. The vapor-liquid interface has an unstable wavey nature. As the void fraction increases, the liquid core takes on a foamy frothy characteristic which finally transits into dispersed flow at some intermediate void. This transition point is on the order of 5-10% quality for nitrogen as its void fraction rises very rapidly with quality. For liquids whose ratio of vapor density to liquid density is much larger as with water and Freon 12 this transition point is generally higher due to a relatively slower increase of void with quality. To this author's knowledge no water data has been obtained using this technique supposedly due to the fear of melting the tube in the start-up procedure. There is an advantage though to using this technique. One is able to obtain film boiling data in the region between the minimum heat flux line and the

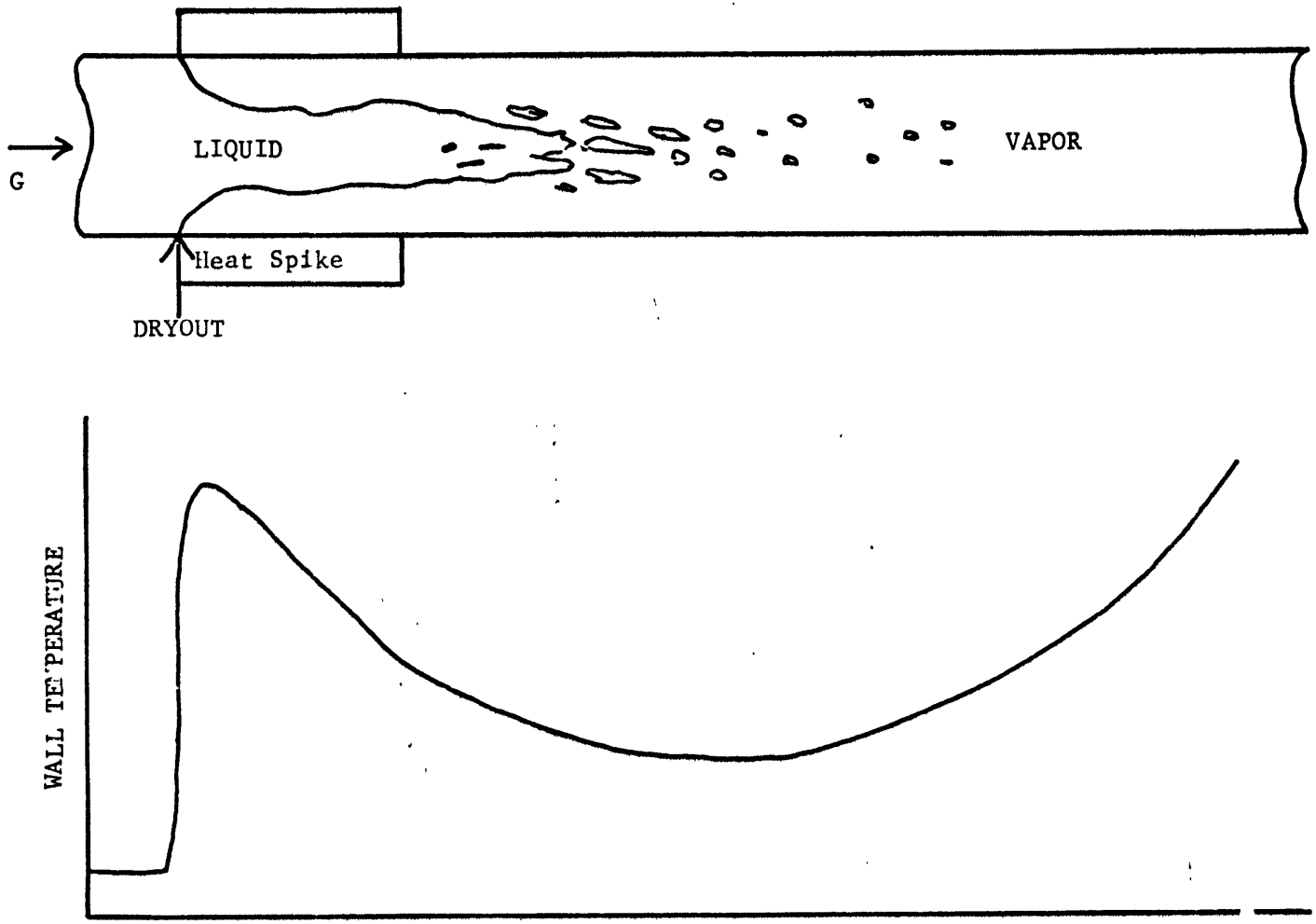

FIGURE 3 FLOW REGIME AND WALL TEMPERATURE PROFILE FOR LOW VOID DRYOUT WITH HEAT SPIKE

critical heat flux line on the boiling curve. That is to say that this flow regime does exhibit the hysteresis effect where upon a particular point in the tube can descend the film boiling curve below the critical heat flux line without traversing over into a wet wall condition until the minimum heat flux is reached.

This is an inherently unstable flow structure for a uniformly heated tube for if the inlet quality to the heated tube is below the quality at which dryout should occur for the given system mass flux and tube heat flux, then the liquid front will want to move into the heated tube to the position where the quality is equal to quality at which dryout was calculated to occur. The forcing function that prevents the liquid interface from moving into the tube for this experimental technique is the heat gain in through the electrical buss bar attached at the inlet end of the heated tube. In the nitrogen experiments of Forslund and Hynek the buss bar was a large copper electrode whose temperature was somewhat higher than the tube wall to which it was attached. This allowed a suffient heat spike at the entrance to prevent the liquid interface from attaching itself to the heated tube. Hynek attached a cooling devise to the electrical buss bar which cooled the inlet region to such an extent that dryout could not be achieved directly at the inlet to the heated tube.

Further experimentation by Iloeje et al[10] using a buss bar which could control the amount of heat into the inlet region of the tube resulted in the determination of a threshhold heat flux above which the minimum test section heat flux at which liquid reattaches the inlet region was unaffected by changes in heat flux in through the buss bar. Below this value the rewetting at the entrance occurred at higher values of test section heat flux for lower heat fluxes in through the buss bar.

This technique of initiating post critical conditions directly at the inlet to the heated tube is similar in purpose to the hot patch technique used by Groeneveld to obtain the lower portion of the film boiling curve. The hot patch provides the spike which initiates film boiling at a quality lower than the system mass flux and heat flux would dictate. The dryout spreads up the remainder of the heated tube as in the nitrogen experiments.

1.4 Scope of Research

An extensive experimental program was undertaken utilizing a unique transient technique to obtain the entire forced convection boiling curve for a vertical tube at one specified mass flux and equilibrium quality combination for nitrogen. The thermodynamic quality varied from 5% to 95% and the mass flux varied from 30,000 to 200,000 lbm/hr.ft^2.

The effect of scaling roughness and heater material on the boiling curve were independentally investigated.

A comprehensive comparison of Hymek's and Groeneveld's dispersed flow film boiling models with data available in the literature was carried out. The original Hynek computer code [8] was modified to include features of the Groeneveld model when those features were deemed better than the comparable feature in Hynek's code.

A generalized post critical heat flux correlation was developed after simplying assumptions were applied to the modified dispersed flow mode. The correlation contains all the thermal variables (excluding any surface effects) known to affect the post critical heat transfer. This correlation can give upper and lower bounds for the heat transfer as well as predict the data. The correlation was not only compared against the transient nitrogen data obtained in this work with good success but also predicted steady state tube data for nitrogen, water and Freon 12 published in the literature with fair success.

II. Experimental Program

2.1 Concept of Forced Convection Transient Film Boiling Experiment

In the process of choosing an experimental technique for this work several important factors were considered. First, an experiment had to be designed that would allow for a detailed analysis of the minimum film boiling point and the surface rewet phenomenon. The main criterion here was that minimum film boiling data be obtained for particular mass flux- quality combinations that was free from axial conduction effects. That investigation was carried out concurrently with this work by O.C. Iloeje [28] for his Ph.d thesis. Secondly, accurate data in the post critical heat flux regime needed to be obtained for particular mass flux-quality combinations in order to lend support to a post critical heat flux correlation. Also provisions had to be incorporated in the experiment to allow for the investigation of roughness, scale and material effects on the two quantities in question. The idea of a transient boiling experiment presented in this work very successfully satisfied these criteria.

The concept of the experimental technique was taken from the knowledge that a sufficiently hot body when immersed in a liquid will quench and in doing so passes through

all the regimes of boiling from dry wall film boiling through the transition region to nucleate boiling.* For this experiment the hot body consisted of a one inch long thick walled tube combined with all the necessary equipment for passing the test fluid of a particular inlet mass flux and quality through it and a system for initially heating the short tube into film boiling. The following sections describe the transient section in detail as well as the main loop related instrumentation.

2.2 Nitrogen Loop

The loop diagram for the experimental apparatus is given in Figure 4. It is a once through system employing liquid nitrogen as the test fluid. Aside from the adaption of the transient test section to the discharge of the main test section, the apparatus is essentially that used by Iloeje et al[10] and a detailed description of the apparatus can be found in that report.

The main test section, a uniformly heated 8 foot long Inconel 600 tube 0.5 "O.D. by 0.4" I.D., operates as a preheater for the transient test section. In this manner a two phase flow mixture with a particular quality and mass flux can be supplied to the transient section. The preheater was operated in one of two states, either a wet wall condition or a drywall condition. The drywall length was

---

*See Section 2.71 for further discussion of this assumption

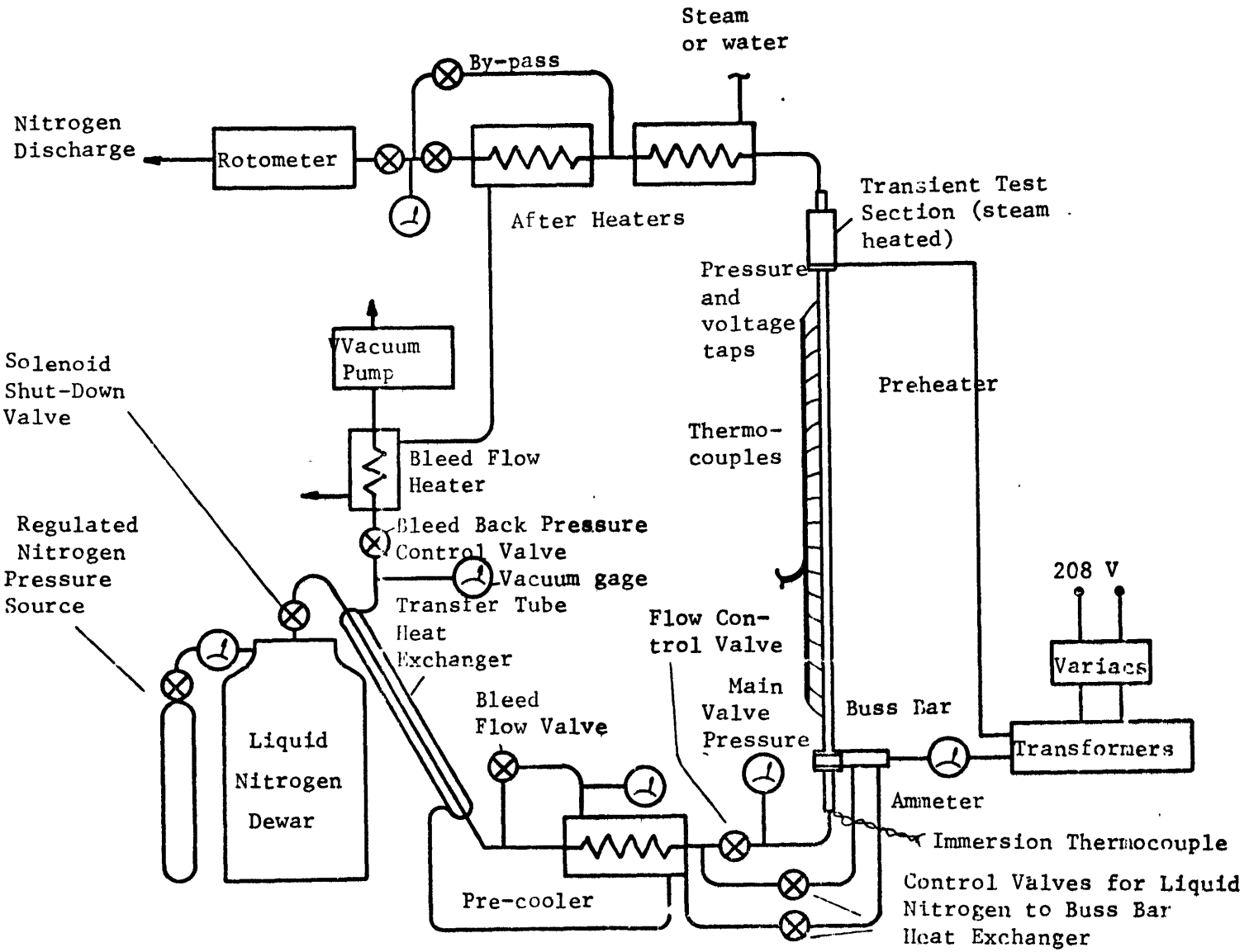

FIGURE 4 NITROGEN TEST LOOP

varied by constructing a movable electrode that could be bolted onto the preheater at any desired position. When using this electrode the electrical supply cable previously attached to the bottom buss bar was transferred to the new. Data was taken for two dryout lengths, four feet and eight feet.

2.3 Transient Test Section

A detailed drawing of the transient test section design 2 is given in Figure 5. The test section consists of a one inch tube .4 I.D. by 1.0 inch O.D. supported and encased by a copper cup arrangement. This cup allows the specimen to be independently heated with steam supplied at a temperature of 220-250^{o}F. The specimen is electrically and thermally insulated from the supporting structure by micarta insulators. (thermal conductivity of 0.2 BTU/hr-ft^{2}) whose contact areas were purposefully reduced to a minimum. A combination of rubber O-rings, silicon rubber sealant and compression of the cover assembly onto the specimen insure that the steam and flowing nitrogen are completely separated. The transient test section assembly was bolted onto the exit of the preheater via connection flanges. Glass wool insulation was wrapped around the transient section to reduce heat gains in through the sides of the section. The electrical supply cable for the top electrode to the preheater was bolted to the brass cover of the transient section.

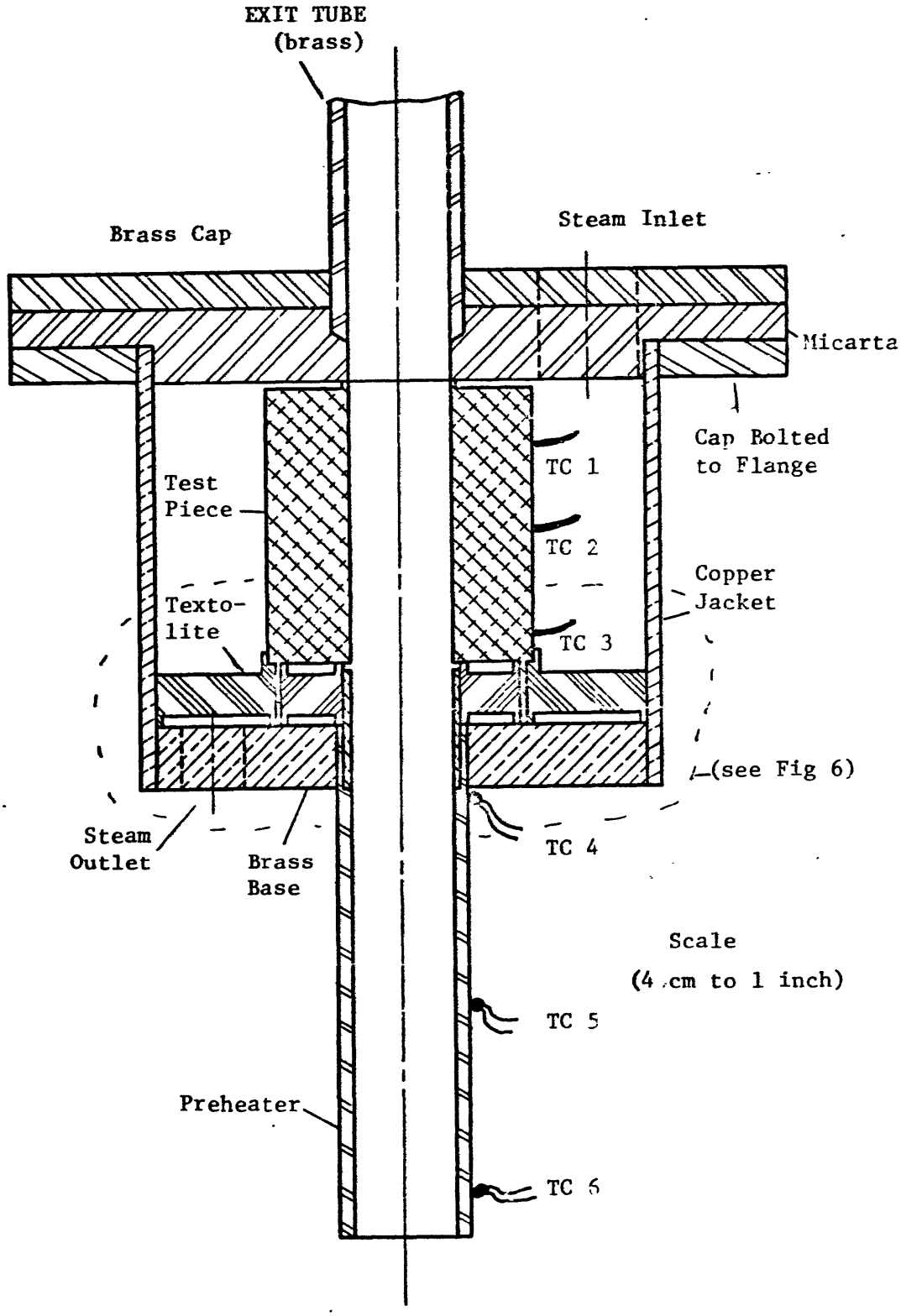

FIGURE 5 TRANSIENT TEST SECTION (DESIGN 2)

The current was thus conducted through the copper casing to the electrode.

The transient test section was specifically designed to allow for the interchangeability of the test specimens. The specimens included smooth Inconel-600, aluminum 1100 and copper pieces; roughened Inconel-600; and oxidized Inconel-600. The smooth surfaces were rough drilled, bored to within .003" - .005" of final size and then finished with a Sunnen Products honing stone No. K12-395. Expected roughness for the Inconel piece is about 5 microinches (arithmetic average) and about 10 micro inches for the copper and aluminum pieces. The actual surface finishes were of this order of magnitude as determined by a profilometer. The roughened Inconel-600 piece was produced by boring and lapping as described for the smooth specimens but at a diameter .003" less than the final .40 inches. A series of left handed and right handed threads, at 20 threads per inch and a depth of about .002 inches were then scribed on the inside surface. The average roughness for this surface was on the order of 400 microinches.

The oxide coating of the Inconel-600 piece was achieved by baking it in an oven for 2 hours at 1000^{o} and another hour at 1500^{o}F. The hot piece was allowed to cool gradually in air at each step. The resulting oxide film was estimated to be .0001 inches or less.

Transient test section design 2 is a modification of an earlier design which was tested and found to have certain deficiencies. These deficiencies centered around design 1's inability to be completely insulated against extraneous heat additions. Figure 6 shows a blowup of the encircled area of Figure 5 where the two designs differ. The finned type arrangement that protrudes from the transient piece in design 1 is bad for two reasons. First it is capable of transferring considerable heat from the base into the transient piece as the small micarta sleeve does not supply sufficient insulation, and secondly, the liquid front attached to the preheater is capable of attaching itself to the fin quite easily thereby causing axial conduction effects. The small contact area and low conductivity of the material that does contact the test specimen in design 2 reduce the heat gains to a greater extent. The copper sleeve at the end of the preheater retards the liquid front in the preheater from coming close to the test specimen. This is because the copper will tend to have a more uniform temperature and any heat that is transferred to it from the brass base will be more uniformly distributed preventing the liquid from attaching it.

This design was so effective in reducing heat losses out the bottome that the small axial temperature gradient in the test piece which was observed to slope down during

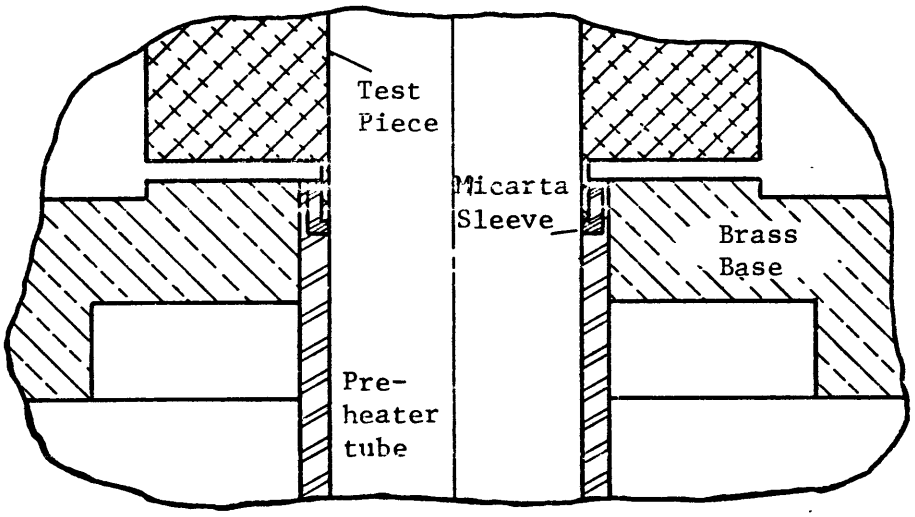

DESIGN 1

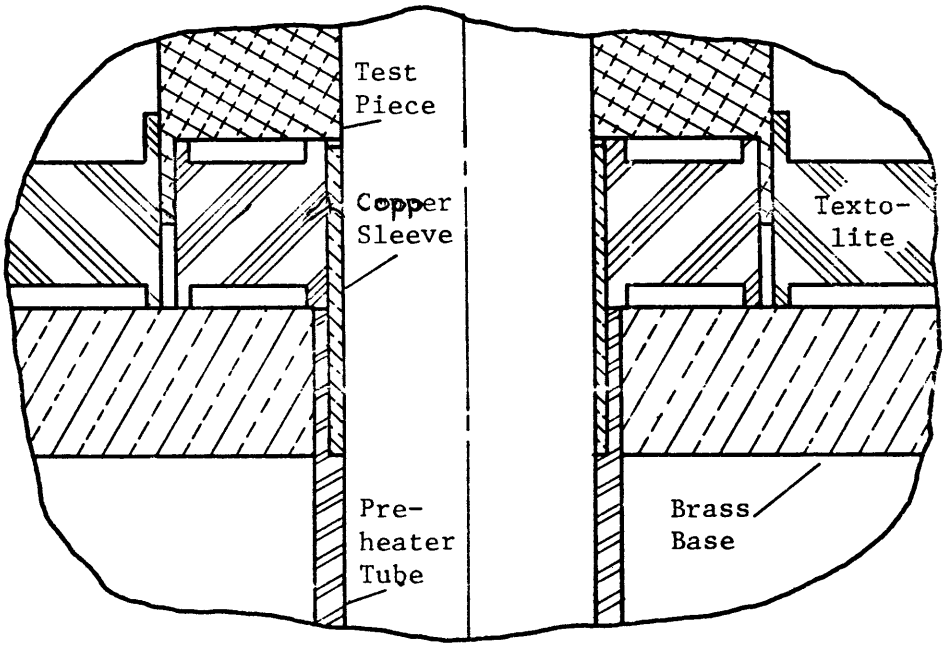

DESIGN 2

Scale
(8 cm to 1 inch)

FIGURE 6 COMPARISON OF DIFFERENCE BETWEEN DESIGN 1 AND DESIGN 2 TRANSIENT SECTIONS

a run with design 1 with the lowest temperature being recorded at the bottom thermocouple reversed itself for runs using design 2 thereby having the lowest temperature being recorded at the top thermocouple. This indicates that design 2 still has some problems with heat losses. Appendix A gives a total estimation of the heat losses from the test piece for the two designs.

2.4 Instrumentation and Data Acquisition

The instrumentation can be divided into two areas: that related to the monitering of the loop operations and that related to the data aquisitions from the transient test section. In all cases copper-constantan thermocouples were utilized as the temperature sensing device.

2.4.1 Test loop instrumentation:

Seven thermocouples were placed on the preheater tube, three on the two inch length preceding the transient section (as shown in Figure 5) and four on the main preheater length. The purpose of these thermocouples was to detect the dryout position in the preheater tube. These thermocouples were measured on a Leeds & Northrup Precision Potentiometer. Other system temperatures such as inlet fluid temperature and exhaust gas temperature from the rotometers were also monitored on this instrument. Measurements of such system quantities as pressure, preheater power and mass flux were obtained as described in Reference (9).

2.4.2 Transient test section instrumentation:

Three thermocouple holes .042 inches in diameter were drilled radially into the test pieces to a depth 1/32 of an inch from the inside radius. The holes were spaced at three axial positions along each test piece with each hole circumferentially spaced 120 degrees apart. The thermocouples were coated with a conducting gel similar to that used for heat sink attachments and inserted in the holes. The thermocouple leads were exited from the steam jacket through conex glands, to the measuring devices.

The measuring equipment for the transient thermocouples consisted of two independent recording devices. The first device, used in recording the top and bottom transient thermocouples, was a Honeywell Speedomax W 24 Point strip chart recorder. The four channel mode was used. The extra two channels were used to monitor thermocouples 1 and 3 on the preheater. This system was a backup to the main data acquisition system to which the middle thermocouple was connected.

At the heart of the data acquisition system was a Model 2000 Sanborn-Ampax FM tape recorder. A solid-state, battery operated amplifier was constructed to boost the ± 5 millivolt thermocouples signal to the required ± 2 volts needed by the recorder. Provisions were made to allow the signal from a reference thermocouple to be recorded on the

tape before the start of each run. This reference signal, used in the data reduction program described in a further section, consisted of a zero reference obtained by placing the reference thermocouple in an ice bath and a maximum reference point obtained by placing the reference thermocouple in a dewar of liquid nitrogen. The temperatures of these two points were obtained by reading the reference thermocouple on the precision potentiometer.

The frequency response of the tape recorder was 650 cycles/second at a recording speed of 3 and 3/4 ips. The strip chart recorder was capable of reading a channel every 1.2 seconds. Being in the four channel model the recorder was able to read one particular thermocouple every 4.8 seconds. Both of these recording devices were able to record the temperature transient of the test specimen whose transient times averaged 30 minutes. (The extreme in total collapse times from 212^{o}F to -320^{o}F depending on the mass flux and quality were 5 minutes to 90 minutes).

2.5 Experimental Procedure

Transient boiling curve data was obtained from the experimental apparatus with the preheater either in a completely wetted mode or in a low quality dryout mode with dryout lengths of 4 or 8 feet. The following sequence of operations were carried out for obtaining film boiling data with wet approach conditions. The steam supply to the

transient section was turned on which allowed the specimen to reach an initial temperature of 220-250°F. Liquid nitrogen subcooled 3-5°F was initiated into the preheater. When the preheater thermocouples registered a temperature near the saturation temperature of the liquid, power was applied to the preheater. The flow rate and power were adjusted to give the desired values of mass flux and exit quality to the transient section for that particular run. During the time needed for steady state to be achieved in the preheater the reference points were recorded on the tape recorder. With the tape recorder reading the data thermocouple the transient was initiated by closing off the steam to the transient section. When the transient was completed, the steam was reinitiated into the transient section, power was increased to produce a new quality for the same mass flux, and the transient procedure was repeated until all qualities for a particular mass flux setting was completed.

The procedures for obtaining film boiling data with dry approach differed only in the startup. The bottom electrode was positioned on the preheater for either a four foot or eight foot heated length. Power was applied to the preheater to raise the wall temperature to about 200°F. Flow was then allowed to enter the preheater resulting in a zero quality dryout starting at the position of the bottom

electrode. Flow rate and power were adjusted to give the desired mass flux and equilibrium quality at the exit of the preheater. The remaining procedures are the same as outlined for the wet wall approach. In some instances especially for the higher quality runs a dryout length of one or two inches was noted for the wet wall approach. This was unavoidable due to the physics of the situation.

2.6 Data Processing:

Figure 7 presents a complete flow diagram of the data from the thermocouple signal to the final boiling curve output. This section is concerned with the segments of the flow chart dealing with data processing. This part of the experimental program was carried out at the Joint Mechanical and Civil Engineering Computer facility using the analog-digital hybrid system as well as the INTERDATA Model 70 and Model 80 digital computer systems. The analog computer was an EAI 680 computer system.

A simple first order filter network, consisting of 3 inverters, 2 potentiometers, and one integrator, was patched into the analog computer to filter and amplify the analog signal from the tape recorder. The data-thermocouple leads acting as an antenna picked up strong 60 cycle noise which had to be removed from the analog signal before accurate digitizing could take place. The amplification was necessary to boost the ± 2 volt signal to ± 10 volts

needed to give maximum sensitivity to the analog-to-digital conversion process. The analog part of Figure 8 can, therefore, be looked upon as a black box whose function is to amplify the oncoming signal by the ratio P1/P2 and filter all frequencies above that given by $10 \cdot N \cdot P_2$ as described in the figure.

The analog-to-digital package is a system that allows the digital computer to read the output of the analog circuit every time a timing pulse is sent to it by the analog computer. This timing pulse is termed the digitizing rate and can be set by the operator to any desired frequency. The output of the analog-to-digital block on Figure 7 is, therefore, an array of voltages whose elements are separated from one another by a constant unit of time specified by the digitizing rate. This array is stored in the digital computer for later processing.

The digital computation phase involves two basic processes: conversion of the voltage array to the actual temperature array and the use of this array to calculate the boiling surface heat flux and wall superheat. The conversion of the voltage array to corresponding temperature values is accomplished in two stages. First, the amplified voltage array is converted back to the original millivolt values using conversion factor generated from the two reference points which had been subjected to the same

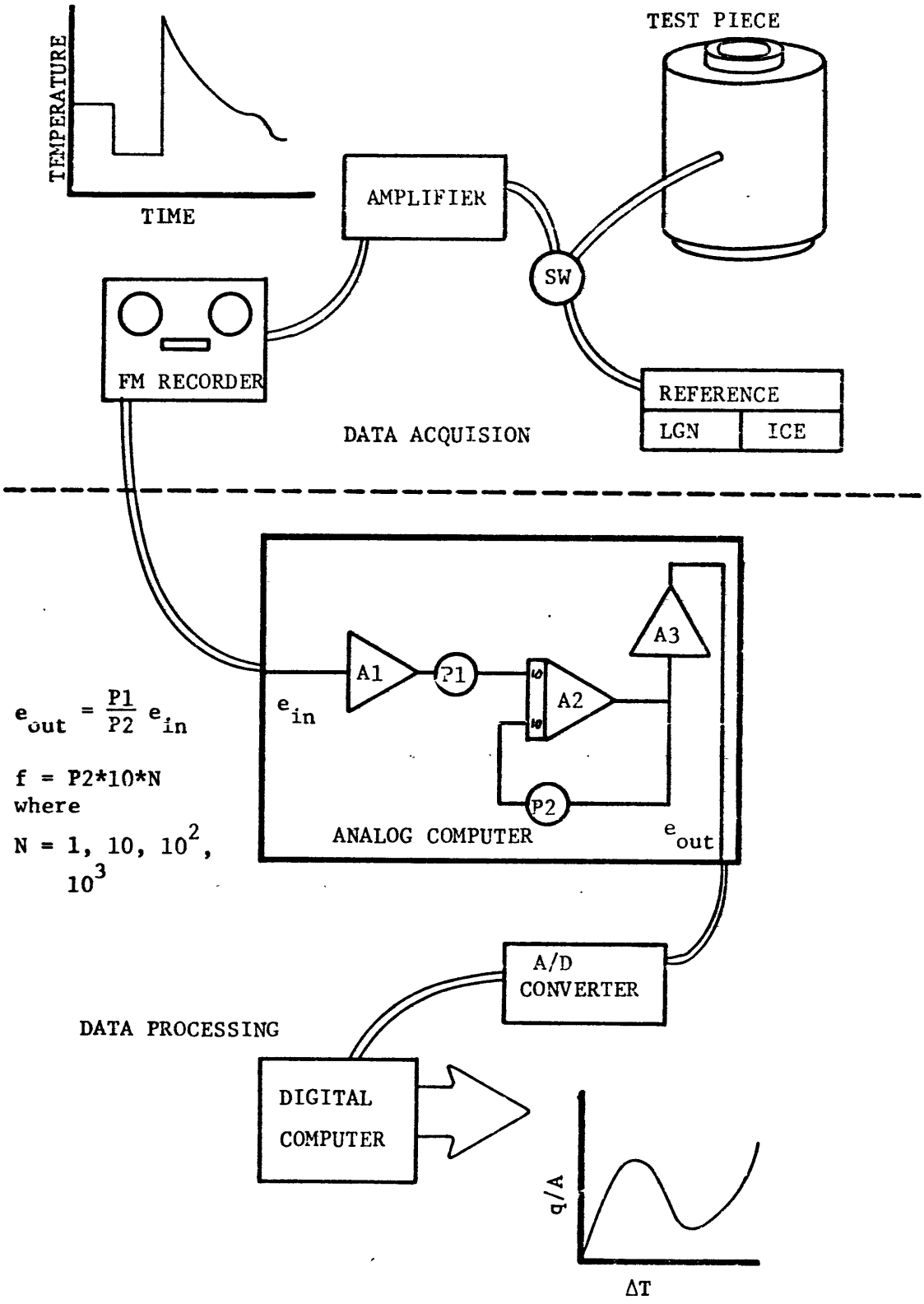

FIGURE 7 DATA FLOW DIAGRAM

processes as the rest of the data. Then the millivolt array is converted to the actual temperature values using a function subroutine consisting of a series of fourth order polynomial curve fits for the copper-constantan thermocouple conversion table.

The main data processing code takes the temperature array for a particular data run and computes the surface heat flux and corresponding wall superheat. The code assumes that the test specimen exhibits no radial or axial temperature profiles allowing the heat flux to be calculated using a lumped heat capacity model. This is a good assumption and the internal temperature gradient will be within 5% of zero if the Biot number ($\bar{h}\ L/K_s$), where L is the characteristic length of the body obtained by dividing the volume by the surface area, is less than .1 [11]. At the maximum post critical heat transfer coefficient of 50 BTU/hr - ft^2-^oF obtained in the experiment the Biot number for the Inconel-600 piece was .22. The same value for the copper and aluminum 1100 pieces were .01 and .013 respectively. The average heat transfer coefficient was generally half the value quoted allowing one to calculate the heat flux from the following equation

$$q/A = \rho\ C_p\ \frac{V}{A}\ \frac{dT}{dt} \qquad (2.1)$$

The temperature dependance of C_p at the low temperature

obtained using liquid nitrogen was included in the calculation of heat flux. With this model the heat flux is directly proportional to the rate of change of the test specimen temperature with time. The code determines the first derivative in the following manner. The temperature array is divided into several segments, and for each segment a least square polynomial curve fit is applied up to order 6. The order of the curve fit is chosen to give the least RMS error between data and curve fit without introducing too strong a wavey character to the first derivative. A fourth order polynomial was generally used in processing the data. The first derivative is obtained directly from the polynomial representation of temperature-time data. This procedure calculates quite well the boiling curve from the film boiling region to the minimum point. The region of the calculated boiling curve to the left of the minimum film boiling wall temperature, including the transition and nucleate boiling regions, is not as well represented quantitatively. The shape is correct but due to the high head fluxes radial temperature gradients reduce the accuracy of the lumped heat transfer model causing the calculated heat fluxes and wall superheat temperatures to be more inaccurate in these regions.

A simple finite difference calculation technique was also performed as a check on the curve fitting method. This procedure consisted of averaging the slope over 4 to 8 time-

temperature increments and applying the calculated heat flux to the middle temperature value to generate the boiling curve from the temperature arrays. There appeared to be little discrepancy between the two methods.

2.7 Experimental Results:

The film boiling data for all the runs (Runs 101-159) using design 2 transient test pieces are tabulated in Appendix C. The results for a selected number of runs (Runs 90-100) employing design 1 transient test pieces are also tabulated. These runs include all those with the preheater in the dryout mode. Most of the data with the preheater in the wet mode is affected to some degree by heat losses as discussed in Appendix A. It is felt that the data obtained in the initial portions of the transient for each of these runs is affected to a much lesser degree by the heat losses than the portion of the transient where the test piece is considerably below the ambient room temperature. Therefore one should only consider the first portions of tabulated data for the runs with low L_{DO}'s. Appendix B gives the equations used in the data reduction process for the system variables and gives an estimated error for these quantities. The following sections discuss the results of a parametric study of heater material, roughness and oxide coating on the post critical heat transfer. A comparison is also made between the transient nitrogen

data taken in this program and some data obtained by Forslund in the steady state mode.

2.7.1 Transient vs. steady state data

There is some contention in the literature that a quench experiment will not reproduce a steady state boiling curve. Bergles and Thompson[12] attempted to ascertain if there were any discrepancies between the steady state and transient boiling curves for the same fluid and heater geometry. Experimentally Bergles and Thompson found the steady state boiling curves differed in some respects from the transient boiling curves for the three fluids, water, Freon 113 and nitrogen, that he tested. The discrepancies for the water and Freon 113 steady state and transient boiling curves were easily explained to be caused by the oxide deposits deposited on the boiling surface during heat up. The combination of wettability and roughness of the oxide coating increased the minimum heat flux and wall temperatures, increased the film boiling heat transfer, increased the critical wall temperature and decreased the critical heat flux. The discrepancies between the transient and steady state boiling curves for nitrogen were localized around the minimum point. The transition point was reduced to a much lower heat flux and wall temperature for the transient experiment than exhibited by the steady state experiment. This phenomenon could not be explained by oxide

scaling as the quench piece was only heated to room temperature. Bergles and Thompson took the position that the steady state boiling curve represented the correct physical phenomenon and tried to explain why the transition point in the transient case was delayed to lower a wall temperature and heat flux than that resulted in the steady state case. It is our contention that the transient case is the more accurate representation of the boiling characteristic and that the steady state experiment conducted by Bergles and Thompson was forced to transit earlier due to axial conduction effects brought on by the power lead as well as the possibility of liquid reattachment to the unheated areas of the test cylinder.

Figure 8 presents a comparison of several of the transient data runs obtained in this program with some steady state nitrogen data taken by Forslund. The transient data appears to be slightly lower than each of the corresponding steady state data points, even though the mass flux and quality differences between the two would cause one to expect slightly higher values. This is attributed to experimental uncertainties in the transient data rather than any transient effects. As the transient times for the tests averaged over thirty minutes per run the transient experiments can be considered nearly quasisteady.

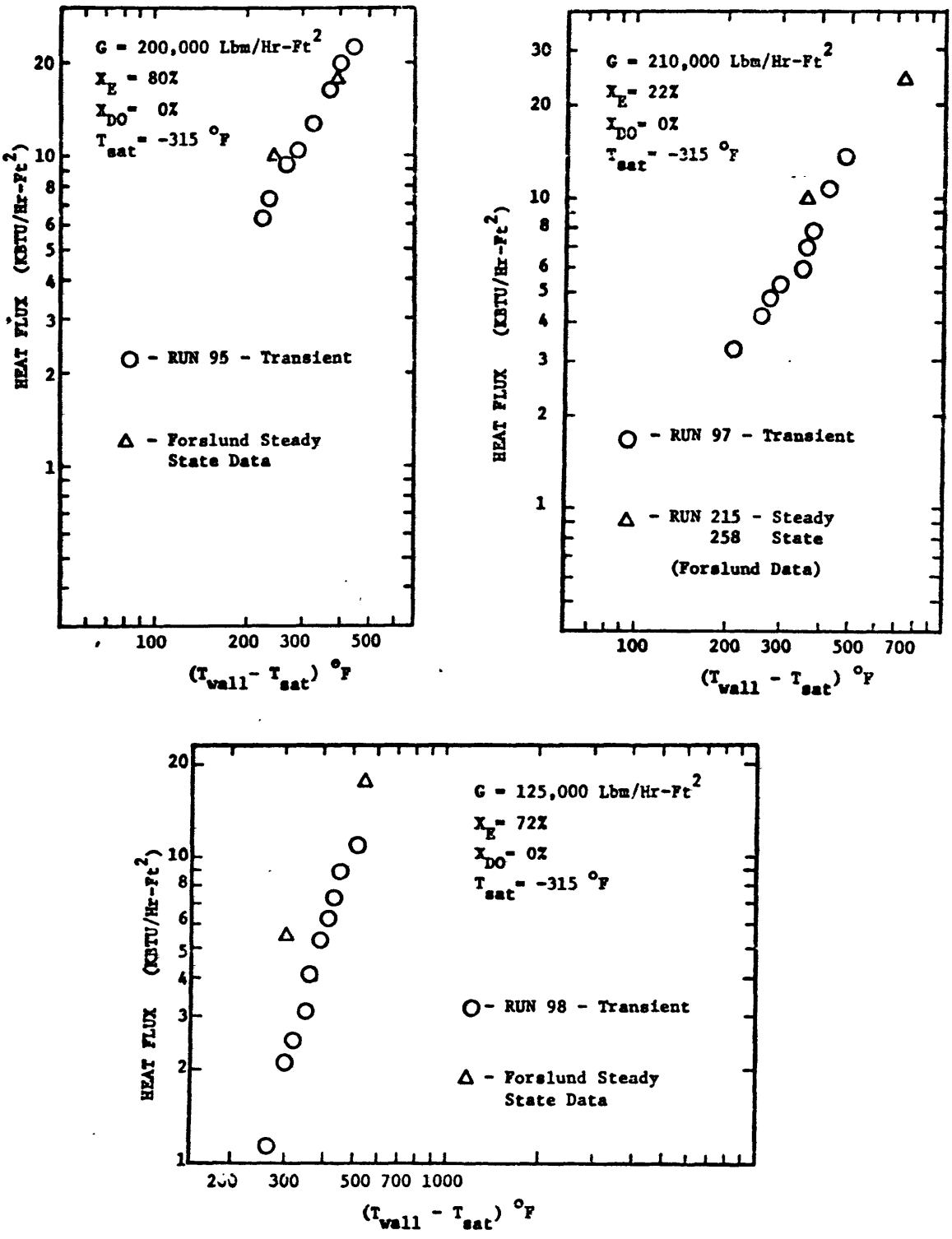

FIGURE 8 TRANSIENT VS STEADY STATE FILM BOILING HEAT TRANSFER

2.7.2 Effect of heater material on post critical heat transfer.

Figure 9 presents a comparison of the three different smooth specimens tested for a mass flux of 60,000 lbm/hr-ft^2 and 210,000 lbm/hr-ft^2. The results for each of the materials produce a fairly large band at each of the two mass flux cases. For the 60,000 lbm/hr-ft^2 case copper gives the highest heat flux for a given wall superheat, followed by aluminum 1100 and then Inconel-600. For the high mass flux case the order from highest to lowest is copper, Inconel-600 and aluminum 1100. There appears to be no consistant material effect in the data, and the banding is considered to be the result of experimental error (Appendix A & B)

Bergles and Thompson[12] in the process of determining the relationships between steady state and transient boiling curves presented some data for copper and inconel. Taking the view that the two processes used gave the same boiling curve, no strong material effects were noted in the film boiling data for the two materials where the surfaces were considered to be free of oxide scale effects.

2.7.3 Effect of roughness on the post critical heat transfer.

The roughness effect on the post critical heat transfer should follow the same trends as observed in single phase heat transfer. By applying the Colburn analogy[13] between

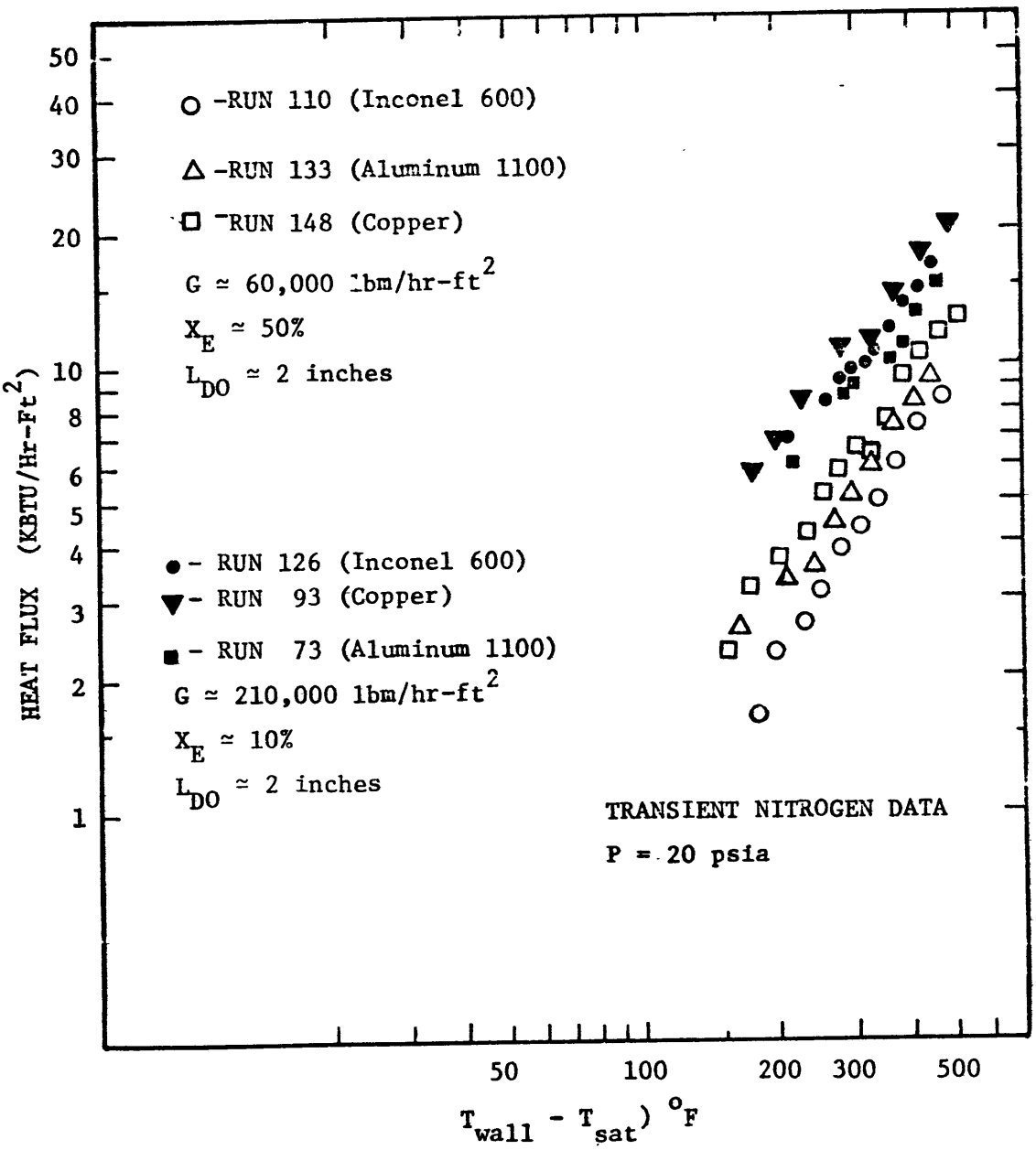

FIGURE 9 EFFECT OF MATERIAL ON DRY WALL FILM BOILING HEAT TRANSFER

heat transfer and fluid friction and considering the heat transfer in post dryout to be entirely due to the wall to vapor component where the vapor mass flux is defined as

$$G_v = \frac{GX}{\alpha} \tag{2.2}$$

one can obtain a functional dependance of roughness on the post critical heat flux in an approximate manner to be

$$q/A = \frac{f}{2} Cp \frac{GX}{\alpha} Pr^{-2/3} (T_w - T_v) \tag{2.3}$$

With all other variables held constant the heat flux will increase with increasing friction factor, f. f is directly related to roughness heights defined by the ratio, e/D, and Reynolds number as given by Moody[14].

The roughness effect on the transient data was not very strong for the 30,000 lbm/hr-ft^2 mass flux tested as seen in Figure 10. Both the low and high quality cases showed no pronounced effect. This is because at the low vapor Reynolds numbers, the difference between the rough and smooth friction factors is small. There are indications though that the roughened surface gives slightly higher heat transfer for the high quality case if one looks at the actual mass fluxes for the two sets of data being compared. The roughened specimen had a mass flux 16% lower than the smooth but had the same heat flux for a given wall superheat.

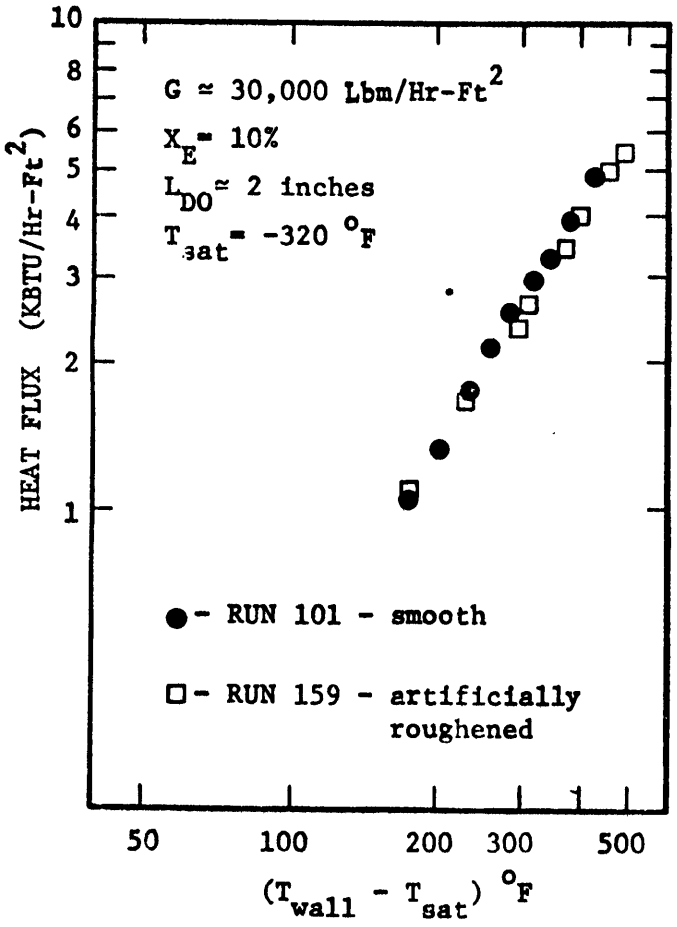

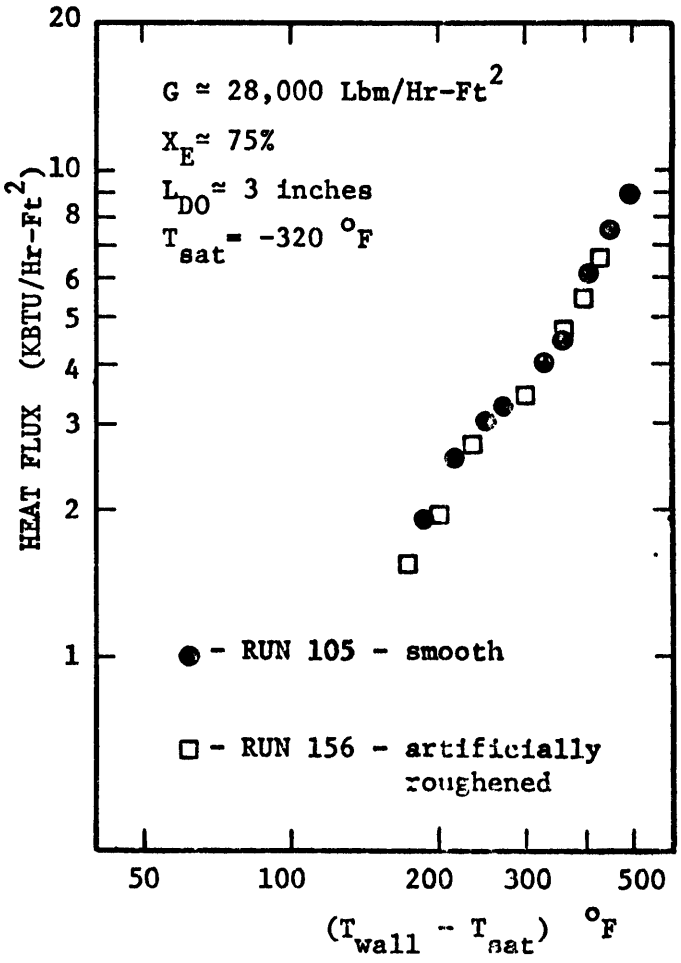

FIGURE 10 EFFECT OF ROUGHENING ON FILM BOILING HEAT TRANSFER

2.7.4 Effect of oxide scale on the post critical heat transfer.

There is considerable evidence in the literature [12, 15, 16, 19] that oxide coatings on the heating surface have large effect on the boiling curve. Figure 11 presents the effects of oxides on the film boiling heat transfer found in this program for several mass fluxes and qualities which is consistant with that observed by other experimenters. For both mass fluxes at each of the different qualities the oxide coated specimen has higher heat fluxes than the smooth specimen. The low qualities gave more pronounced effects than the higher qualities. It is felt that the heat losses or gains, if present as discussed in Appendix A, will affect all the data used in the comparison and will not influence the differences observed between the smooth and oxide coating runs. The following is postulated to be the reason for the observed oxide effect.

It is postulated that there is sporadic liquid contact in the dry wall film boiling region. (Visual observations have been observed and the heat transfer effects have been measured for liquid-metal contact of single droplets on horizontal heated plates [17, 18, 19]). The contact time may be of an infinitesimal ly small duration but is sufficient for the liquid to sense the wall. If the contact temperature which can be estimated to be

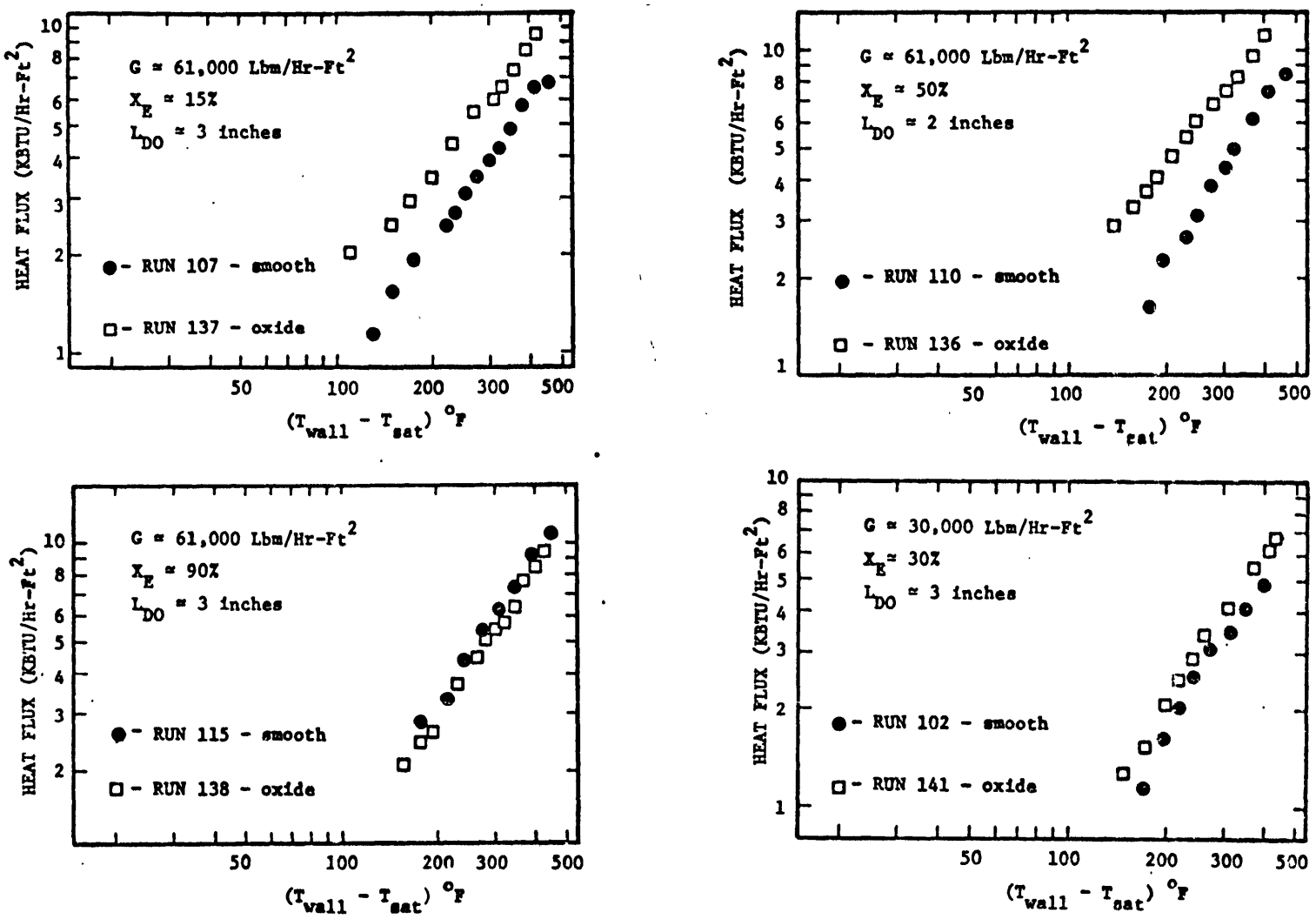

FIGURE 11 EFFECT OF OXIDE SCALE ON FILM BOILING HEAT TRANSFER

$$\frac{T_{cb} - T_{Lo}}{T_{wo} - T_{cb}} = \frac{\sqrt{(k\rho c)_w}}{\sqrt{(k\rho c)_L}} \qquad (2.4)$$

at the instant of contact from the solution of two semi infinite bodies of different inital temperatures is greater than the maximum liquid temperature*, the liquid will not remain in contact but immediately be expelled from the surface. However, if the surface is covered by an oxide coating, several effects will allow the liquid to remain for a longer period of time. First the contact temperature will be initially lower due to the lower $(k\rho c)$ ratio of the oxide as evidenced by equation (2.4 and if the base temperature is higher than the maximum liquid superheat a certain amount of time will be necessary to heat the surface temperature of the oxide to the maximum liquid temperature. During this heat up time the liquid is evaporating producing good heat transfer. Second, if the oxide is porous or highly wetting the liquid will spread out covering a larger portion of the heater and adhere more strongly to the heater than if the surface was clean. Both these processes will increase the heat transfer. The quality effect can be linked by the fact that the probability of the liquid contact will increase as the void fraction decreases. The momentum of the small drops, characteristic of high

* The maximum liquid temperature is defined by Groeneveld [7] as a thermodynamic liquid temperature for a given pressure above which the liquid state can not be maintained. It can be obtained from homogeneous nucleation theory [29].

void film boiling, towards the heated surface is too small to resist the repelling force due to the liquid evaporating from the surface of the drop.

The explanation of the oxide effect presented here is somewhat contradictory to the idea that the minimum film boiling temperature is identical to the maximum liquid temperature (Groeneveld [7]) and as such no liquid contact can result in film boiling. Instead of the minimum film boiling temperature being thermally controlled, a theory has been developed (Iloeje[28]) that indicates that the minimum film boiling point is the result of the changing importances of three heat transfer mechanisms: the mechanism controlling heat transfer to liquid in direct contact with the heater, the mechanism controlling heat transfer to liquid that comes near the heater surface without touching (dry collisions) and the mechanism of forced convection heat transfer to vapor. The first term, starting from the maximum nucleate boiling temperature where total liquid contact is assumed, decreases with increasing wall superheat. The last two terms increase with increasing wall superheat. The addition of the three terms produces a minimum in the boiling curve. Anything that affects each of the separate terms will influence the minimum point. Iloeje considers that any droplet can contact the surface regardless of the wall temperature if it has sufficient radial momentum towards

the wall. His model can not predict the effect of wet collisions with the wall whose temperature is above the maximum liquid superheat as the vigorous evaporative heat transfer mechanism is not understood.

It is felt that this concept of the three step process is a major advancement towards the full knowledge of the boiling curve and helps one to understand in the light of surface effects such data as McDonough, Milich, and King's[27] and Plummer and Iloeje's[16] where the transition boiling data was considerably above the maximum liquid superheat. Assuming the minimum film boiling temperature to be determined by the maximum liquid superheat would discount this data as suspect when in actuality it is real data which is probably influenced by surface effects. (In the data analyzed by Plummer and Iloeje actual physical evidence of oxide was found upon examination of the test section).

III. Two-Step Dispersed Flow Film Boiling Heat Transfer Model

3.1 General Properties of Model

The dispersed flow model [5,6,7,8] assumes that the two phase mixture beyond the dryout-point is composed of spherical drops uniformly distributed in the vapor phase. In simple terms the model allows heat to be transferred from the wall to the bulk flow in two steps; first from the wall to the vapor phase and from the vapor to the entrained droplets. The model also allows for direct heat transfer to the drop via direct collisions with the heating surface. The model begins at the point of dryout where equilibrium conditions are assumed. There the vapor temperature is at the saturation temperature, and the quality is that given by thermodynamic conditions. At this point initial drop size, vapor and liquid velocities are calculated from continuity, momentum and critical Weber number equations. The Weber number is a ratio of inertia to surface tension forces and in essence restricts the diameter of the drop given the droplet and vapor velocities. To move the solution downstream the gradients of vapor temperature, droplet diameter, actual quality and liquid velocity are derived. These quantities are derived from energy, momentum and continuity considerations. The

empirical nature of the model comes in through the use of friction factor and heat transfer coefficient for a droplet moving in a super-heated vapor, the single phase transfer coefficient from heater surface to the super-heated vapor and heat transfer coefficient used to define behavior of direct wall to droplet heat transfer.

The Hynek and Groeneveld treatments of the basic quantities of the model differ in some instances. The purpose of this chapter is to present the fundamental equations for the two step model as used by Hynek and Groeneveld and to compare each calculation procedure with intention of ascertaining their strong and weak points. The two models are compared with data and a hybrid model is presented which is generally as consistant or somewhat better in predicting the data than either the Hynek or Groeneveld model.

3.2 Conditions at Dryout

3.2.1 Groeneveld Technique:

In calculating the dryout conditions Groeneveld employs the void fraction definition and a slip correlation developed for predryout annular flow by Ahmad[20]. Groeneveld modified the slip predicted by Ahmad's correlation to be halfway between S_{Ahmad} and S = 1 to account for the discrepancy in flow regimes. The void fraction at dryout

is therefore, given by

$$\alpha_{DO} = \frac{X_{DO}}{X_{DO} + \frac{\rho_v}{\rho_\ell}(1-X_{DO})S} \tag{3.1}$$

where S is determined from

$$S = \frac{1}{2}\left[\left(\frac{\rho_\ell}{\rho_v}\right)^{.205} / \left(\frac{GD_T}{\mu_\ell}\right)^{0.016} - 1\right] + 1 \tag{3.2}$$

The average vapor and liquid velocities are found from

$$(V_\ell)_{DO} = \frac{(1-X_{DO})G}{\rho_\ell(1-\alpha_{DO})} \tag{3.3}$$

$$(V_g)_{DO} = \frac{G\,X_{DO}}{\rho_v \alpha_{DO}} \tag{3.4}$$

Groeneveld assumes the droplet diameter to be critical at the point of dryout, and furthermore he assumes that the diameter can be predicted by a critical Weber number criterion given by

$$(W_e)_{crit} = \frac{\rho_v(V_g - V_\ell)\delta}{\sigma} \tag{3.5}$$

He selects a value of 6.5 for the critical Weber number based on Isshiki's[21] water data. Substituting in the values of $(We)_{crit}$, $(V_\ell)_{DO}$ and $(V_g)_{DO}$ gives δ_{DO}

3.2.2 Hynek Technique:

Hynek solves the momentum, continuity and critical Weber number equations along with the assumption that the liquid acceleration is related to the vapor acceleration by

$$\frac{dV_\rho}{dZ} = X_A \frac{dV_g}{dZ} \tag{3.6}$$

and the assumption that the vapor acceleration is related to the heat flux under isothermal conditions with $A_v = A$ by

$$\frac{dV_g}{dZ} = \frac{(q/A)}{\rho_v h_{fg} D_T} \tag{3.7}$$

to obtain two equations relating $(V_g)_{DO}$ to $(V_\ell)_{DO}$.

$$(V_g)_{DO} = (V_\ell)_{DO} + \sqrt[4]{\left[g\left(1 - \frac{\rho_v}{\rho_\ell}\right) + \frac{4(q/A)X_{DO}(V_\ell)_{DO}}{\rho_v h_{fg} D_T}\right] \frac{\rho_\ell (W_e)_{crit} \sigma}{.75 C_D \rho_v^2}} \tag{3.8}$$

and

$$(V_g)_{DO} = \frac{G\, X_{DO}}{\rho_v \left[1 - \frac{G(1-X_{DO})}{\rho_\ell (V_\ell)_{DO}}\right]} \tag{3.9}$$

These two equations require an iterative solution. A fortran subroutine, developed by Hynek is given in Appendix D which gives $(V_g)_{DO}$ and $(V_\ell)_{DO}$ for any desired set of conditions. Hynek chose a value of 7.5 for the critical Weber number based also on the Isshiki data. Knowing the liquid and vapor velocities at dryout the droplet diameter is obtained from the critical Weber number criterion given by equation (3.5).

3.2.3 Discussion:

Tabulations of dryout slip and void fraction calculated, by each model are presented in Table 1 for a selected set of mass fluxes and heat fluxes with dryout quality ranging from 10-90% for liquid nitrogen. The Hynek slip is strongly influenced by dryout quality and mass flux. The Groeneveld slip has no dryout quality variable and the mass flux variable is quite small being raised to the 0.016 power. Groeneveld has no heat flux variable in the slip ratio, and while the Hynek model does include heat flux, an increase of heat flux by a factor of 4 for the same mass flux and quality changed the resulting slip by less than 1 percent. For Nitrogen the maximum slip the Groeneveld method was 1.7 compared to a value of 41. for Hynek's at the same conditions of X_{DO} = 10% and G = 30,000 lbm/hr-ft^2. This resulted in a dryout void of 89% for the Groeneveld method as compared

$G \times 10^{-3}$ (lbm/hr-ft)	$q/A \times 10^{-3}$ (Btu/hr-ft^2)	X_{DO}	HYNEK S_{DO}	HYNEK α_{DO}	GROENEVELD S_{DO}	GROENEVELD α_{DO}
30.	5.	.1	41.17	.260	1.694	.895
		.5	4.13	.969	1.694	.987
		.9	2.06	.998	1.694	.999
	10.	.1	41.18	.260	1.694	.895
		.5	4.58	.966	1.694	.987
		.9	2.3	.998	1.694	.999
	20.	.1	41.22	.260	1.694	.895
		.5	5.39	.960	1.694	.987
		.9	2.68	.998	1.694	.999
100.	5.	.1	5.45	.726	1.671	.896
		.5	1.41	.989	1.671	.987
		.9	1.27	.999	1.671	.999
	10	.1	5.52	.724	1.671	.896
		.5	1.49	.989	1.671	.987
		.9	1.32	.999	1.671	.999
	20.	.1	5.68	.718	1.671	.896
		.5	1.6	.988	1.671	.987
		.9	1.43	.999	1.671	.999
250.	5.	.1	1.715	.894	1.654	.897
		.5	1.2	.991	1.654	.987
	10.	.1	1.758	.892	1.654	.897
		.5	1.204	.991	1.654	.987
	20.	.1	1.832	.888	1.654	.897
		.5	1.261	.990	1.654	.987

(D_T = .4 inches)

Representative Values of S_{DO} and α_{DO} for the Hynek and Groeneveld Initialization Techniques

TABLE 1

to 26% void for the Hynek technique. While it is possible that the Hynek model fails at this set of conditions due to the fact that the flow pattern might not be dispersed flow, the value of 26% for the void seems intuitively more correct than the 89% value. As the mass flux and dryout quality increase to the point where the dryout void is high (greater than 85-90%), both techniques give reasonably close values. The more physical nature of the Hynek model as well as its ability to give more reasonable results outweight its awkwardness.

3.3 Gradients in Post Dryout

Groeneveld revised the Bennett post dryout gradierts to include pressure drop effects and flashing effects. Groeneveld found that these terms can be neglected except in the case of Freon 12 at high heat flux-mass flux conditions. Therefore, the simplified post dryout gradients of Groeneveld which are identical to those used by Hynek are presented here.

Liquid droplet velocity gradient:

$$\frac{dV_\ell}{dZ} = \frac{3\ C_D \rho_v (V_g - V_\ell)^2}{4\delta\ \rho_\ell V_\ell} - \left[1 - \frac{\rho_v}{\rho_\ell}\right] \frac{g}{V_\ell} \qquad (3.10)$$

Droplet diameter gradient:

$$\frac{d\delta}{dZ} = \frac{-2(q/A)_{\text{vapor to drop}}}{h_{fg}\rho_\ell V_\ell} - \frac{4\delta(q/A)_{\text{wall to all drops}}}{3(1-X_A)D_T G\ h_{fg}} \qquad (3.11)$$

Actual quality gradient

$$\frac{dX_A}{dZ} = \frac{-3(1-X_o)\delta^2}{\delta_o{}^3} \frac{d\delta}{dZ} \qquad (3.12)$$

where $X_o = X_{DO}$ and $\delta_o = \delta_{DO}$ to start .

Equilibrium quality gradient (thermodynamic)

$$\frac{dX_E}{dZ} = \frac{4q/A}{G\, h_{fg} D_T} \qquad (3.13)$$

Vapor temperature gradient:

$$\frac{dT_v}{dZ} = \frac{h_{fg} \frac{dX_E}{dZ} - [h_{fg} + C_{pv}(T_v - T_{sat})]\frac{dX_A}{dZ}}{X_A C_{pv}} \qquad (3.14)$$

3.4 Droplet Breakup

The point at which droplet breakup occurs is determined by the critical Weber number for both the Hynek and the Groeneveld model. Hynek used 7.5 whereas Groeneveld used 6.5.

When the critical Weber number is reached in the Groeneveld model the new droplet diameter is set equal to the critical droplet size given by

$$\delta_{crit} = \frac{(W_e)_{crit}\,\sigma}{\rho_v (V_g - V_\ell)^2} \qquad (3.15)$$

The values, δ_o and X_o, in the actual quality gradient are updated to δ_{crit} and X_A at shatter. The droplet flux [droplets/ft^2-fr.] is increased to a new value given by

$$N_d = \frac{6\ G[1 - (X_A)_{\text{at shatter}}]}{\pi\ \delta_{crit}^3\ \rho_\ell} \qquad (3.16)$$

A new velocity gradient is calculated from which new values of V_g and V_ℓ are determined. The Weber number is rechecked. If the Weber number is still critical the cycle is repeated until the Weber number is just subcritical.

The Hynek model assumes the droplet to shatter in two as the critical Weber number is reached. This results in the doubling of the droplet population and a reduction of each drop diameter by $1/\sqrt[3]{2}$. The values of X_o and δ_o are updated. The same procedure as Groeneveld used is applied to ascertain if the new Weber number after shattering is less than the critical value.

Unlike the large discontinuity in drop diameter resulting from shattering in the Hynek model the trend of the droplet diameter change for the Groeneveld model is more gradual. The Weber number in the post dryout calculations tends also to remain near the critical value for the Groeneveld method as the drop diameter doesn't change

much after shattering.*

3.5 Heat Transfer Correlations:

The dispersed flow model is by reason of the extremely complicated flow structure a semi-theoretical model which depends on empirical correlations to describe the heat transfer behavior of the component parts.

3.5.1 Vapor to droplet:

There is general agreement between the two models that the analogy between heat and mass transfer modified by the Froessling ventilation factor will predict the vapor to drop heat transfer. While Groeneveld derives a simple technique for determining the diffusive resistance associated with this heat transfer mechanism, he subsequently neglects it as did Hynek citing that high turbulence levels are sufficient to wipe out this resistance. The vapor to drop heat transfer is given by

$$(q/A)_{\substack{\text{vapor}\\ \text{to drop}}} = \frac{2(T_v - T_{sat})k_v}{\delta}\left[1 + .276\, Re_{drop}^{1/2}\, Sc^{1/3}\right] \quad (3.17)$$

where Hynek assumes $Sc = Pr_{vapor}$

and Groeneveld assumes $Sc = \dfrac{\mu_g R}{k_g(\gamma-1)}$

from Kinetic theory of gases

---

* A provision was made in the dispersed flow film boiling code to reduce the diameter by 10% if after four cycles of the shattering process at a tube position the Weber number was still critical.

3.5.2 Wall to vapor:

There are a number of single phase vapor heat transfer coefficients applicable for the wall-to-vapor heat transfer term. These correlations are differentiated by the fluid on which they were based. Two such correlations tested in this work were that developed by Forslund for nitrogen and that developed by Heineman[22] for superheat steam. Groeneveld modified a generalized heat transfer coefficient developed by McAdams[23]. These three equations are presented here

Forslund:
$$h_{w,v} = \frac{k_v}{D_T} .035\ Re_v^{.743}\ Pr_v^{.4} \qquad (3.18)$$

Heineman:
$$h_{w,v} = \frac{k_f}{D_T} .0157\ Re_f^{.84}\ Pr_f^{1/3}\ \left(\frac{D_T}{L_{DO}}\right)^{.04} \quad \left(6 < \frac{L_{DO}}{D_T} < 60\right) \qquad (3.19)$$

$$h_{w,v} = \frac{k_f}{D_T} .0133\ Re_f^{.84}\ Pr_f^{1/3}\ \left(\frac{L_{DO}}{D_T} > 60\right) \qquad (3.20)$$

Modified McAdams:
$$h_{w,v} = \frac{k_v}{D_T} .023\ Re_v^{.8}\ Pr_v^{1/3}\ \left(\frac{\mu_v}{\mu_w}\right)^{.14} \left[1 + .3\left(\frac{D_T}{L_{DO} + .01\ D_T}\right)^{.7}\right] \qquad (3.21)$$

3.5.3 Wall to drop:

At low qualities and correspondingly low void fractions Forslund found that large discrepancies were present between the experimental data and his core flow analysis using only

a wall-to-vapor heat transfer term. He postulated that a direct wall-to-droplet term made up the difference and derived a heat transfer coefficient based on Baumeister's[30] work related to sessile drops on horizontal heated plates. A correlating constant was employed to take into account the droplet velocity and concentration and evaluated from data comparisons. His term is given as

$$h_{w,\delta} = K_1 K_2 (\pi/4)\ (6/\pi)^{2/3} (1-\alpha)^{2/3} \left[\frac{k_f^3 h_{fg}^* g \rho_f \rho_\ell}{(T_w - T_{sat}) \mu_f \sqrt[3]{\frac{\pi}{6}\delta}}\right]^{1/4} \quad (3.22)$$

where $(1-\alpha) = \dfrac{G(1-X_A)}{\rho_\ell V_\ell}$

and $h_{fg}^* = h_{fg}\left[1+\frac{7}{20}\dfrac{C_p (T_w - T_{sat})}{h_{fg}}\right]^{-3}$

Groeneveld questions the validity of extrapolating the use of the heat transfer coefficient for sessile drops to predict the wall-drop interaction in dispersed flow. He feels both the droplet velocity and its rotation invalidates the solution for a sessile drop. The proper evaluation of the wall-to-droplet term requires the knowledge of the drop dynamics as it is projected towards the wall as well as the droplet-wall interaction ear the heating surface. Groeneveld estimates the wall to droplet term by a simple heat conduction term assuming a linear temperature profile between the wall and drop.

$$h_{w,\delta} = \frac{k_{v,f}(1-\alpha)}{\delta_{film}} \text{EXP}[-\frac{2D_T}{L_{DO}}] \qquad (3.23)$$

where

$(1-\alpha)$ is that fraction of wall facing the liquid droplets.

$\text{EXP}[-2^{D}T/L_{DO}]$ is estimated to account for the reduced wall-droplet interaction just beyond dryout.

δ_{film} is the average distance of droplets above the heated surfaces.

A theoretical analysis of droplet trajectories in post dryout dispersed flow is currently being investigated by O.C. Iloeje[28] which indicates that δ_{film} is strong function of wall temperature. Therefore the choice of one value for δ_{film} for predicting wall-to-droplet effects in a uniformly heated tube will of necessity be in error somewhere in the tube. An optimum value of δ_{film} can be chosen, though, from comparison of model with post dryout data.

Figure 12 gives a quantitative comparison of the two wall-to-droplet terms for a mass flux of 130,000lbm/hr-ft^2

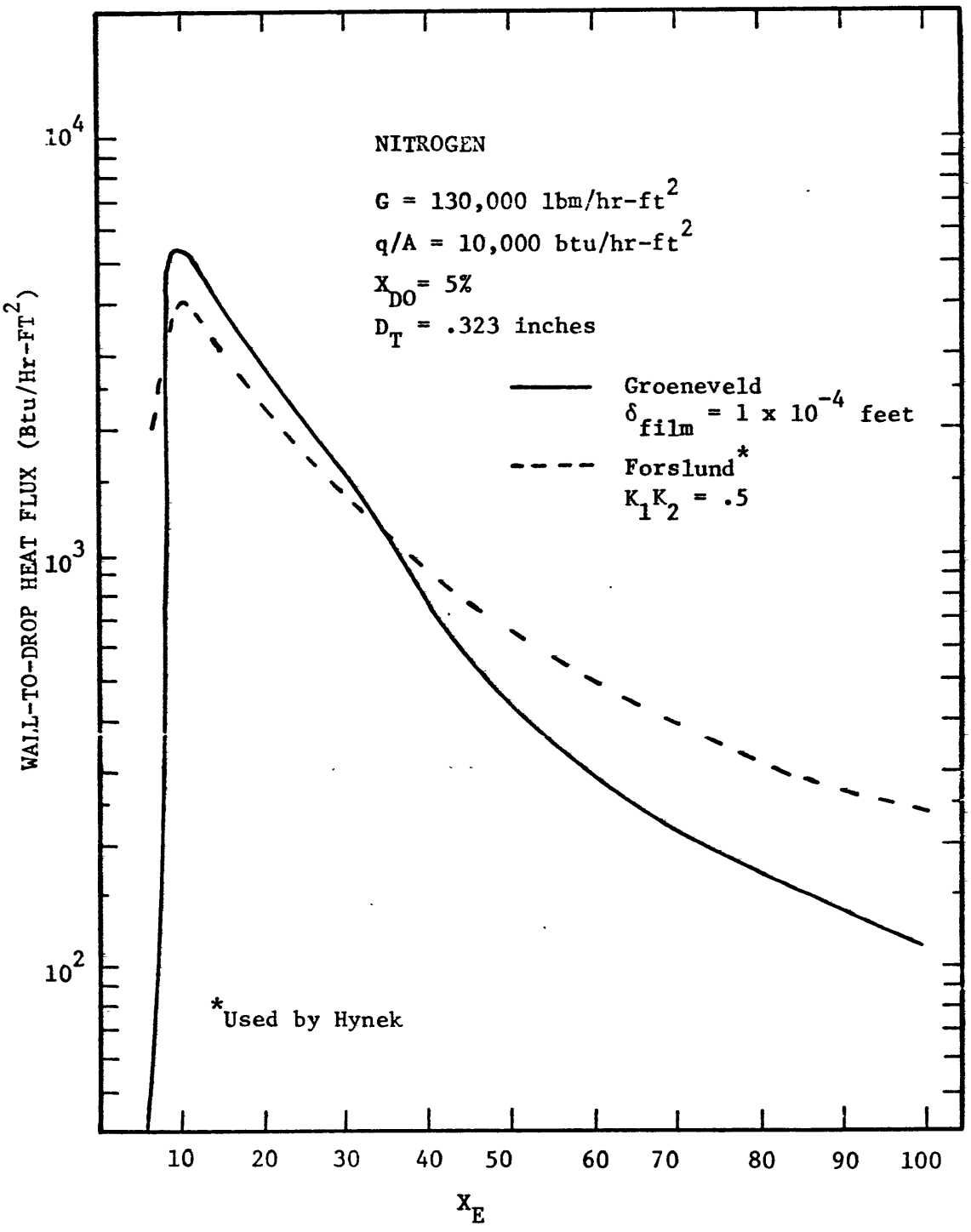

FIGURE 12 COMPARISON OF FORSLUND'S AND GROENEVELD'S WALL-TO-DROP HEAT FLUX TERMS FOR A SELECTED SET OF CONDITIONS

using liquid nitrogen as the test fluid. δ_{film} was determined to be 1 x 10^{-4} ft from comparison of model with experimental data for this mass flux. Using the same technique a value of 0.5 was chosen for K_1K_2 . As can be seen from the figure the Groeneveld term is zero near the dryout point (as determined by the exponential term) whereas the Forslund term is finite. The two terms coincide as the solution is moved away from the dryout point. This happens at about 40 diameters away from dryout which is the point where the exponential term in Groeneveld's heat transfer coefficient has a 5% effect. As the void fraction tends to one, both droplets terms reduce to zero.

Due to the 2/3 power on the liquid fraction term, $(1-\alpha)$, in the Forslund term instead of the one power as used by Groeneveld, Forslund's wall to drop term tends toward zero at a slower rate.

From observations of temperature length data, low quality dryouts exhibit a low heat transfer coefficient after dryout which builds to a maximum and decreases again as the quality increases from the dryout value. The Groeneveld wall-to-drop term is consistant with this trend. The Groeneveld term was adopted for use in the generalized post critical correlation developed in Chapter 4 for this reason as well as for its more intuitively

justifiable basis.

3.6 Total Heat Transfer in Disperse Flow Film Boiling

The total heat transfer calculated by the model is the sum of the wall-to-vapor heat flux and the wall-to-droplet heat flux given by

$$(q/A)_{\substack{\text{heater}\\\text{surface}}} = h_{w,v}(T_w - T_v) + h_{w,\delta}(T_w - T_{sat}) \qquad (3.24)$$

A finite difference computer code, FILMBOIL, was developed using a combination of techniques used by Groeneveld and Hynek. This is given in Appendix D. The code uses the Hynek initialization procedure, the Groeneveld droplet breakup and the Groeneveld wall-to-droplet heat transfer coefficient. Provisions were made to select either the modified McAdams equation or Heineman equation for the wall-to-vapor heat transfer coefficient depending on what fluid was being tested. This code was compared against Forslund's nitrogen data, Bennett's water data and Groeneveld's Freon 12 data, to ascertain the variations of δ_{film} need to predict the respective data.

3.6.1 Comparisons of model with nitrogen data

Figure 13 represents the resulting comparisons of FILMBOIL with Forslund's nitrogen data. This data was taken in zero quality dryout mode and is a good example of the low void dryout explained in the introduction. The

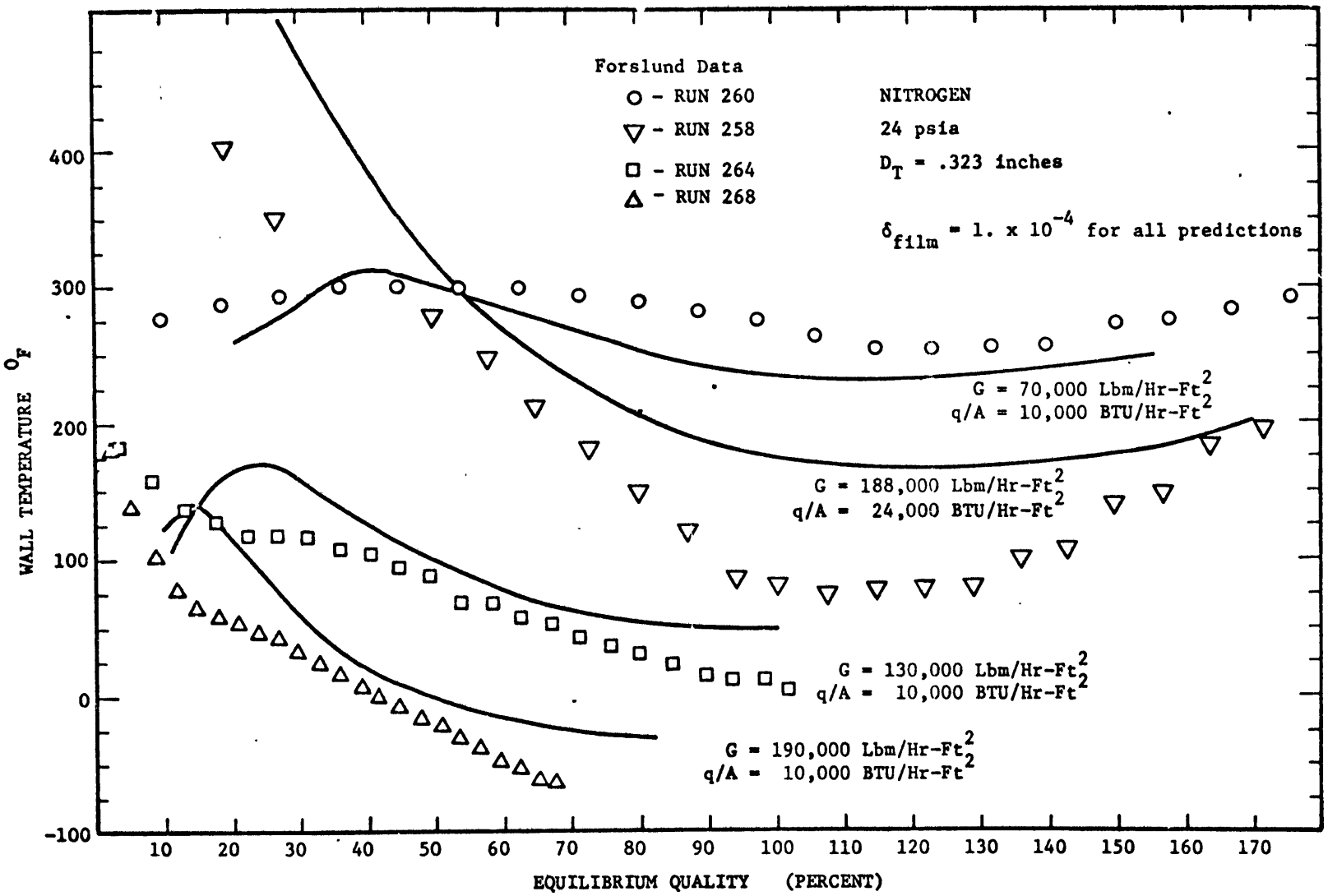

FIGURE 13 COMPARISON OF FILMBOIL WITH FORSLUND'S STEADY STATE NITROGEN DATA

inlet qualities for the four runs presented here are about -2% indicated a slight inlet subcooling. The calculation procedure was started at a quality of 5% which is a small distance away from the dryout point. The code cannot be started at a zero quality value as that is a singular point for some of the equations in the code. The modified McAdam's single phase vapor equation was used in the code for this comparison analysis. $\delta_{film} = 1 \times 10^{-4}$ feet predicts the nitrogen data quite well and shows no heat flux or mass flux dependence for the three mass fluxes and the two corresponding heat fluxes presented. The model diverges somewhat in the low quality region as can be expected. The flow regime in all probability is not that of dispersed flow but more like a froth flow. The prediction converges to the data as the equilibrium quality increases to a value of 10-30%.

3.6.2 Comparison of model with water data

The water data taken by Bennett is all high void dryout data. Figure 14 gives the resulting comparisons of this data with the dispersed flow model. The Heinemen vapor heat transfer coefficient was used for this set of comparisons. The predictions for these runs were very insenstive to the value of δ_{film} chosen. A range of 0.5×10^{-4} to 5×10^{-4} ft did not appreciable affect the results given in the figure. For $\delta_{film} = 4 \times 10^{-4}$ feet the

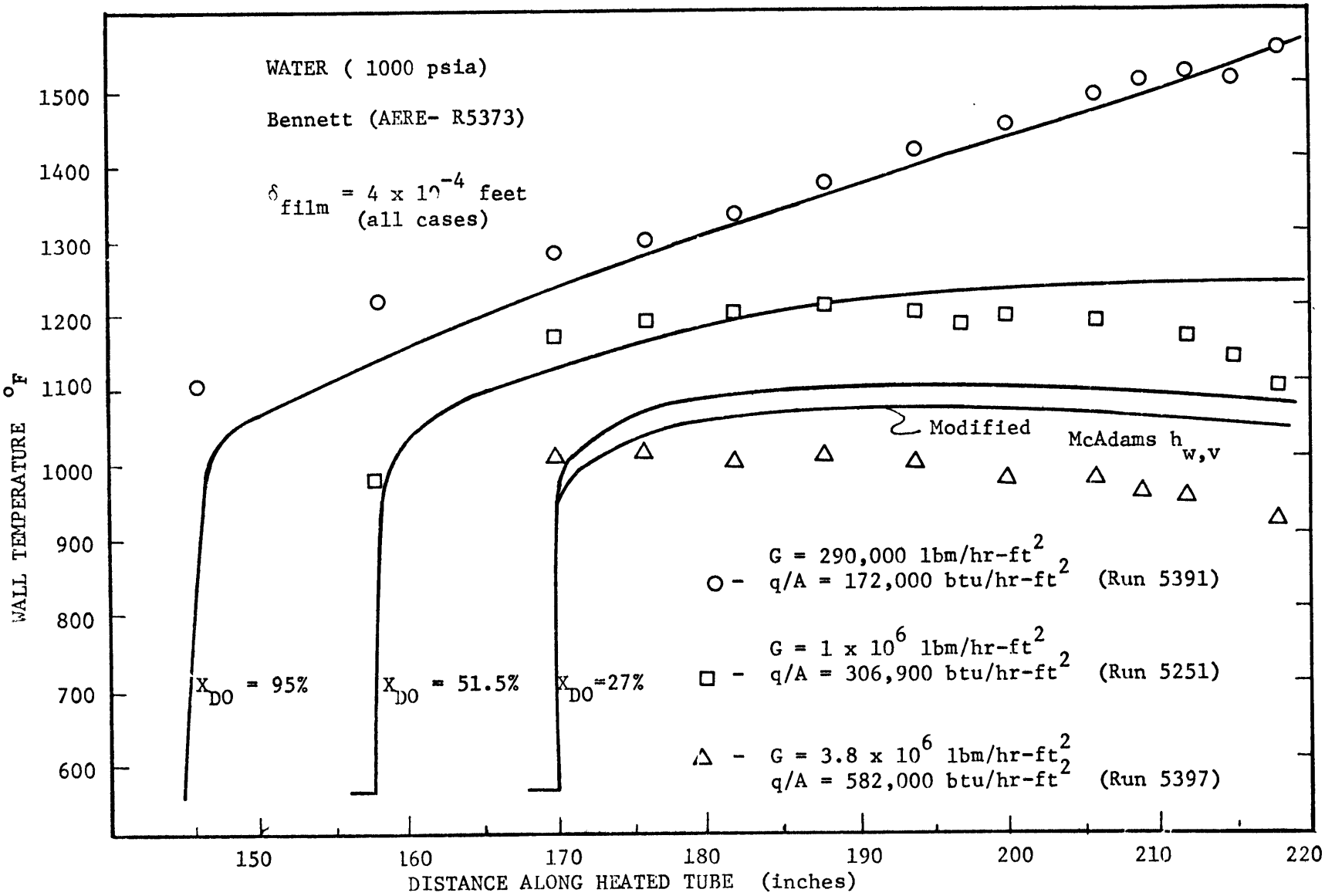

FIGURE 14 COMPARISON OF FILMBOIL WITH BENNETT'S STEADY STATE WATER DATA

two low mass flux runs (Runs 5359 and 5251) are predicted quite well, but there is a hundred degree overprediction in the case of the 3.8×10^6 lbm/hr-ft^2 run (Run 5397). As the void fraction is too high for δ_{film} to have much effect, the reason for the discrepancy must lie in the vapor heat transfer coefficient. A check on the range of variables used in the correlation revealed first that the property data used in the correlation was within 2% of the values used in this work.* This discounts one possible source of error. The Reynolds numbers encompassed in the correlating procedure were in the range of 20,000 - 370,000. However, the saturated vapor Reynolds number for Run 5397 is 3.5×10^6 or an order of magnitude higher than the maximum value correlated in the Heineman equation. It is possible that the discrepancy arises from extrapolating the correlation too far. Using the McAdams equation reduces somewhat the discrepancy between the prediction and data as shown in Figure 10 for the 3.8×10^6 lbm/hr-ft^2 case. The McAdams equation was found to underpredict the other two mass fluxes. Groeneveld compared a 3×10^6 lbm/hr-ft^2 mass flux run of Bennett's using an optimized vapor heat transfer

*See Appendix F for a listing of all property data used in this thesis. Included in Appendix F are polynomial curve fit equations for temperature dependence on the transport properties.

coefficient developed by Hadoller[24] with very good results. As the correlation is not published in the literature it could not be used here. This problem of uncertainties in the vapor heat transfer coefficient coupled with the fact that the data is in the high void region makes the choice of δ_{film} somewhat arbitrary for the case of water. This in some measure explains why Bennett did not use a direct wall to droplet term in his model.

3.6.3 Comparison of model with Freon 12 data.

The ability of the model to predict the Freon 12 data presented by Groeneveld is somewhat poorer than in the cases of the other two fluids as indicated in Figure 15. Using the modified McAdams equation and a $\delta_{film} = 1 \times 10^{-4}$ ft gives a fairly accurate prediction of the high quality-low mass flux case given by Run 8602.12, but this combination does not predict well at all the rapidly decreasing temperature - length profile exhibited after dryout for the low quality-high mass flux case given by Run 8620.14. Two values of δ_{film}, 2×10^{-4} and $.75 \times 10^{-4}$ ft, are presented to indicate the effect of its decrease on the resulting temperature profile. As is expected the decreasing of δ_{film} affects the first half of the profile much more than the second half due to the generally lower void fraction. Therefore, increasing δ_{film} to affect a better prediction of the experimental profile will only succeed in giving an in-

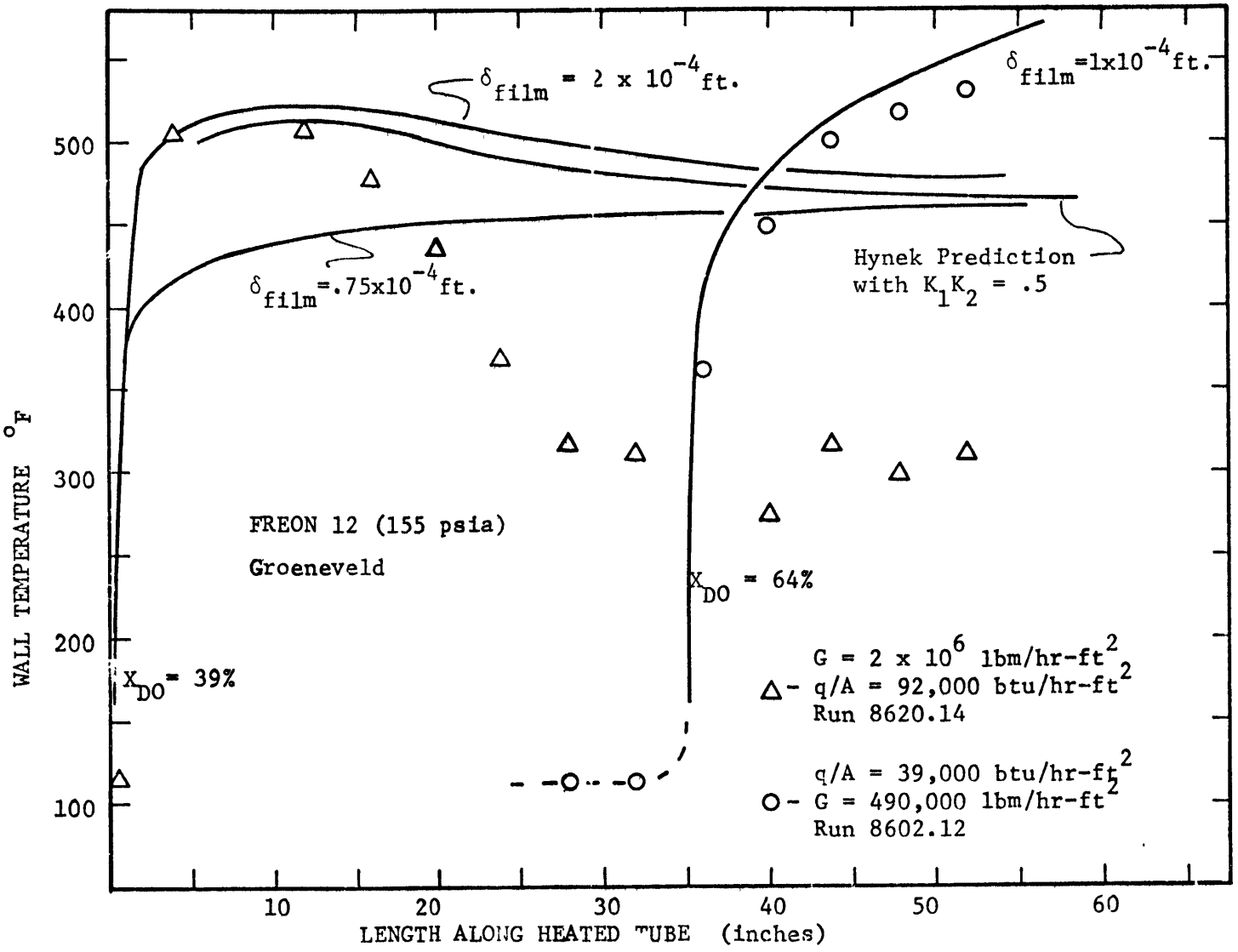

FIGURE 15 COMPARISON OF FILMBOIL WITH GROENEVELD'S STEADY STATE FREON 12 DATA

correct trend of increasing wall temperature with length. Groeneveld observed this same problem of trying to predict the Freon 12 profiles and postulated that the inaccuracy in the Freon 12 properties could be responsible as well as the use of a generalized correlation for the vapor heat transfer to Freon 12. Another possible explanation for the models' overprediction of the low quality run could be related to the oxide effects and increased wettability discussed in section 2.7.4. If in some manner the tube was made more wettable the low void runs such as Run 8620.14 would display a higher heat transfer than the model predicts where as the high void runs such as 8602.12 would not due to the liquid droplets being too small to approach the wall. DuPont bulletin B2 indicates that a one percent decomposition rate per year was found for Freon 12 when subjected to steel at 400°F. This figure resulted from exposures for a six day period where an initial higher rate of decomposition was disregarded. Groeneveld indicated that Freon 12 was susceptible to decomposition at temperatures above 600°F in the presence of moisture. This temperature was not reached in his experimental program. In a private communication Groeneveld indicated that the test section appeared clean after the experimental program was completed.

3.7 Discussion of Generalized Dispersed Flow Model

While the dispersed flow film boiling model adapted from the Hynek and Groeneveld models and used in this work appears not to greatly improve the accuracy of predicting post critical heat transfer, it is fundamentally more self consistant in its basic components than either of the parent models as previously discussed. Strictly speaking the model is valid only in the dispersed flow regime which is generally found at void fractions exceeding 80%. But by using the Hynek initialization method the froth regime encountered at void fractions above 10% can be transformed to a hypothetical dispersed flow regime whose initial drop sizes and velocities are given by the Hynek method. From the comparison with the nitrogen data which, as Forslund visually determined, was in the froth regime this extrapolation technique appears to work quite well. It is postulated, therefore, that the dispersed flow model can be used in any post critical flow regime with the accuracy increasing as the actual flow regime more closely resembles that of dispersed flow. There is a limiting mass flux, however, below which the model will not work, and that is the value necessary to give a sufficient vapor velocity to carry the liquid out the tube. This critical mass flux is derived in Appendix E assuming that the liquid fraction can be represented as droplets for any quality dryout. Using the Groeneveld wall-to-droplet term

allows for a more physical understanding of the correlating term, δ_{film}, than K_2K_2 used by Forslund to extrapolate Baumeister's theory for heat transfer to a drop sitting on a flat plate. While it is physically reasoned that the average height that the droplet population remains away from the heated surface is a function of the surface temperature, choosing an average value of 1×10^{-4} feet tends to predict the heat transfer data for the three fluids tested. δ_{film} is also capable to a certain extent of correcting for the errors associated with the vapor heat transfer coefficient by making up in the droplet term the underprediction of the vapor correlation. The modified McAdams equation for single phase vapor heat transfer gives reasonable results for the three fluids tests. It is felt that a greater degree of accuracy can be obtained by using a vapor correlation taylored for the particular fluid and operating conditions desired. The final variable which is very sensitive in the model is the position and quality of the dryout point. The technique of predicting post dryout wall temperatures used in this work is simplified because the dryout points were known in advance. (For zero quality dryouts a small positive value was used, and the calculation procedure was started there). For cases where the dryout point is not specified CHF correlations have to be relied on. This could introduce considerable uncertainties in the

predictions. The sensitivity on the quality variable is reduced for those dryout cases where the wall temperature profiles decrease after dryout with quality as is the case for low quality-high mass flux dryouts.

The general use of the dispersed flow film boiling code to predict the behavior of systems in post dryout is relatively combersome. The integration procedure is sensitive to the step size chosen. A small step size is needed just after dryout where the wall temperature profile is rapidly changing. This can subsequently be gradually increased to reduce computation costs. In the next chapter procedures are presented which reduce the dispersed flow film boiling model to an algebraic equation in terms of system variables which is capable of predicting post critical heat transfer equally well.

IV Generalized Post Critical Heat Transfer Correlation

4.1 Concept of Correlation

The complexitity of predicting the post critical heat transfer is a result of the departure from the equilibrium state after dryout. This nonequilibrium is manifested in the superheating of the vapor phase with the result that the mass fraction of vapor, termed in this work the actual quality, is always less than that value calculated by an equilibrium energy balance. The degree to which the vapor is superheated and the actual quality deviates from the equilibrium at any point downstream of the dryout for a particular fluid is related to the distance from dryout, the dryout quality, the mass flux and to some extent the heat flux as can be deduced from the analysis of the dispersed flow model presented in Chapter 3. Figure 16 reproduced from Forslund's thesis demonstrates quite well the nonequilibrium of post crtical heat transfer. The mass flux and equilibrium quality effects on the actual quality are indicated. As the mass flux increases the nonequilibrium at any distance from dryout decreases. This figure also indicates a small diameter effect on the nonequilibrium.

The premise of the post critical heat transfer prediction scheme presented in this chapter is that the thermal nonequilibrium in post dryout indicated by Figure 16 can be approximated

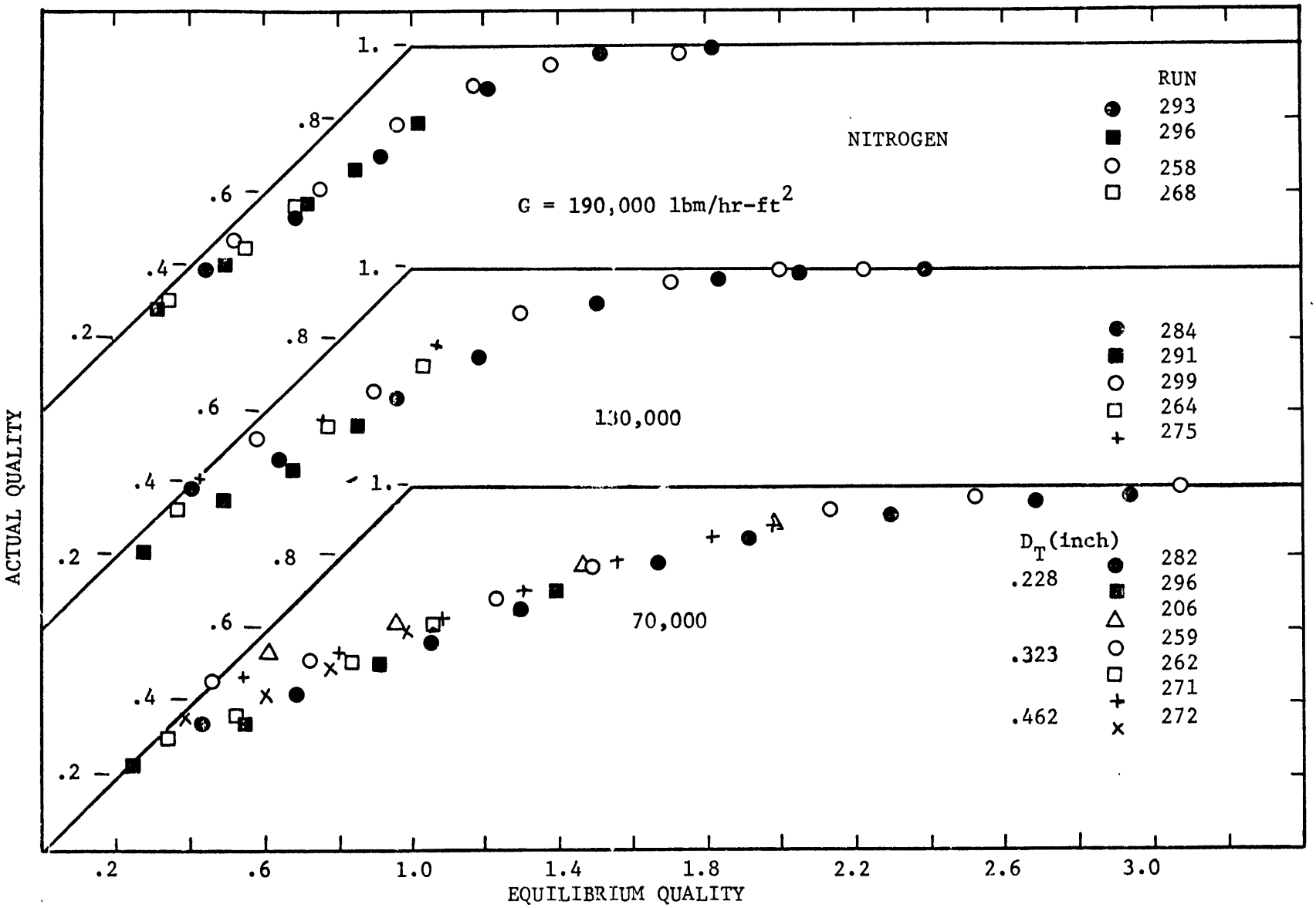

FIGURE 16 CALCULATED X_A VS X_E FOR NITROGEN AT SEVERAL MASS FLUXES (FROM FORSLUND REF. 5)

with the following linear relationship between X_A and X_E

$$(X_A - X_{DO}) = \kappa\ (X_E - X_{DO}) \qquad (4.1)$$

where κ is viewed as a correlating constant. A reexamination of the two-step dispersed flow model of Chapter 3 in light of Equation (4.1) resulted in the development of the generalized post critical heat transfer correlation.

The general form of the correlation is taken directly from the two step heat transfer process.

$$q/A = h_{w,v}\ (T_w - T_v) + h_{w,\delta}(T_w - T_{sat}) \qquad (4.2)$$

where $h_{w,v}$ as well as $h_{w,\delta}$ can be defined in terms of void fraction and actual quality to be

$$h_{w,v} = .023\ \frac{k_v}{D_T}\left(\frac{G\ X_A\ D_T}{\mu\alpha}\right)^{.8} Pr_v^{1/3}\left(\frac{\mu_v}{\mu_w}\right)^{.14}\left[1+.3\left(\frac{D_T}{L_{DO}+\ .01\ D_T}\right)^{.7}\right] \qquad (4.3)$$

and

$$h_{w,\delta} = \frac{k_{v,f}}{\delta_{film}}\ (1-\alpha)\ \exp\left[-\frac{2D_T}{L_{DO}}\right] \qquad (4.4)$$

The quantities needed to determine the heat flux in the post critical region are the vapor temperature, T_v, the void fraction, α, δ_{film} and κ as defined in equation (4.1). The following sections describe the formulations for T_v and α and the procedures for obtaining values of δ_{film} and κ to predict post critical heat transfer data. The resulting correlation procedure is compared with the transient

nitrogen data taken in this investigation as well as with steady state nitrogen data in the literature.

Procedures for obtaining a bounded solution for the heat transfer in post dryout are presented and a preliminary check of the correlating model is made with water and Freon 12.

4.2 Determination of Vapor Temperature in Post Dryout

With the approximation to the actual quality curve as given in equation (4.1) the vapor temperature can be obtained immediately upon writing the energy balance between the evaporating liquid and superheating vapor. This equation is simply

$$X_E h_{fg} = X_A[h_{fg} + C_{pv}(T_v - T_{sat})] \qquad (4.5)$$

Substituting equation (4.1) into (4.5) and rearranging gives the vapor temperature as

$$(T_v - T_{sat}) = \frac{h_{fg}(1 - \kappa)}{C_{pv}} \frac{X_E - X_{DO}}{X_{DO} + \kappa(X_E - X_{DO})} \qquad (4.6)$$

For liquid nitrogen, C_{pv} is not a function of T_v which allows one to obtain T_v directly in terms of X_E, X_{DO} and κ. For water at 1000 psia and to some extent Freon 12 at 155 psia C_{pv} is a function of T_v. This necessitates iterating equation (4.6) with C_{pv} vs T_v data.

4.3 Determination of Void Fraction After Dryout

The slip ratio and void fraction can be determined at dryout from Hynek's initialization procedure. Determining the void fraction, hence, the vapor velocity after dryout requires the simultaneous solution of the drop diameter gradient, equation (3.12), the droplet velocity gradient, equation (3.10), continuity equation, similar to equation (3.9) together with the droplet break up criterion, equations (3.15 and 3.16).

The drop diameter gradient can be integrated directly when equation (4.1) is differentiated and substituted into equation (3.12). The resulting drop diameter gradient becomes

$$d\delta = - \frac{\kappa \, \delta_{DO}^3 \, dX_E}{3(1-X_{DO})\delta^2} \tag{4.7}$$

Integrating (4.7) from $\delta = \delta_{DO}$ at $X_E = X_{DO}$ to $\delta = \delta'$ at $X_E = X_E'$ gives

$$\delta'^3 - \delta_{DO}^3 = - \kappa \delta_{DO}^3 \frac{(X_E' - X_{DO})}{(1 - X_{DO})} \tag{4.8}$$

rearranging (4.8) gives the drop diameter as a function of X_{DO}, X_E and κ to be

$$\delta = \delta_{DO} \left[1 - \frac{\kappa (X_E - X_{DO})}{(1 - X_{DO})} \right]^{1/3} \tag{4.9}$$

The droplet velocity gradient becomes

$$\frac{dv_\ell}{dz} = \frac{3C_D\rho_v(V_g - V_\ell)^2}{4V_\ell\rho_\ell\delta_{DO}} \left[1 - \frac{\kappa(X_E - X_{DO})}{(1 - X_{DO})}\right]^{-1/3} - \frac{g}{V_\ell}\left[1-\frac{\rho_v}{\rho_\ell}\right] \quad (4.10)$$

The vapor velocity can be eliminated using the continuity equation

$$V_g = \frac{G\ X_A}{\rho_v\left[1 - \frac{G(1-X_A)}{\rho_\ell V_\ell}\right]} \quad (4.11)$$

where X_A is given by equation (4.1). Equation (4.10) and (4.11) must be solved together with the critical Weber number criterion, equations (3.15) and (3.16), to obtain the values of liquid and vapor velocities necessary to determine the slip ratio and void fraction. The solution of these two quantities will be in terms of system variables and κ. The critical Weber number is utilized in the same manner as discussed in Section 3.4 for the updating of δ_{DO} and X_{DO} in equation (4.9) after each shatter. It is obvious from the fact that equation (4.10) is a non linear differential equation that a closed form solution cannot be directly obtained from this set of equations. An approximate closed form solution was obtained indirectly, however which represents quite accurately the void fraction after dryout.

The procedure consists of solving the above set of equations for V_g and V_ℓ on a digital computer using a Runge-Kutta integration scheme and applying a simple correlation technique to the resulting slip ratios in terms of the important variables. As V_g and V_ℓ are each functions of G, q/A, X_E, X_{DO} and κ, a parametric study of each of these variables was undertaken to ascertain their effect on the resulting slip ratio in post dryout. In the parametric study, G was varied from G_{crit} (defined in Appendix E) to 500,000 lbm/hr-ft^2. X_{DO} was varied from 5% to 50%. κ was varied from 1.0 to 0.2. X_E is the dependent variable. Figures 17 and 18 give the results for nitrogen for $\kappa = 1.0$ and $\kappa = 0.5$ respectively. The slip ratio varies in a rather simple predictable manner. It starts at the dryout slip, S_{DO} (determined from Hynek's procedure given G, X_{DO} and q/A at the dryout point), and decreases as X_E increases until $S = 1$ at $X_A = 1$ (the point where $\kappa(X_E - X_{DO})$. A simple equation of the form

$$\left(\frac{1-S}{1-S_{DO}}\right) = \left[1 - \frac{\kappa(X_E - X_{DO})}{(1 - X_{DO})}\right]^D \qquad (4.12)$$

gives the observed trends for the slip ratio. The variables, G and q/A are hidden in the determination of S_{DO}. As S does not physically remain at S_{DO} for all values of X_E where $\kappa = 0$ as equation (4.12) indicates, D must be an inverse

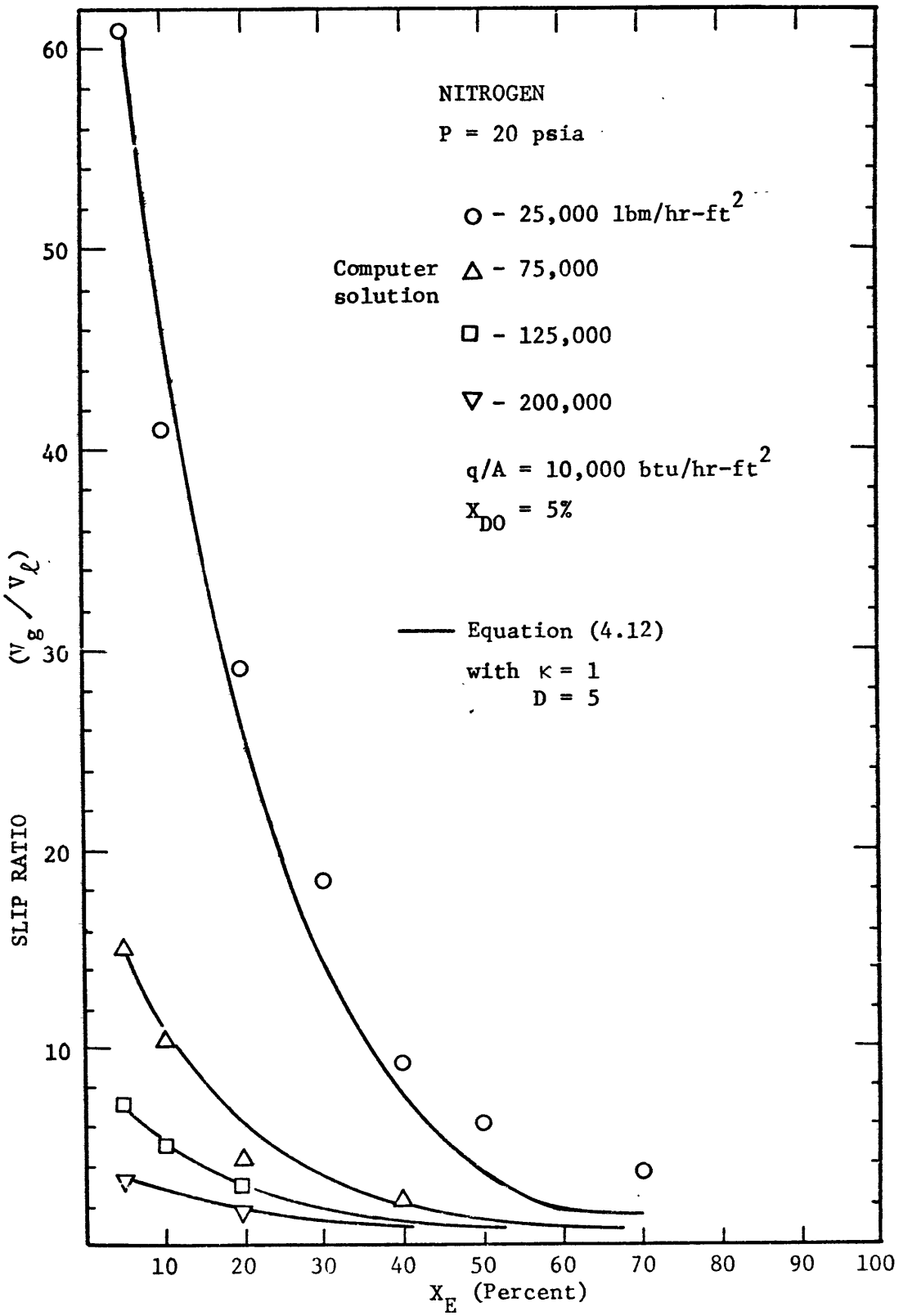

FIGURE 17 COMPARISON OF COMPUTER GENERATED SLIP RATIOS WITH SLIP CORRELATION (EQN. 4.12)... $\kappa = 1$

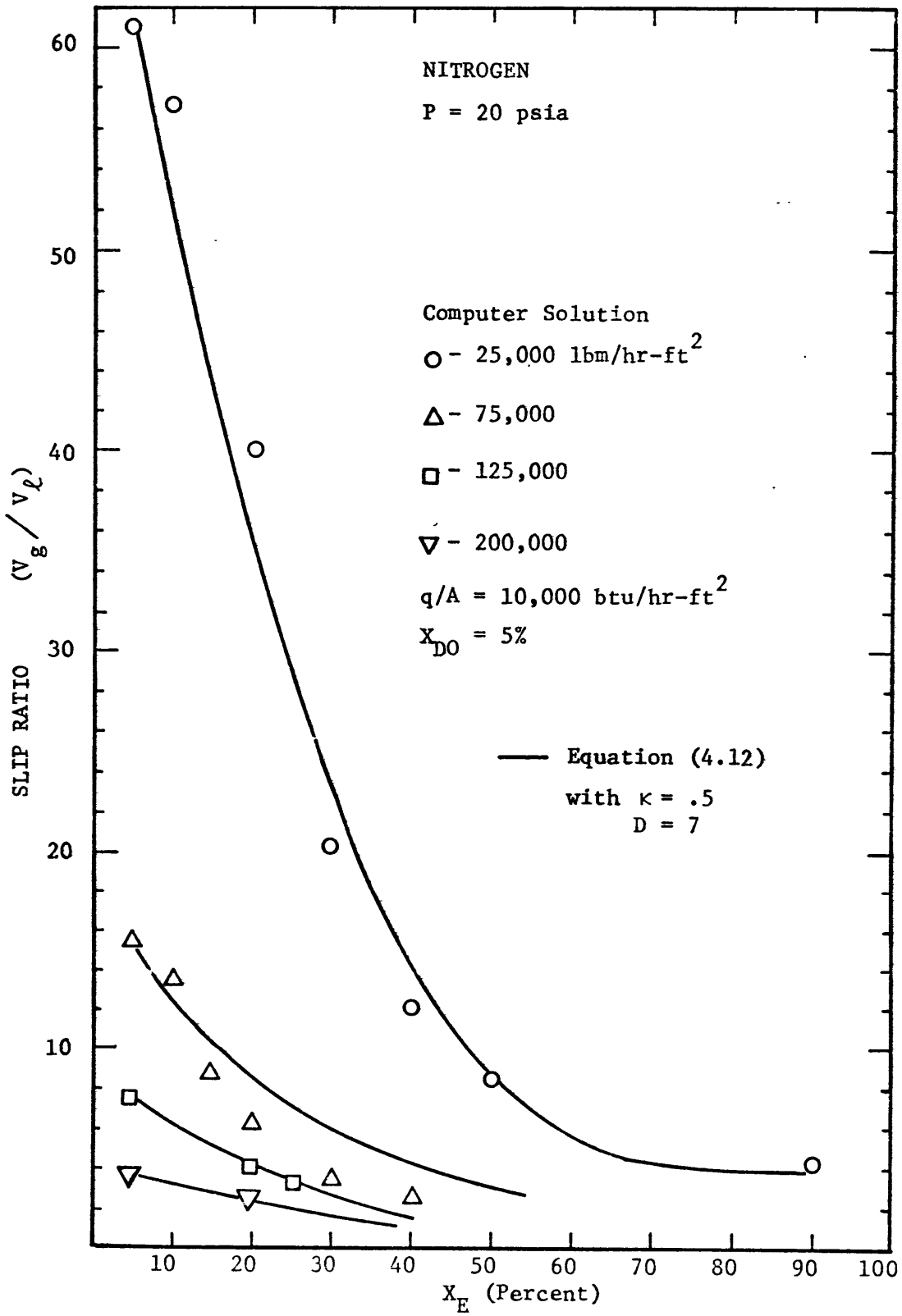

FIGURE 18 COMPARISON OF COMPUTER GENERATED SLIP RATIOS WITH SLIP CORRELATION (EQN. 4.12)... $\kappa = .5$

function of κ so that D will increase as κ decreases to the point where $D = \infty$ at $\kappa = 0$. Equation (4.12) is plotted on Figure 17 using a value of D = 5 and predicts reasonably well the four mass fluxes given. A value of D = 7 gives a reasonable result for the case of $\kappa = .5$ given in Figure 18. This indicates that whatever G effect there might be on D is quite small and restricted to only the lowest values of G. If one then proceeds to correlate S vs X_E at the lowest value of S_{DO} for a given κ the resulting correlation will of necessity improve as G or X_{DO}, hence S_{DO}, increases.

Considering now that D is only a function of κ a series of curves similar to those presented in Figures 17 and 18 were developed for nitrogen, Freon 12 and water. The resulting values of D vs κ for each of the three fluids are tabulated in Table 2. Also given in Table 2 are the coefficients to the equation

$$D = \frac{A}{\kappa^B} \tag{4.13}$$

which gives the correct functional dependence of κ on D. For the case of nitrogen D must equal 5 when $\kappa = 1.0$, and D must approach infinity when κ approaches 0 . Equation (4.13) will give this dependence.

The void fraction in post dryout can now be obtained from the definition of void fraction. Substituting in (4.12)

Fluid	κ	D	A	B
Nitrogen				
	1.0	5.0		
	.5	7.0		
	.2	10.0		
	0.0	∞		
			5.0	.486
Water				
	1.0	2.5		
	.5	3.0		
	.2	4.0		
	0.0	∞		
			2.5	.264
Freon 12				
	1.0	1.0		
	.5	1.3		
	.2	1.9		
	0.0	∞		
			1.0	.37

Tabulation of κ vs D for Correlating
Post Dryout Slip Ratios

TABLE 2

and (4.13) the resulting void fraction becomes

$$\alpha = \frac{X_A}{X_A + \frac{\rho_v}{\rho_\ell}\{1 - (1-S_{DO})[\frac{(1 - X_A)}{1 - X_{DO}}]^{A/\kappa}\}^B (1-X_A)} \quad (4.14)$$

where X_A is determined from (4.1) and the values for A and B obtained from Table 1 for one of the three fluids correlated.

Figure 19 compares (4.14) against the computer solution of the void fraction for nitrogen, water, and Freon 12 at the conditions G = 250,000 lbm/hr-ft^2 and X_{DO} = 5% with κ = 0.5. The temperatures dependence of the vapor density was included using equation (4.5) to determine T_v as a function of X_E and κ. As can be seen in Figure 19 the approximate closed form solution given by equation (4.14) is a very good representation of the computer solution for void fraction. The discrepancies associated with the approximate slip correlation are not wholly transferred to the void fraction equation. No effort will be made to quantify the errors associated with the use of (4.14) as indeed one does not know really how well the differential equations predict the behavior of an actual system. It is observed though that the approximate solution satisfies the end points of $X_A = X_{DO}$ and $X_A = 1$ and gives a reasonable reproduction of the exact solution of the differential

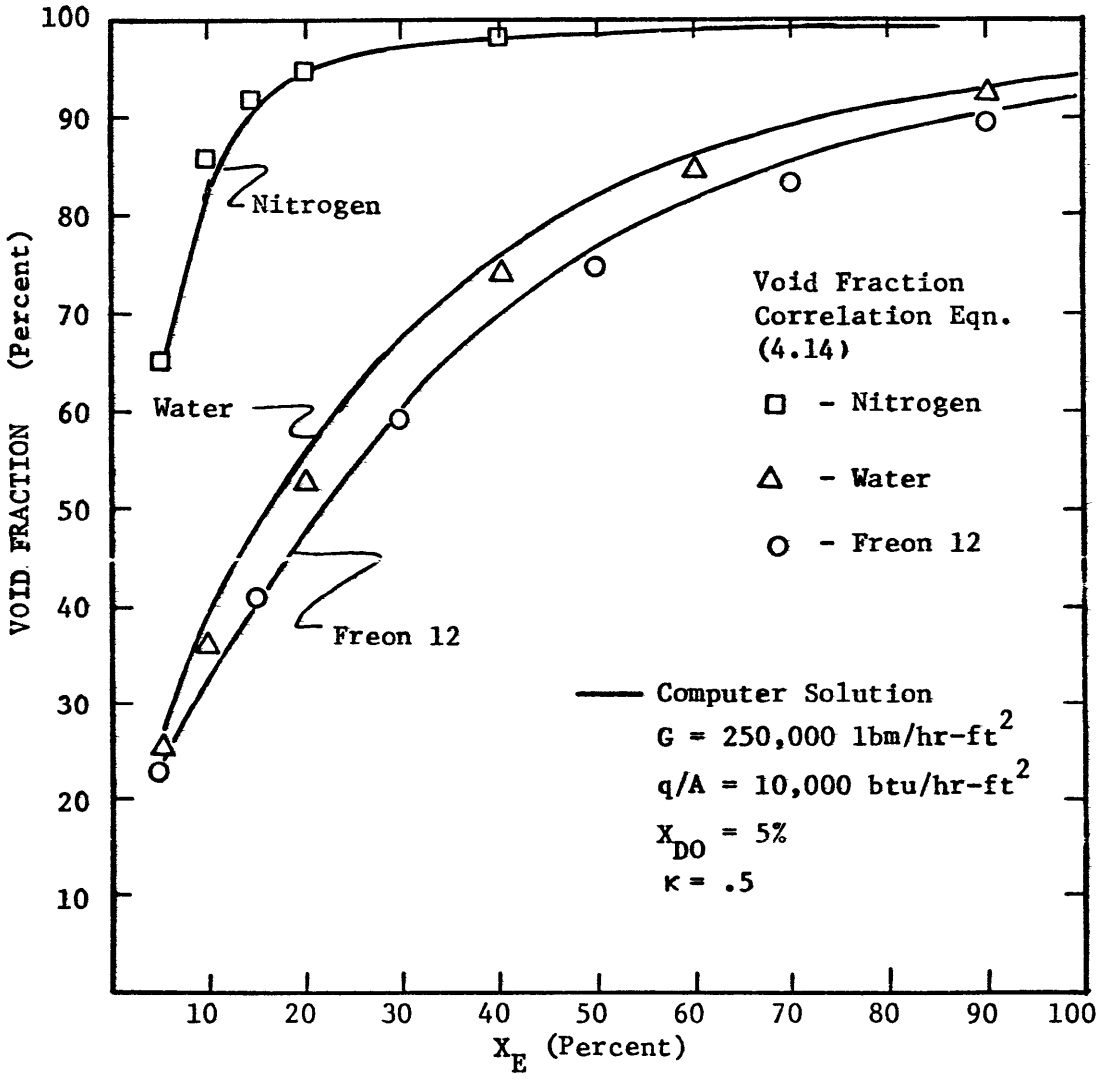

FIGURE 19 COMPARISON OF CORRELATED VOID FRACTION IN POST DRYOUT FOR SEVERAL FLUIDS AGAINST COMPUTER SOLUTION OF GOVERNING EQUATIONS

equations describing the phenomenon. The accuracy of reproduction is increased as the void fraction increases to a point where the approximate calculation nearly equals the computer solution at void fractions above 50%.

4.4 Correlation of Post Critical Heat Transfer For Nitrogen

Substituting, now, equations (4.6) and (4.14) back into equation (4.2) gives the basic framework for the post critical heat transfer correlation in terms of two as yet unspecified constants, δ_{film} and κ. The resulting substitution gives

$$q/A = .023 \frac{k_v}{D_T} \left(\frac{GX_A D_T}{\mu\alpha}\right)_v^{.8} Pr_v^{1/3} \left(\frac{\mu_v}{\mu_w}\right)^{.14} \cdot$$

$$\left[1 + .3\left(\frac{D_T}{L_{DO} + .01D_T}\right)^{.7}\right] \left[(T_w - T_{sat}) - \frac{h_{fg}(1-\kappa)(X_E - X_{DO})}{C_{\rho v} X_A}\right]$$

(4.15)

$$+ \frac{k_{v,f}(1-\alpha)}{\delta_{film}} \exp\left[-\frac{2D_T}{L_{DO}}\right] (T_w - T_{sat})$$

where $$\alpha = \frac{X_A}{X_Z + \frac{\rho_v}{\rho_\ell}\left\{1-(1-S_{DO})\left[\frac{(1-X_A)}{(1-X_{DO})}\right]^{5/\kappa .486}\right\}(1-X_A)}$$

$$X_A = X_{DO} + \kappa (X_E - X_{DO})$$

S_{DO}.....Iteration of equations (3.8) and (3.9)

[Subroutine DOCAL]

The general form of the post critical heat transfer equation is

$$q/A = f(X_E, X_{DO}, L_{DO}, G, \Delta T_{sat}, \delta_{film}, \kappa) \qquad (4.16)$$

The dryout length, L_{DO}, is calculated by

$$L_{DO} = \frac{Gh_{fg}D_T}{4} \int_{X_{DO}}^{X_E} \frac{dX'_E}{q/A} \qquad (4.17)$$

where q/A is the heat flux distribution between X_{DO} and X_E. For uniformly heated tubes L_{DO} is not an independent variable since it is calculated from q/A, X_{DO}, X_E, and G. For the test section used here L_{DO} is an independent variable being determined by the heat flux in the preheater.

The determination of the two correlating parameters, δ_{film} and κ, in equation (4.18) is achieved in the following manner. First the value of κ is selected via a technique to be described next. Anticipating the value of κ, δ_{film} will be determined from comparisons of equation (4.18) with transient nitrogen data. Although δ_{film} has been optimally determined in Chapter 3 such that the differential dispersed flow model affects the best

prediction of the temperature-length data, it is expected that a different value of δ_{film} will be necessary for the post critical heat transfer correlation to correct, somewhat, the errors involved in assuming a linear variation of X_A vs X_E .

4.4.1 Evaluation of κ

To determine κ the X_A vs X_E curve must be known. As physical measurements are cumbersome and involves a large amount of data scatter (see Forslund[5]) alternative methods are required. There are two methods available. First a good estimation of the actual quality can be obtained from post critical heat transfer data by assuming that all heat is transferred by the vapor. This assumption together with the energy balance for obtaining the vapor temperature provide the two following equations for obtaining X_A vs X_E given q/A and T_w.

$$q/A = .023 \frac{k_v}{D_T} \left(\frac{GX_A D_T}{\mu\alpha}\right)_v^{.8} Pr_v^{1/3} (T_w - T_v) \tag{4.18}$$

$$\text{where} \quad \alpha = \frac{X_A}{X_A + \frac{\rho_v}{\rho_\ell} S(1 - X_A)} \tag{4.19}$$

$$X_E\, h_{fg} = X_A [h_{fg} + C_{\rho v}(T_v - T_{sat})]$$

As a first approximation the slip, S, in equation (4.19)

can be obtained from the homogeneous model (i.e. S=1). A more exact method would be to use equations (4.13) and (4.14) for the cases where the correlating constants have been determined.

Figure 16 presents the results Forslund obtained from his data upon applications of equations (4.18) and (4.19). A second method which was used extensively in this investigation consists of generating X_A vs X_E curves from the two step model using FILMBOIL. Using FILMBOIL to generate the X_A vs X_E curve is especially helpful to predict κ for cases where no physical data is as yet available (i.e. water and Freon 12 data at low mass fluxes and qualities).

With the X_A vs X_E curve in hand the value of κ is obtained by visually obtaining the best fit of the curve. This requires some explanation as we have to be consistant in the evaluation procedure if some quantification of variables affecting κ is to be expected. In essence what we are trying to do is fit a straight line to a curve. Of necessity this approximation has a limited range of accuracy. In this investigation κ was evaluated such that equation (4.1) approximated X_A over the largest possible range of X_E without introducting significant error in X_A. The general evaluation criterion used was that κ be decreased from 1 to a value that caused X_A calculated from equation

(4.1) to differ from the generated X_A vs X_E curve by .02 to .03 in a range to the left of the intersection of equation (4.1) with the calculated X_A curve. A sample of this graphical evaluation technique is given in Figure 20 where κ is evaluated from an X_A vs X_E curve generated from FILMBOIL for Nitrogen at G = 70,000 lbm/hr-ft^2 and X_{DO} = 5%. The intersection point and maximum allowable deviation point are clearly indicated. For this case the approximate solution starts to deviate significantly at an $(X_E - X_{DO})$ of 100%.

Before going further into the evaluation procedure, a general idea of what influences κ is necessary in order to localize the evaluation and eventual correlation procedures to the relevant variables. As κ is in essence a measure of the nonequilibrium of the flow in post dryout, whatever tends to affect the degree of non equilibrium will have an affect on κ. Returning again to Figure 16 one can obtain considerable insight into the variables that affect κ. G is definitely a strong variable on κ. A value of κ = .55 in equation (4.1) appears to predict X_A for most of the range of X_E for G = 70,000 lbm/hr-ft^2 whereas a value of κ = .71 predicts the case G = 190,000 lbm/hr-ft^2. Figure 16 also indicates that heat flux and tube diameter have a negligible effect on the nonequilibrium. The next and last variable considered to affect κ is the

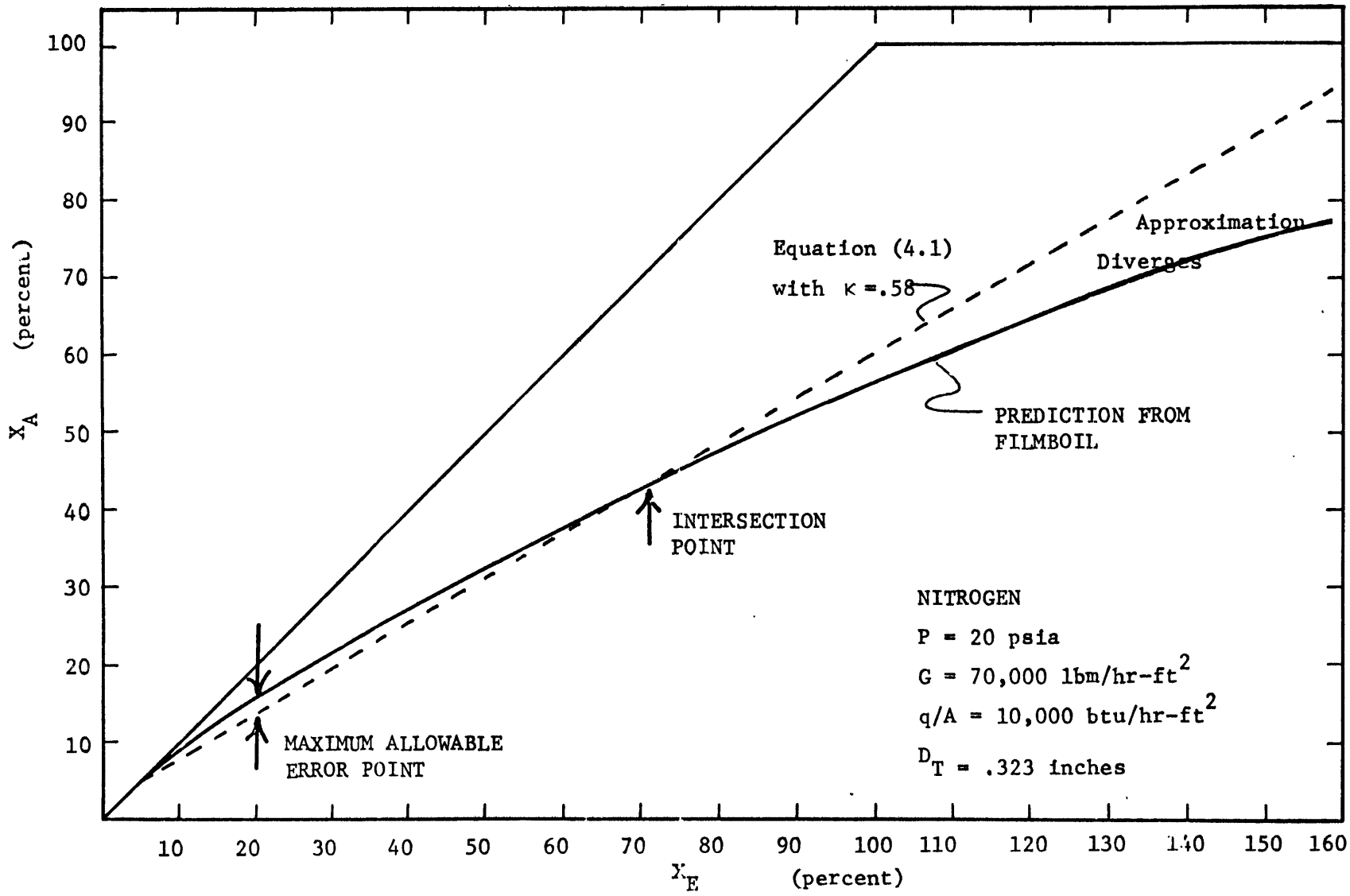

FIGURE 20 BEST FIT PROCESS FOR THE DETERMINATION OF κ

dryout quality. This variable can be rationalized from the observation that at progressively higher dryout quantities there is less liquid to evaporate and cool the vapor. Because the vapor superheats faster the amount of non equilibrium increases proportionately. Figure 21 graphically depicts this variable affect. It consists of X_A vs X_E curves calculated from Filmboil for water at $G = 250{,}000$ lbm/hr-ft^2 at two values of dryout quality $X_{DO} = 20\%$ and $X_{DO} = 80\%$. The straight line approximation is also plotted for each of the two X_A vs X_E curves. $\kappa = .62$ closely approximate the $X_{DO} = 20\%$ case and $\kappa = .7$ for the $X_{DO} = 80\%$ case. This indicates almost a linear relationship between κ and the quantity $(1-X_{DO})$. As X_{DO} increases κ decreases. Graphically this relationship results because all X_A vs X_E curves with X_{DO} greater than zero will eventually merge with the X_A vs X_E curve for $X_{DO} = 0$. In order to do this the slope of the linear approximation to the curves with higher dryout qualities must decrease. Including X_{DO} as a parameter in some measure includes the q/A affect which is not explicitly a variable.

With these two variables, G and $(1-X_{DO})$, an extensive investigation was carried out to determine the best fit value of κ for nitrogen using computer generated curves of X_A vs X_E and the evaluation technique just described.

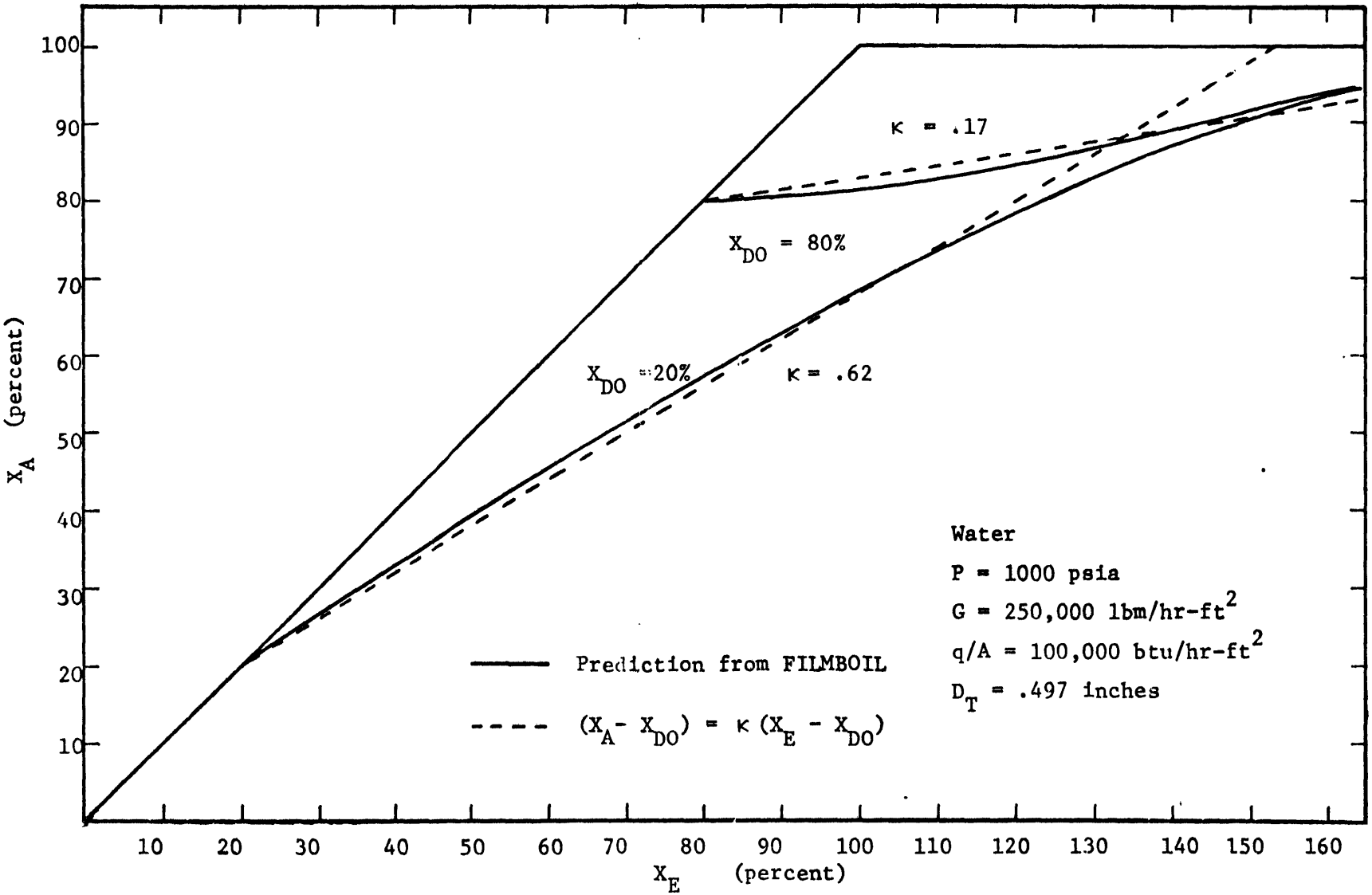

FIGURE 21 DEMONSTRATION OF DRYOUT QUALITY EFFECT ON κ

Included, also, in this investigation were evaluations of κ vs G and $(1-X_{DO})$ for water and Freon 12. The results of this investigation are tabulated in Table 3.

As a tabulation is not the most effective way of using the results as well as anticipating a quantitative need of κ for the final nitrogen correlation an attempt was made to develop a generalized curve for the best fit value of κ in terms of a nondimensionalized form of the two independant parameters, G and X_{DO} based on the three fluids investigated. The following nondimensional equation was selected to represent the variation of κ with X_{DO} and G

$$\kappa = f\left(\left(\frac{G^2 D_T}{\rho_v T}\right)^m (1-X_{DO})^n\right) \qquad (4.20)$$

The nondimensional form of G was developed from the Weber number assuming the velocity difference could be estimated by G/ρ_v. This Weber number formation was initially chosen to account for the fact that small droplets reduce the nonequilibrium. However, the drop diameter vs length curve in post dryout was shown by Forslund to be relatively unaffected by G whereas increasing q/A significantly shifts the curve downward. The reason G decreases nonequilibrium whereas q/A does not is that for a given drop size a higher G results in a larger number of drops per unit volume which increases the cooling area seen by the vapor.

Fluid	D_T (feet)	$G \times 10^{-6}$ (lbm/hr-ft^2)	X_{DO}	κ	$\Pi^\dagger$
Freon 12	.02558	1.5	.02	.7	255.9
Freon 12	.02558	.485	.02	.59	82.7
Freon 12	.02558	.2	.02	.56	34.1
Freon 12	.02558	1.5	.25	.59	67.2
Freon 12	.02558	1.5	.50	.39	8.8
Freon 12	.02558	.485	.10	.57	54.1
Freon 12	.02558	.485	.30	.43	15.4
Freon 12	.02558	.485	.65	.14	0.5
Water	.0414	1.0	.02	.75	172.1
Water	.0414	.490	.02	.72	84.3
Water	.0205	.20	.02	.63	
Water	.0414	1.0	.10	.74	112.4
Water	.0414	1.0	.30	.64	32.0
Water	.0414	1.0	.55	.45	3.5
Water	.0414	.74	.64	.40	0.9
Water	.0414	.49	.10	.67	55.1
Water	.0414	.49	.40	.51	7.3
Water	.0414	.485	.75	.36	0.1
Water	.0414	.490	.79	.20	0.05
Nitrogen	.027	.70	.02	.77	348.2
Nitrogen	.0333	.214	.02	.71	118.3
Nitrogen	.019	.190	.02	.71	79.3
Nitrogen	.027	.130	.02	.62	64.7
Nitrogen	.0333	.123	.02	.62	67.9
Nitrogen	.027	.070	.02	.58	34.8
Nitrogen	.0333	.030	.02	.50	16.6
Nitrogen	.027	.070	.30	.36	6.6
Nitrogen	.027	.070	.60	.22	0.4
Nitrogen	.0333	.033	.78	.10	0.05

Tabulation of Best Fit Value of κ

TABLE 3

$^\dagger \Pi = G\sqrt{D_T/\rho_v\sigma}\,(1 - X_{DO})^5$

This discussion indicates that the parameter chosen to nondimensionalize G has really no physical significance. The parameter was retained however for lack of a reasonable alternative*. The resulting plot of κ vs

$$K \text{ vs } G\sqrt{D_T/\rho_v \sigma}(1-X_{DO})^5$$

is given in Figure 22. Values of m = 1/2 and n = 5 were chosen to reduce the observed banding of the points as much as possible. The larger dependance of $(1-X_{DO})$ on κ relative to G is reasonable in light of discussion in Section 4.5. A distinction is made for those points whose dryout quality is less than 10% as those points will be unaffected by the power on the $(1 - X_{DO})$ term. In fact looking at these points will give a good idea of how well the Weber number formulation for G correlates the three fluids. There appears to be significant deviations between points for different fluids above and beyond that expected to be obtained from the subjective evaluations of κ even though there is a definite trend with little data scatter for each individual fluids. This becomes more obvious when one takes into account all the data for each fluid. The best fit values of κ for water fall on one line which

* A Reynolds number formulation was discarded because D_T would be given equal weight as G where in fact it has little affect on κ.

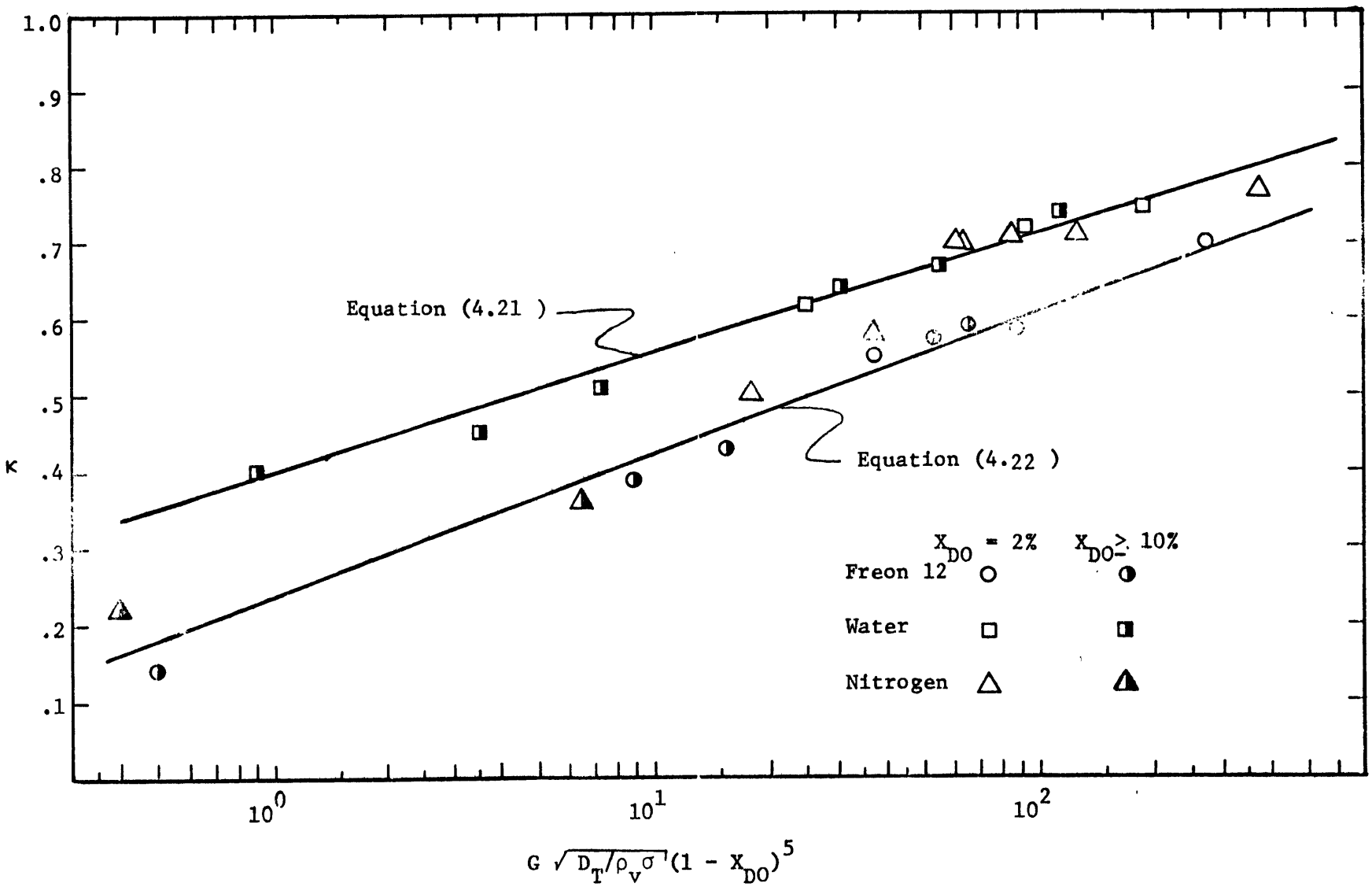

FIGURE 22 CORRELATION OF BEST FIT VALUE OF κ VS $G\sqrt{D_T/\rho_v\sigma}(1 - X_{DO})^5$

is significantly above the data for the other two fluids. Freon 12 data falls on another line with Nitrogen data dividing itself among the two lines. At high G and low X_{DO} the best fit values of κ for nitrogen fall on the water line and at low G and high X_{DO} the data falls on the Freon 12 line. To facilitate the evaluation of κ two equations were developed for these lines.

$$\kappa_{\text{Water}} = .0674 \log_e \left[G\sqrt{\frac{D_T}{\rho_v \sigma}}(1-X_{DO})^5\right] + .402 \qquad (4.21)$$

$$\kappa_{\text{Freon 12}} = .0811 \log_e \left[G\sqrt{\frac{D_T}{\rho_v \sigma}}(1-X_{DO})^5\right] + .236 \qquad (4.22)$$

Equation (4.21) can be used to predict the best fit value for water and equation (4.22) for Freon 12. It is recommended that one use Figure 22 to determine the best fit value of κ for liquid nitrogen. For the actual data comparison of nitrogen data with equation (4.15) to determine the correlating constant, δ_{film} as presented next the data for κ in Table 3 is used.

4.4.2 Determination of δ_{film} from Transient and Steady State Nitrogen Data.

With the generated table of κ vs G and $(1-X_{DO})$ for nitrogen an extensive comparison of the transient nitrogen data obtained in this investigation was undertaken. The

transient data of particular interest is that obtained in Runs 94-100 where the preheater tube was in the dry mode. The data for these runs will therefore have a considerable superheat effect. Figures 23-29 present the results of the evaluation procedure of δ_{film} for these particular data runs. These figures present data for two mass fluxes, G = 215,000 and 130,000 lbm/hr-ft^2 and a range of qualities for each mass flux. In all cases $\delta_{film} = 4x10^{-4}$ft predicts the data extraordinarily well. A value of $\delta_{film} = 1x10^{-4}$ ft as obtained for the differential two steps model in the post critical heat transfer correlation gave too high a prediction for the transient data . It is extremely difficult to explain this discrepancy of δ_{film} between the two models as there are so many competing effects that are influenced by the approximation procedure used in the post critical heat transfer correlation. A cursary check of the approximation procedure embodied in equation (4.1) on the main variables affecting the total heat transfer (T_v, X_A, α) indicated that in applying the approximation to the differential two step model a smaller value of δ_{film} (i.e. a larger wall-to-drop heat flux) would be needed instead of the observed higher value. All computer codes used in the application of the equations for both models were scrupulously checked and found free of errors. The author concludes that an involved analysis of

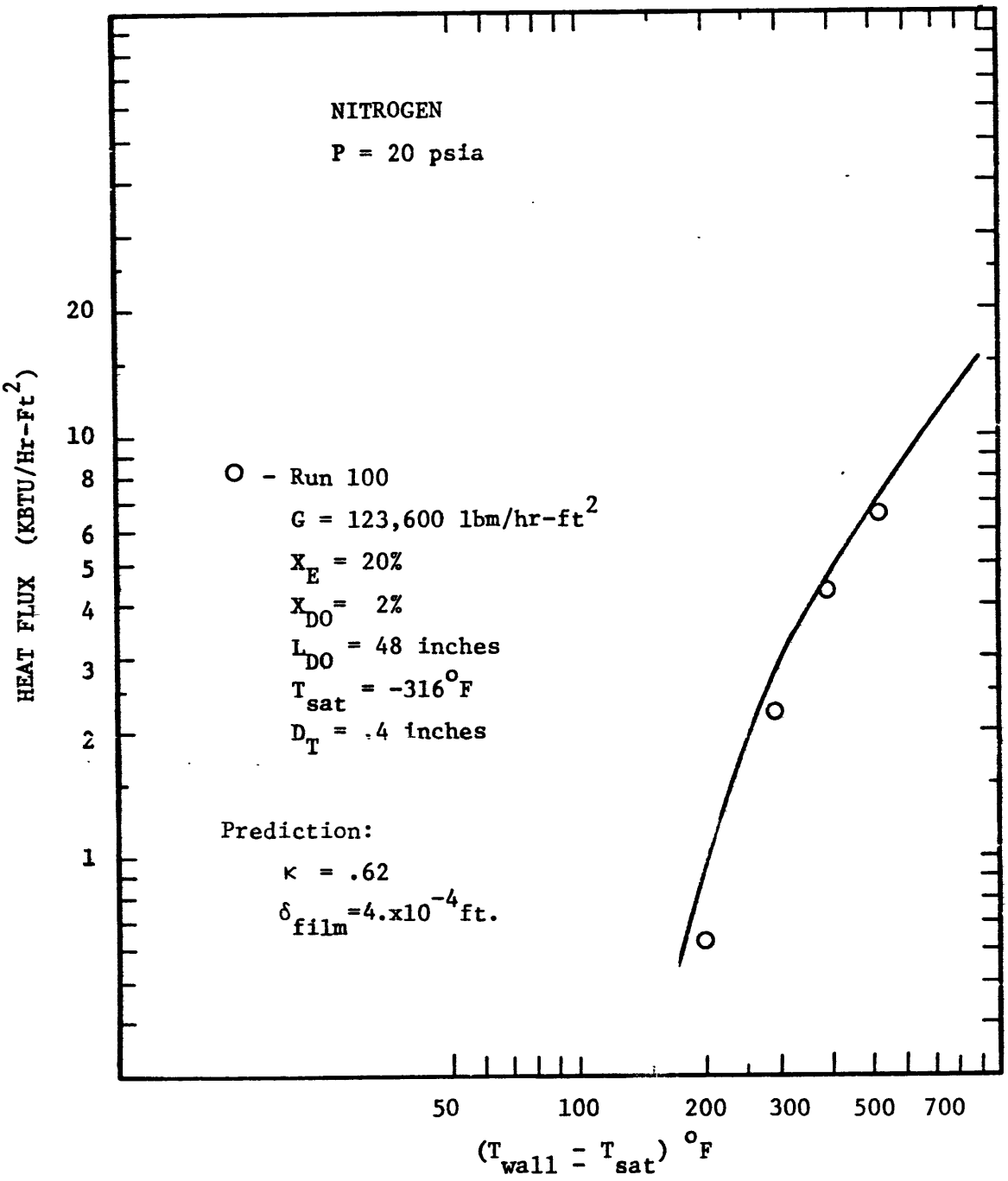

FIGURE 23 COMPARISON OF POST CRITICAL HEAT TRANSFER CORRELATION WITH TRANSIENT NITROGEN DATA - LONG DRYOUT LENGTH

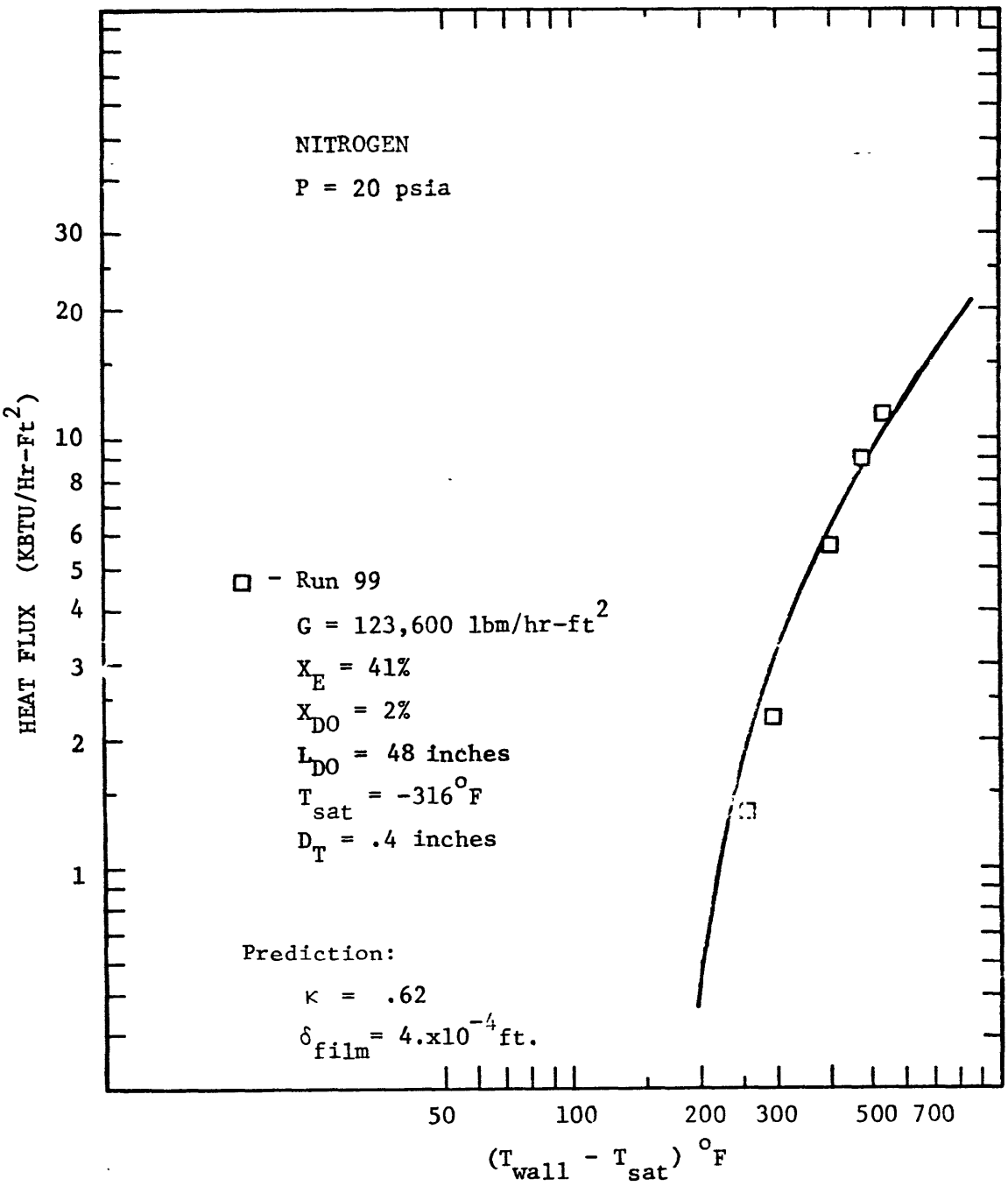

FIGURE 24 COMPARISON OF POST CRITICAL HEAT TRANSFER CORRELATION WITH TRANSIENT NITROGEN DATA - LONG DRYOUT LENGTH

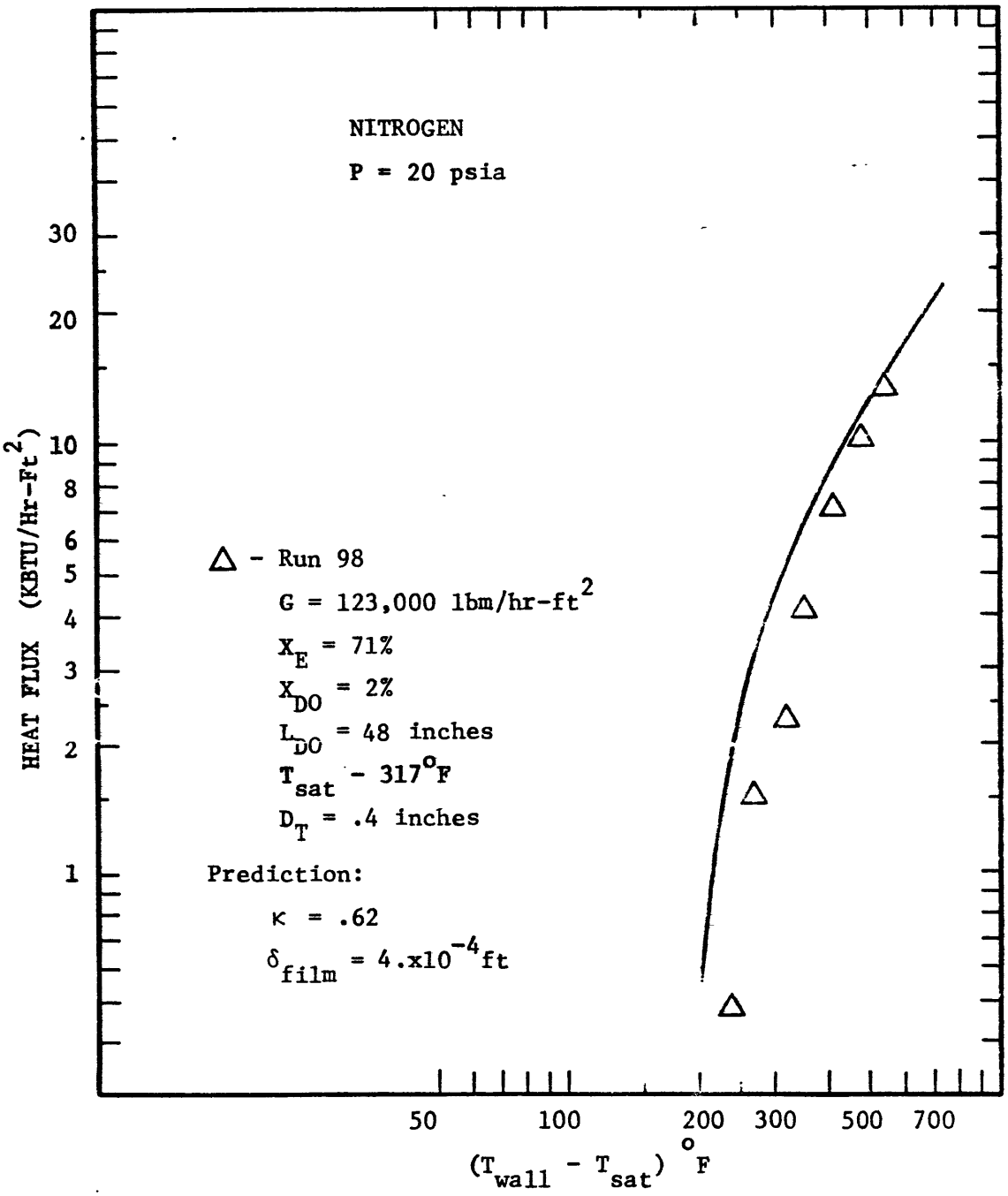

FIGURE 25 COMPARISON OF POST CRITICAL HEAT TRANSFER CORRELATION WITH TRANSIENT NITROGEN DATA - LONG DRYOUT LENGTH

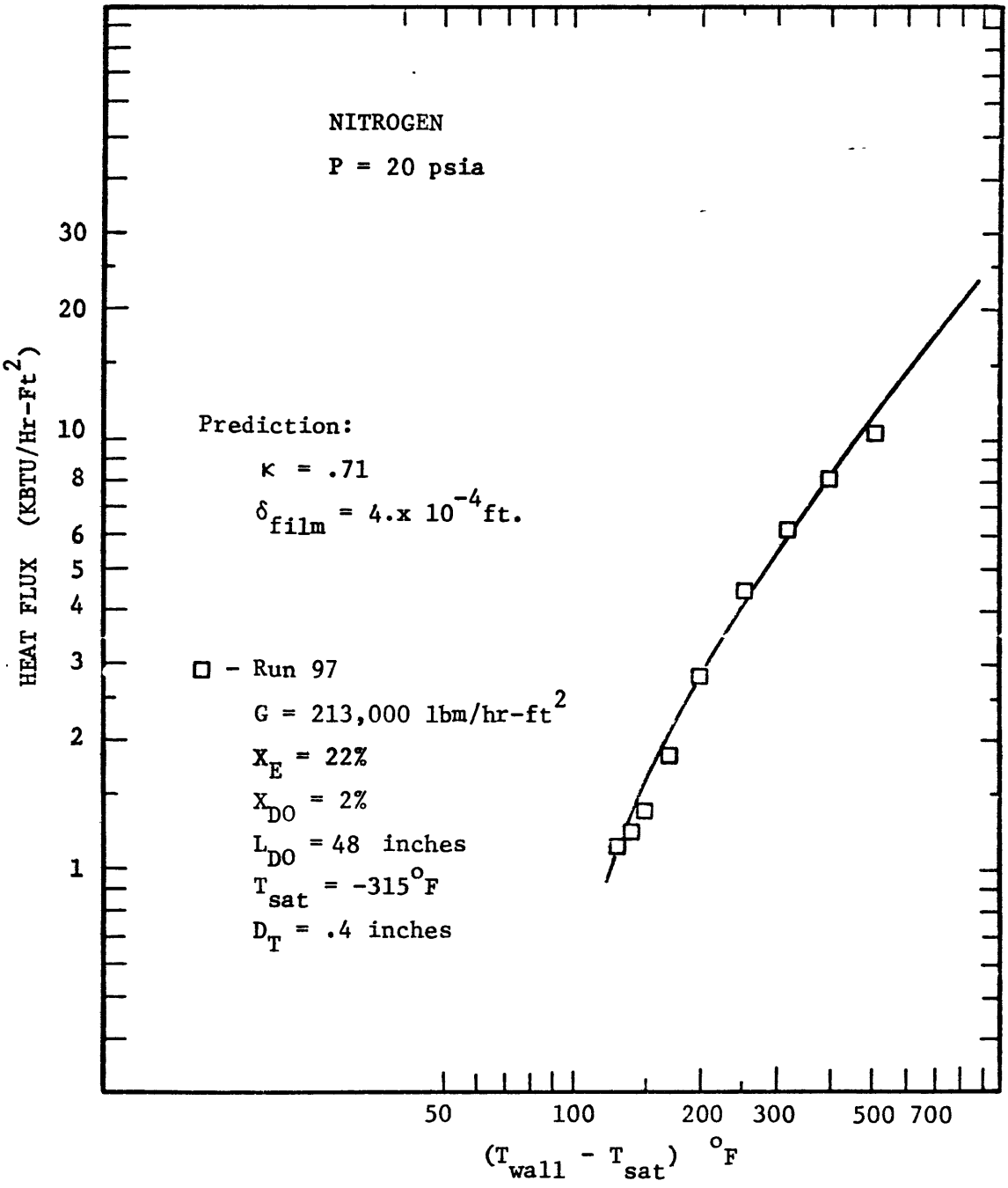

FIGURE 26 COMPARISON OF POST CRITICAL HEAT TRANSFER CORRELATION WITH TRANSIENT NITROGEN DATA - LONG DRYOUT LENGTH

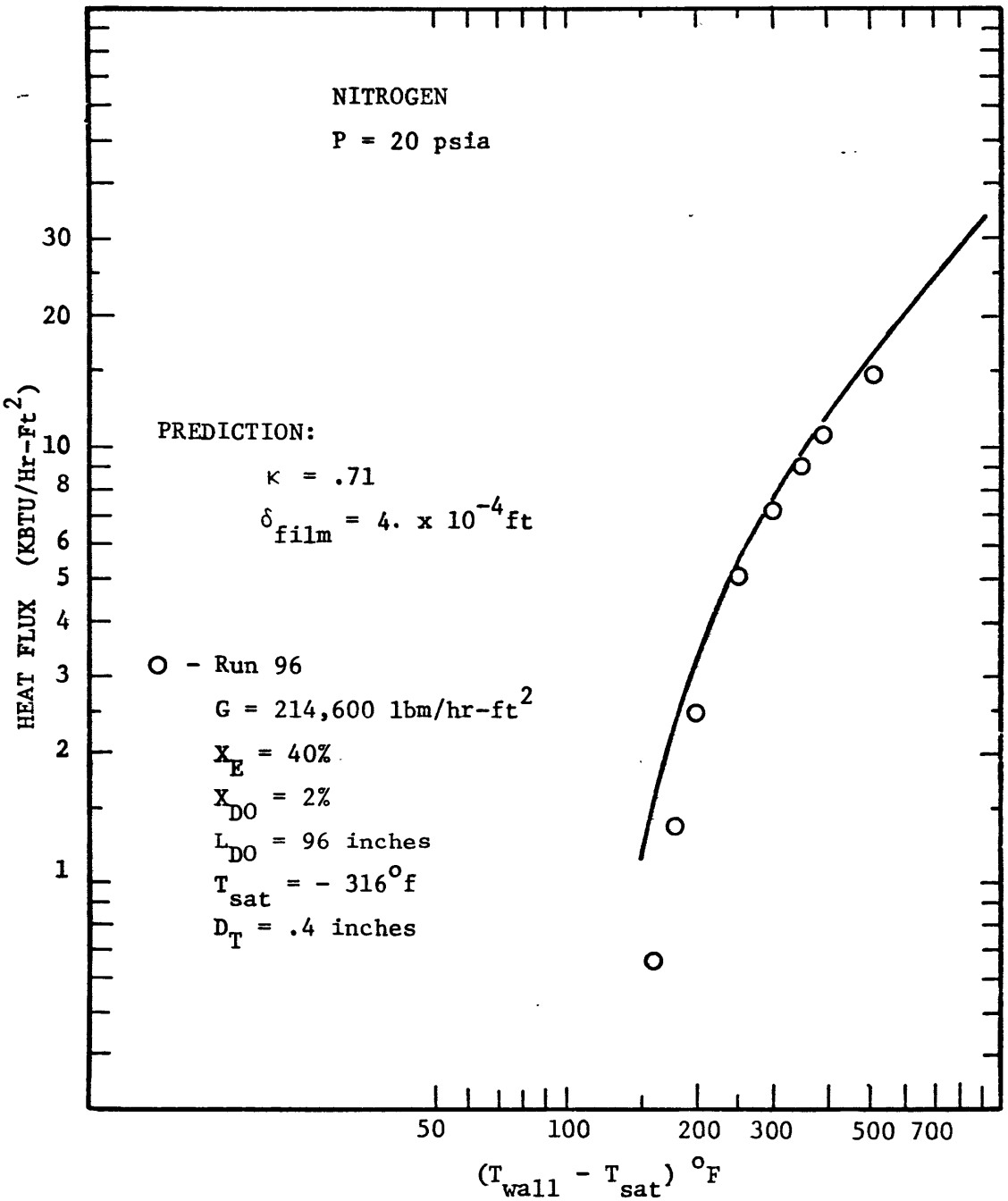

FIGURE 27 COMPARISON OF POST CRITICAL HEAT TRANSFER CORRELATION WITH TRANSIENT NITROGEN DATA - LONG DRYOUT LENGTH

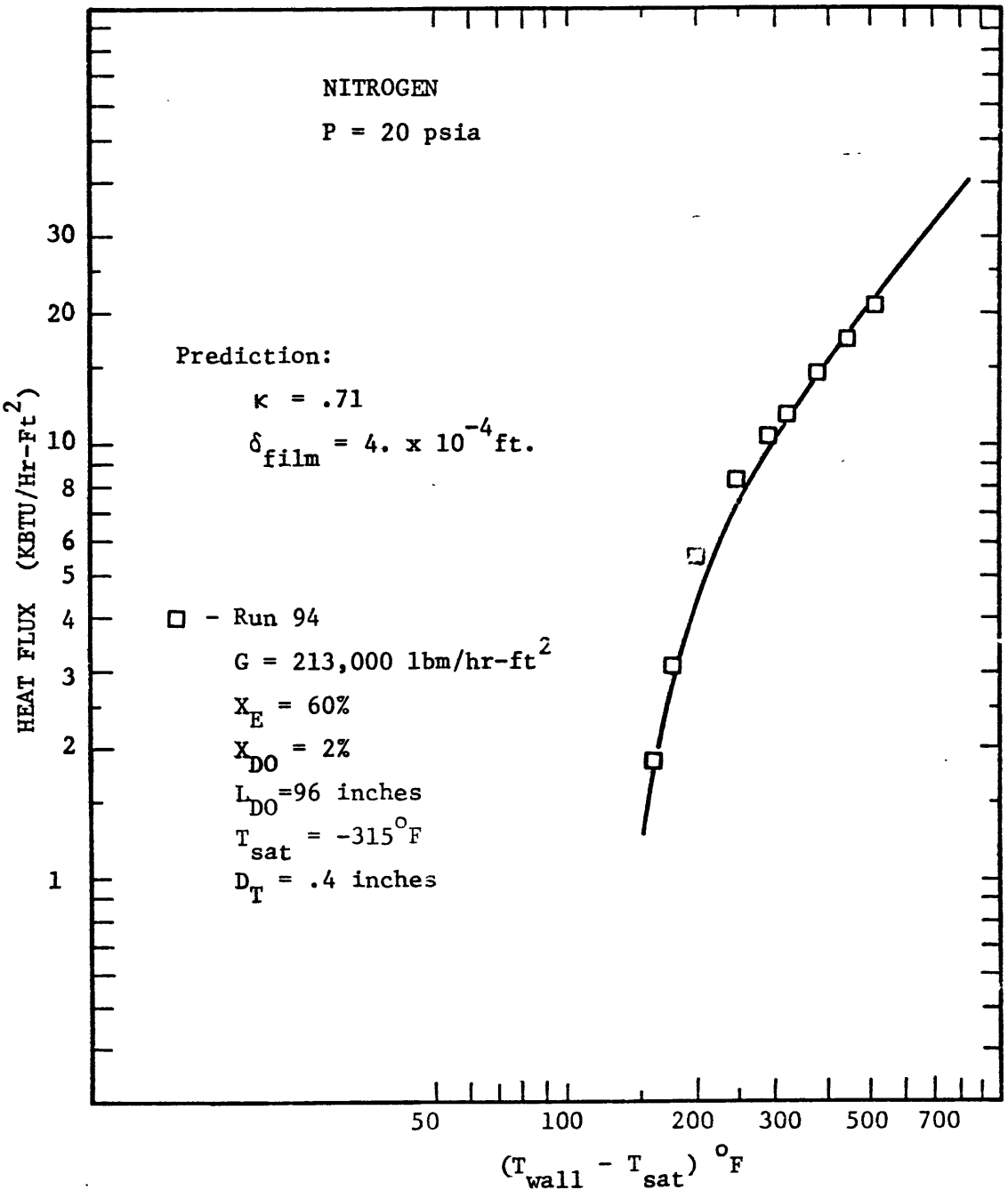

FIGURE 28 COMPARISON OF POST CRITICAL HEAT TRANSFER CORRELATION WITH TRANSIENT NITROGEN DATA - LONG DRYOUT LENGTH

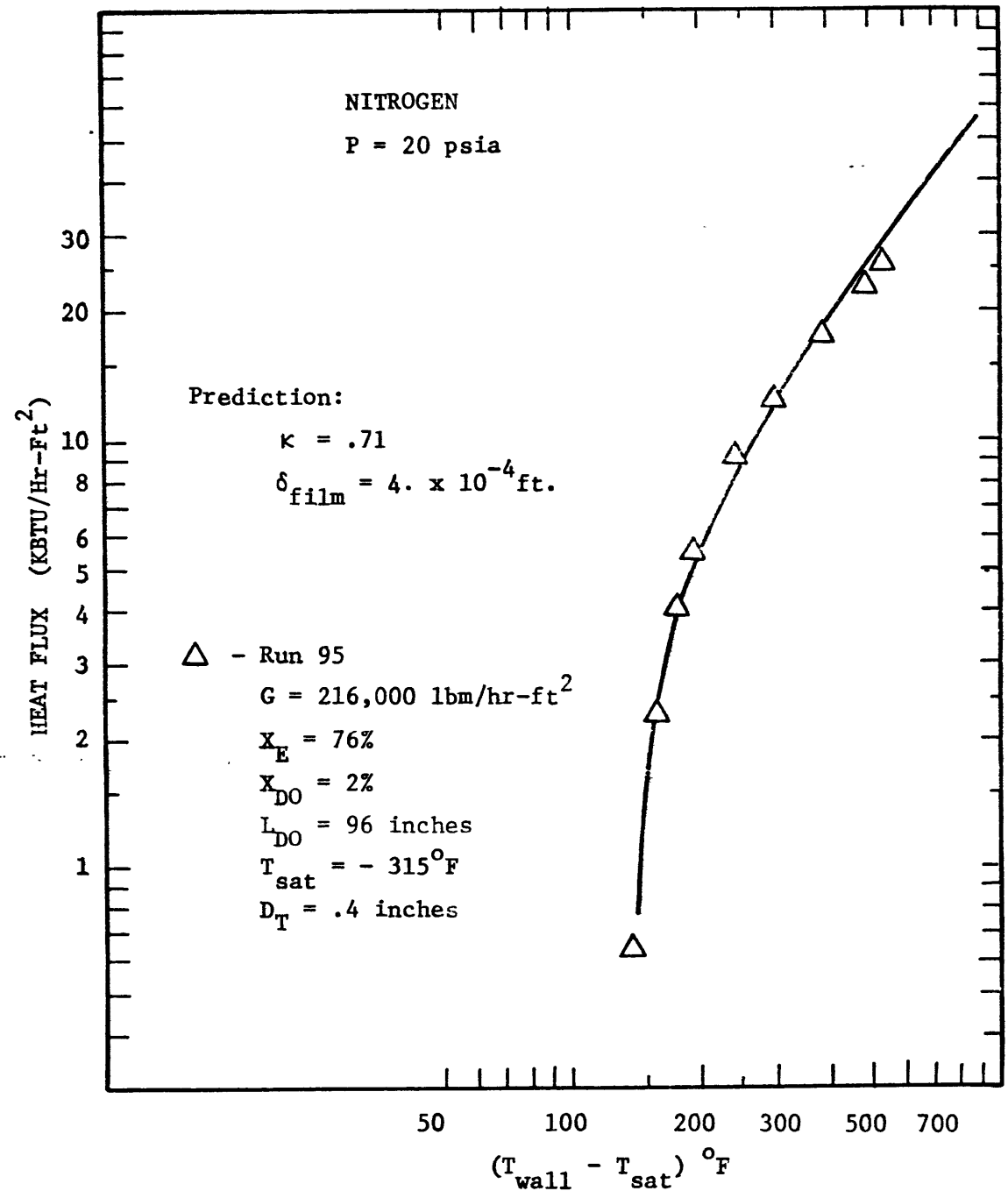

FIGURE 29 COMPARISON OF POST CRITICAL HEAT TARNSFER CORRELATION WITH TRANSIENT NITROGEN DATA - LONG DRYOUT LENGTH

this discrepancy is not warranted once the view that δ_{film} is a correlating constant for the set of equalions composing the post critical heat transfer correlation that is determined by data comparison. To be consistant in the idea that δ_{film} is a correlating constant no further adjustment should have to be made in it to predict other nitrogen data. This is a somewhat naive attitude if δ_{film} is taken in its physical sense of an average height which drops remain above the heated surface.

The most convincing support of $\delta_{film} = 4 \times 10^{-4}$ for nitrogen comes in comparing the prediction scheme with the transient nitrogen data for low values of L_{DO} . A low value of L_{DO} means that very little superheat of the vapor can be affected and that the equilibrium value of κ (i.e. $\kappa = 1$) should predict the data. This automatically reduces the problem of evaluating two correlating constants as δ_{film} is the only variable left to be correlated. As the bulk of the transient nitrogen data consists of low L_{DO} data an extensive check on δ_{film} can be achieved. One must keep in mind that only the higher range of $(T_w - T_{sat})$ is certain of being free from heat losses as explained in Appendix A.

Figures 30-34 present the results of some selected runs where L_{DO} equaled 3 inches or less. It is seen that $\delta_{film} = 4 \times 10^{-4}$ does a very good job of predicting this

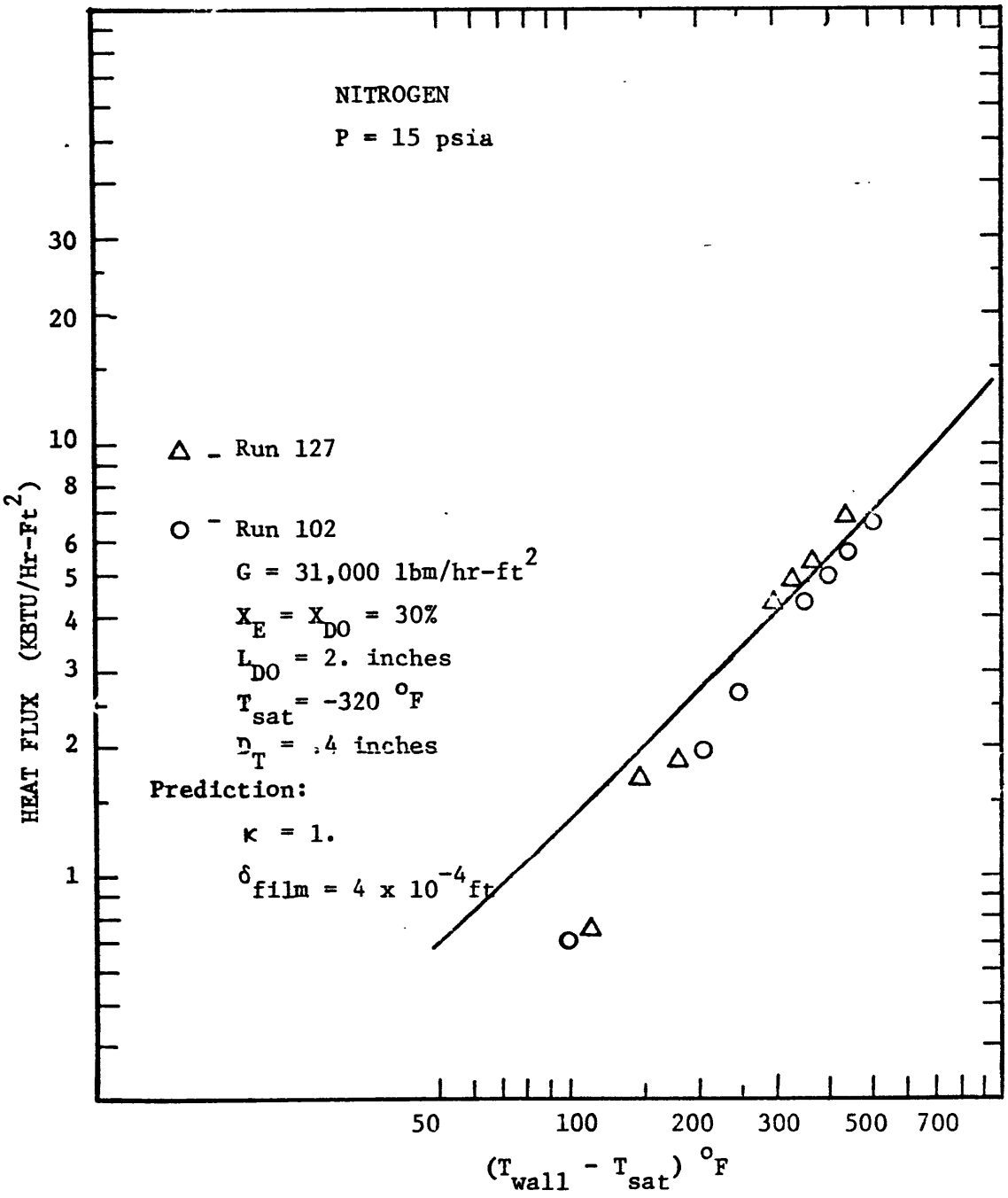

FIGURE 30 COMPARISON OF POSTCRITICAL HEAT TRANSFER CORRELATION WITH TRANSIENT NITROGEN DATA - SHORT DRYOUT LENGTH

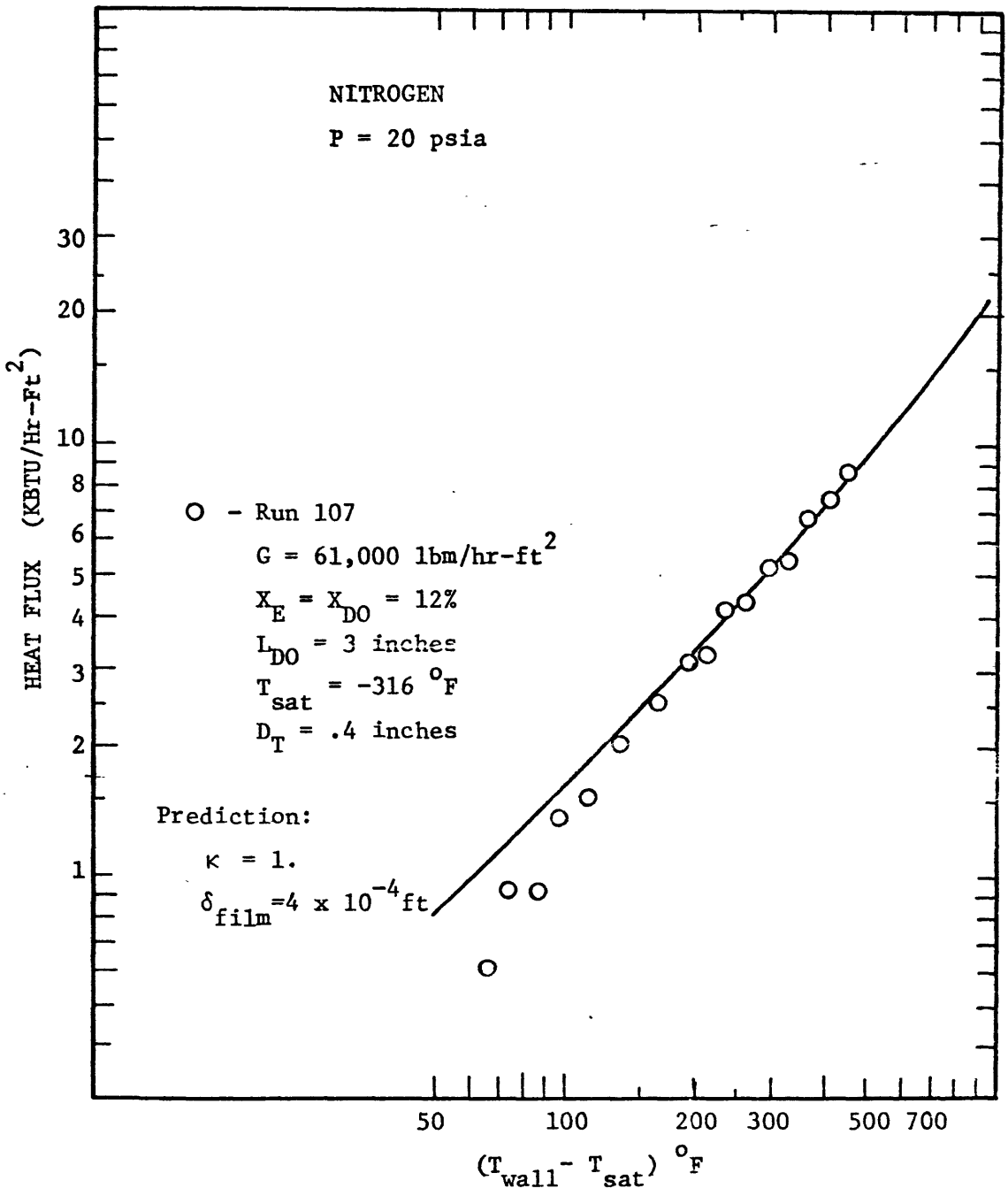

FIGURE 31 COMPARISON OF POST CRITICAL HEAT TRANSFER CORRELATION WITH TRANSIENT NITROGEN DATA- SHORT DRYOUT LENGTH

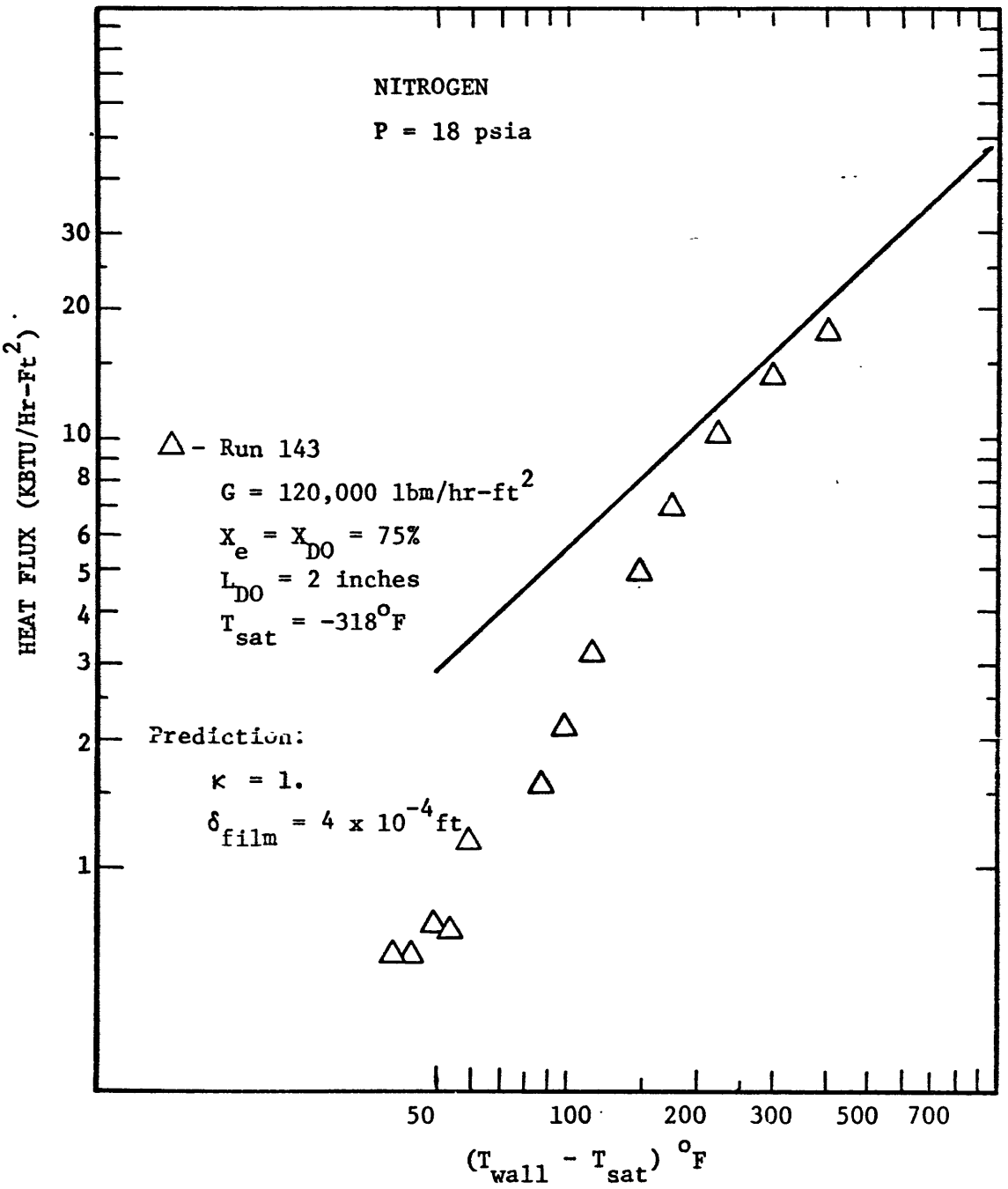

FIGURE 32 COMPARISON OF POST CRITICAL HEAT TRANSFER CORRELATION WITH TRANSIENT NITROGEN DATA - SHORT DRYOUT LENGTH

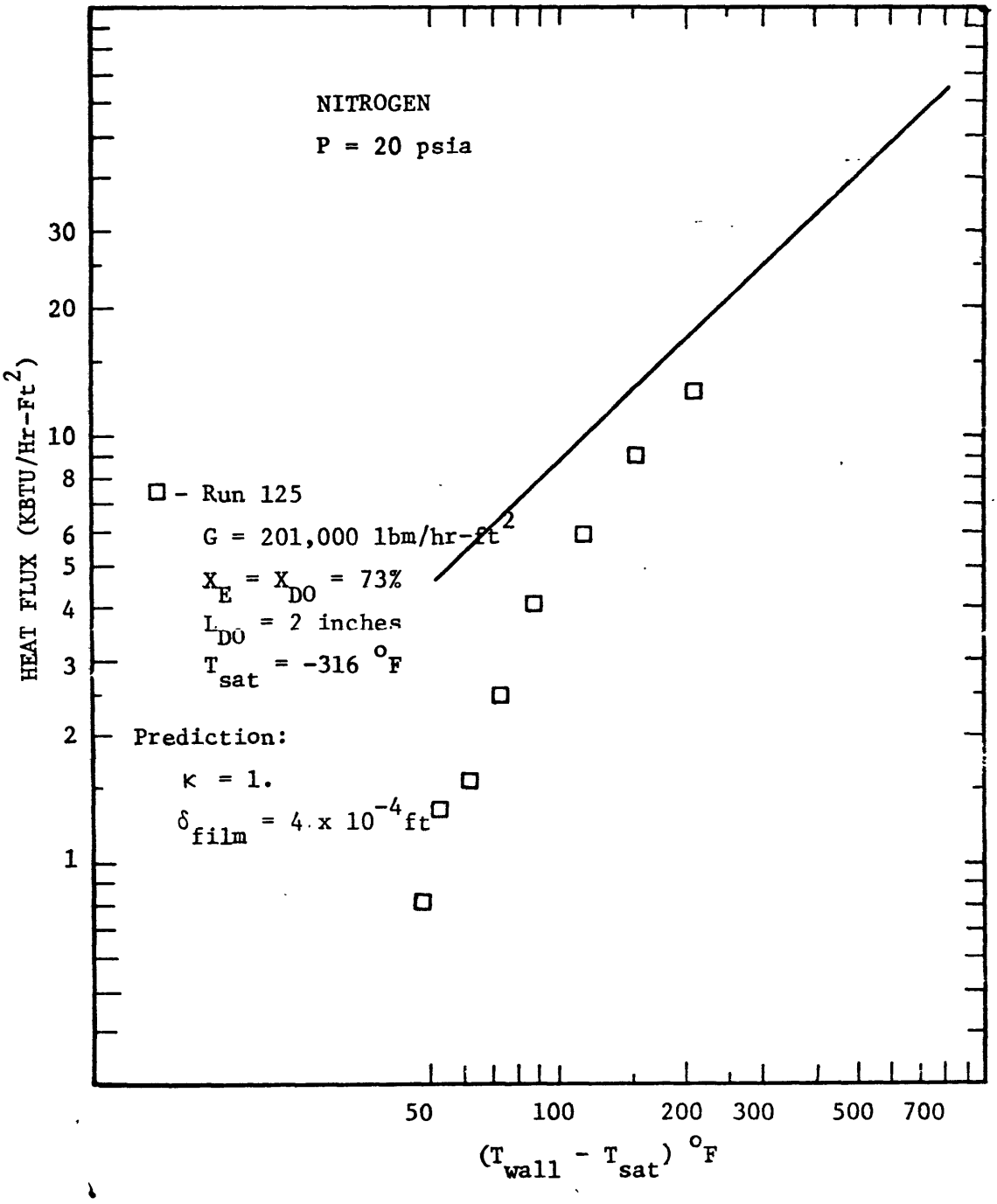

FIGURE 33 COMPARISON OF POST CRITICAL HEAT TRANSFER CORRELATION WITH TRANSIENT NITROGEN DATA - SHORT DRYOUT LENGTH

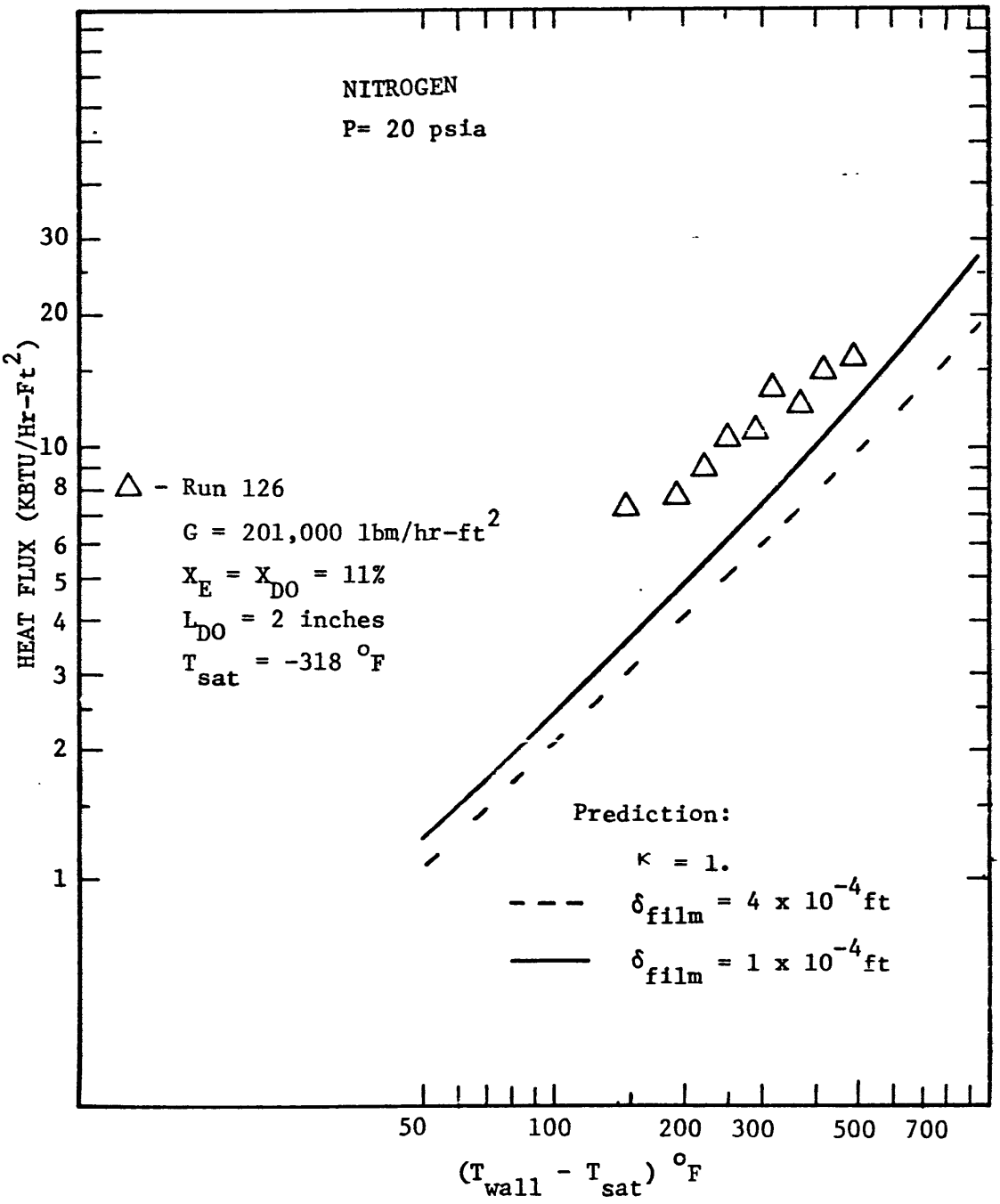

FIGURE 34 COMPARISON OF POST CRITICAL HFAT TRANSFER CORRELATION WITH TRANSIENT NITROGEN DATA - SHORT DRYOUT LENGTH

data. Also shown on some of these curves is the value of heat flux for $\delta_{film} = 1 \times 10^{-4}$. This value is generally outside the data scatter observed. In Figure 33 the data at low values of $(T_w - T_{sat})$ is considerably below the prediction. This is a clear indication of heat gains affecting the data as discussed in Appendix A. As $(T_w - T_{sat})$ increases, the discrepancy decreases and appears to asymptote to the prediction at elevated $(T_w - T_{sat})$ values (hence towards less heat gains). Figure 34 indicates that more heat flux than that provided by $\delta_{film} = 1 \times 10^{-4}$ ft is needed to predict the data. As this is a high mass flux-low quality run, it is felt that heat is being conducted out the top of the transient section due to a wetted interface at the discharge to the transient test section (again refer to Appendix A for more complete description).

The concluding check of the post critical heat transfer correlation for nitrogen comes with the comparison of the steady state temperature-length tube data obtained by Forslund and Hynek. If the correlation predicts this data equally well with $\delta_{film} = 4 \times 10^{-4}$ ft then the uncertainties involved in basing the correlation on data suspected of heat losses is significantly reduced as the problems of insulating a tube are much less involved than that involved with the transient section used in this investigation. Figures 35-39 present the full range of steady state

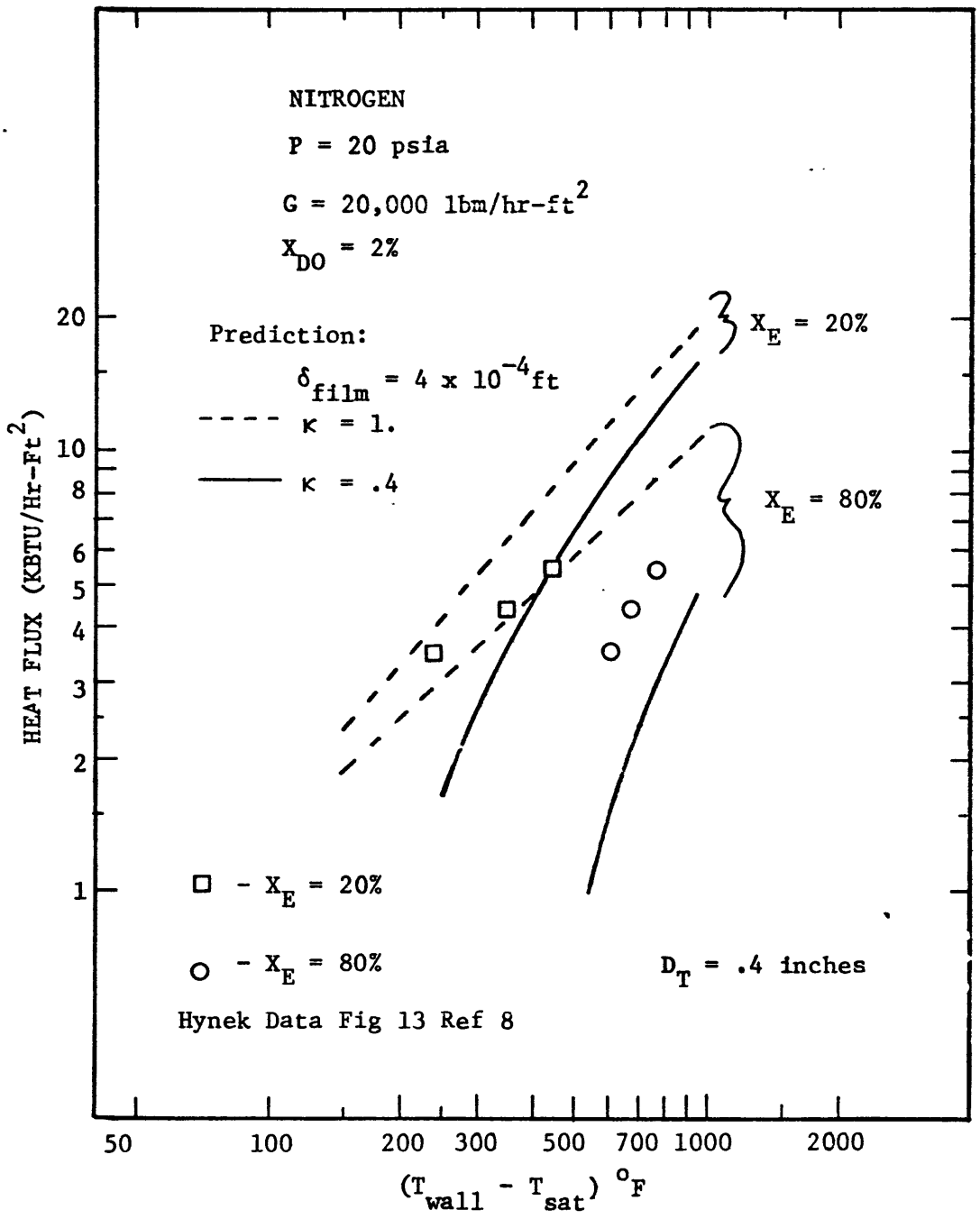

FIGURE 35 COMPARISON OF POST CRITICAL HEAT TRANSFER CORRELATION WITH UNIFORMLY HEATED TUBE NITROGEN DATA - G = 20,000 LBM/HR-FT^2

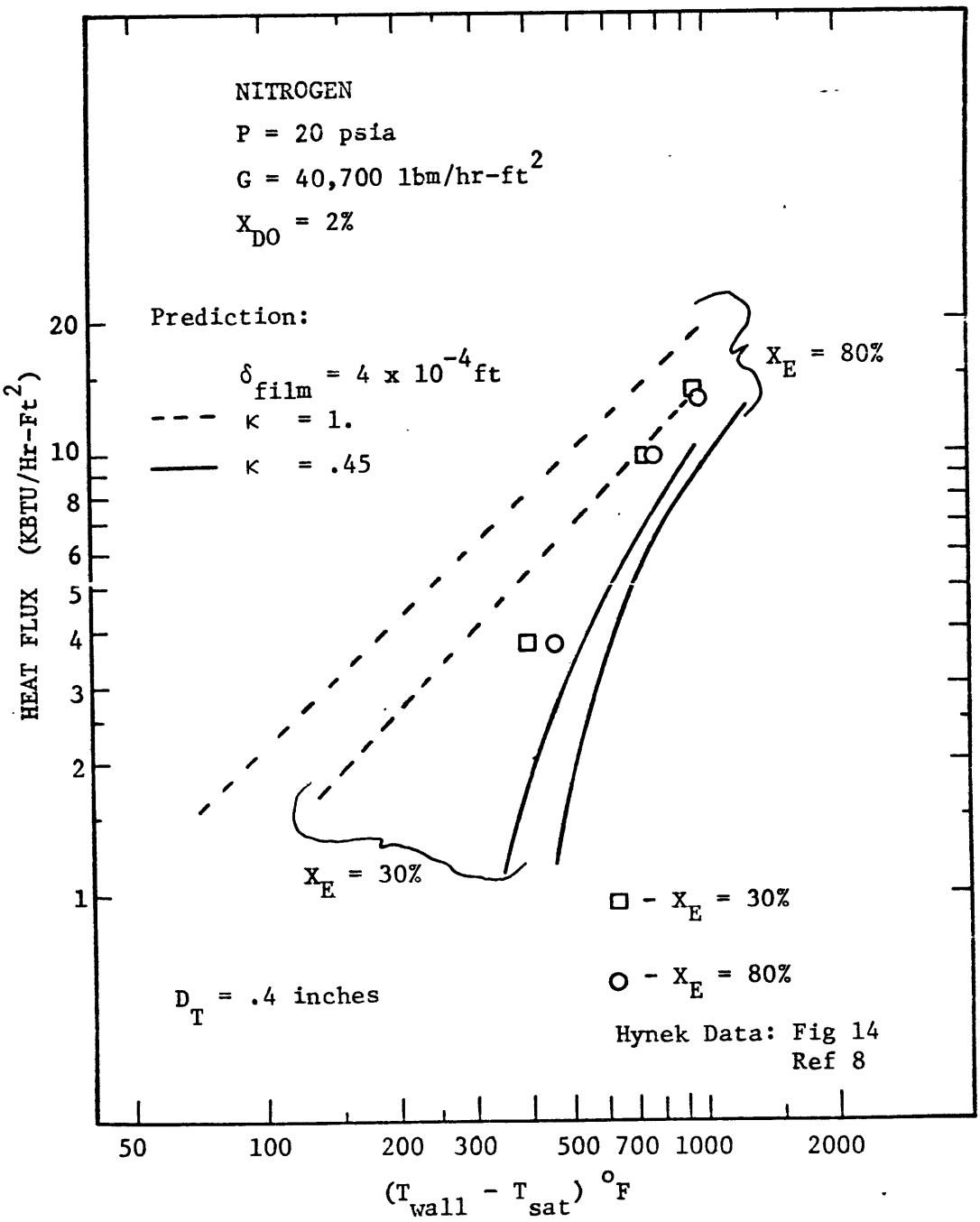

FIGURE 36 COMPARISON OF POST CRITICAL HEAT TRANSFER CORRELATION WITH UNIFORMLY HEATED TUBE NITROGEN DATA - G = 41,000 lbm/hr-ft^2

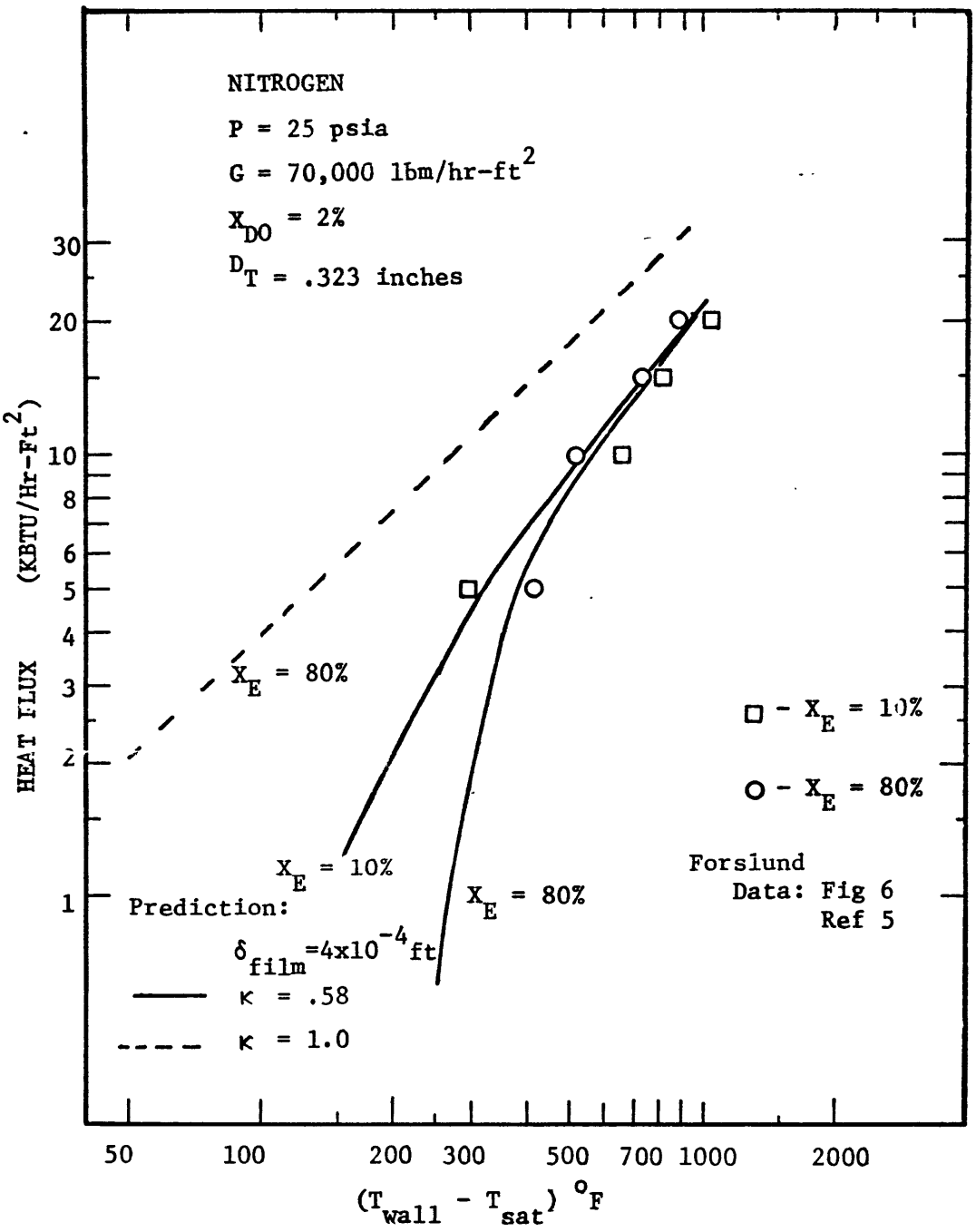

FIGURE 37 COMPARISON OF POST CRITICAL HEAT TRANSFER CORRELATION WITH UNIFORMLY HEATED TUBE NITROGEN DATA - G = 70,000 LBM/HR-FT^2

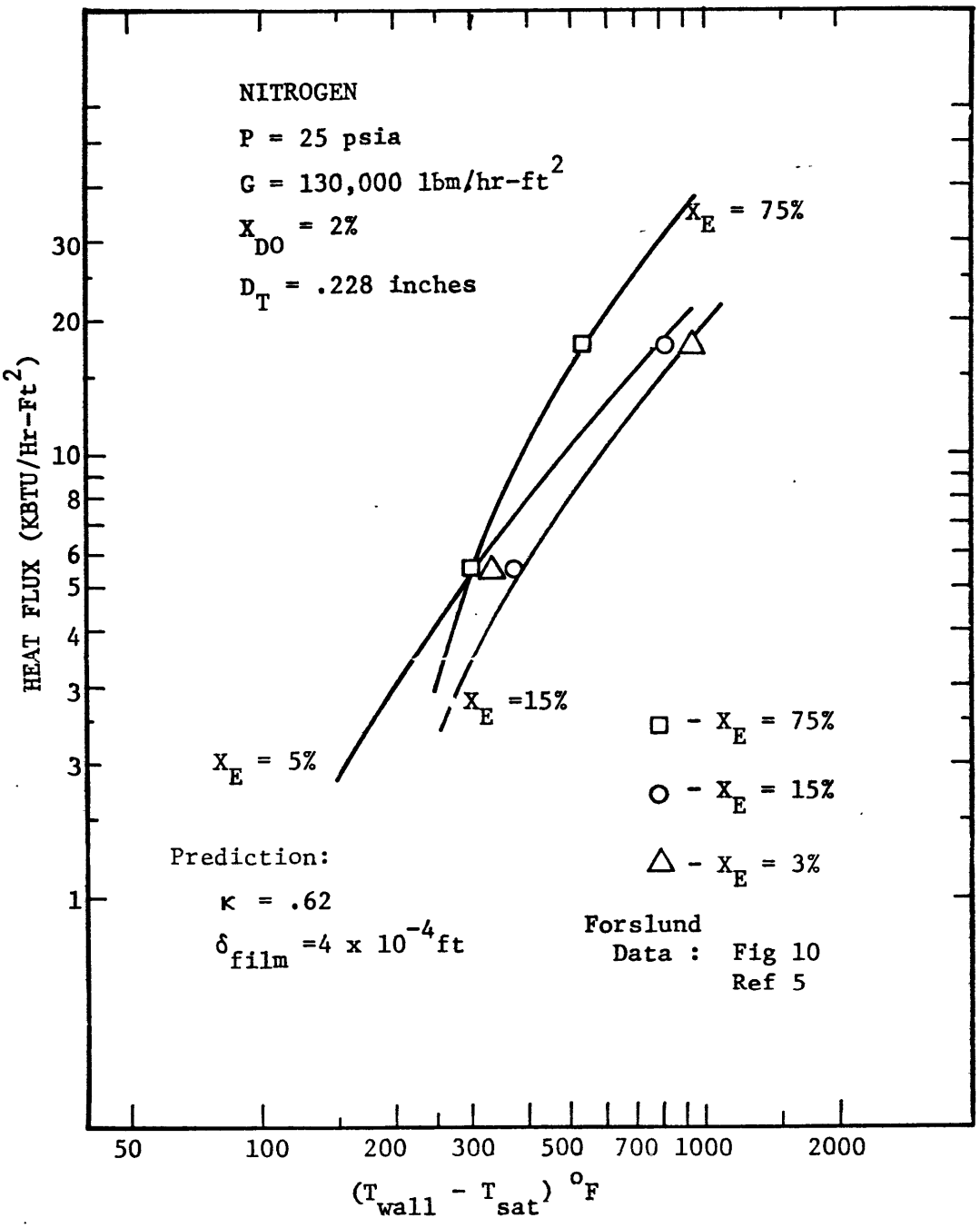

FIGURE 38 COMPARISON OF POST CRITICAL HEAT TRANSFER CORRELATION WITH UNIFORMLY HEATED TUBE NITROGEN DATA - G = 130,000 LBM/HR-FT^2

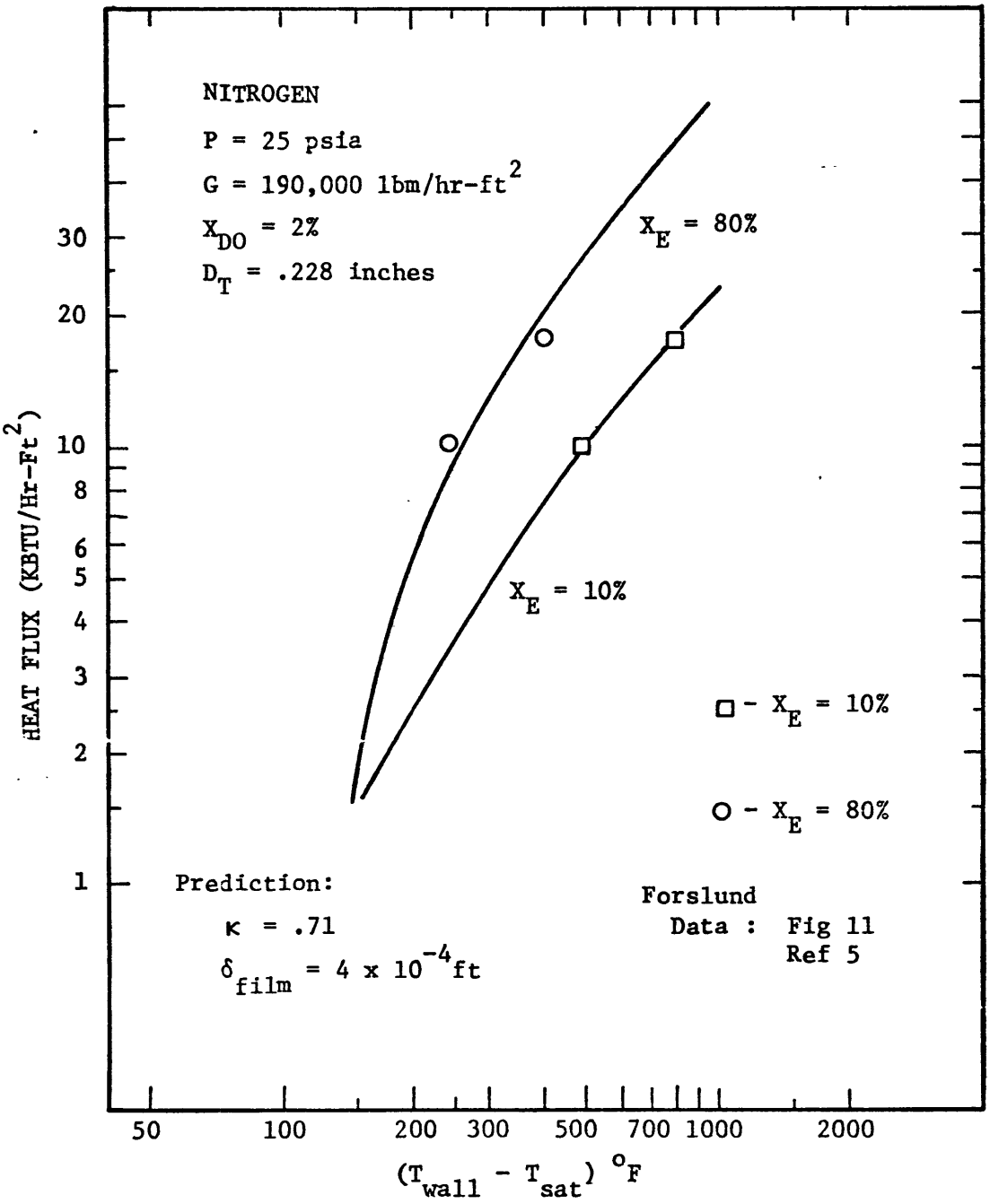

FIGURE 39 COMPARISON OF POST CRITICAL HEAT TRANSFER CORRELATION WITH UNIFORMLY HEATED TUBE NITROGEN DATA - G = 190,000 LBM/HR-FT^2

nitrogen data available in the literature. These figures encompass a G range of 20,000 - 190,000 lbm/hr-ft^2 and an X_E range of 5-80% , Again $\delta_{film} = 4 \times 10^{-4}$ ft provides excellent correlation of the data. The accuracy of the prediction scheme decreases somewhat for the 20,000 and 40,000 lbm/hr-ft^2 cases. This is understandable considering that a significant portion of the data for these G's is probably in a froth flow regime. It should be noted that this is the same data from which a value of $\delta_{film} = 1 \times 10^{-4}$ was obtained for the differential two step model discussed in Chapter 3.

4.4.3 Discussion of Post Critical Heat Transfer Correlation for Nitrogen

From the two previous sections the final unknowns are added to the post critical heat transfer correlation for nitrogen given by equation (4.15). κ is now evaluated from Figure 22 on Table 3. δ_{film} is set equal to 4×10^{-4} feet. The purpose of this section is to discuss the application of the correlation; its properties and limitations.

This prediction scheme appears quite formidable as indeed the physics of post critical heat transfer dictates. However the application of these equations to a particular problem is considerably simpler than the differential two step model discussed in Chapter 3. The equations are completely determinant given G, X_{DO} and X_E for q/A in terms of $(T_w - T_{sat})$. These equations require iterations in a maximum of two places in the calculation procedure. For every application the dryout slip, S_{DO}, has to be iterated using equation (3.8) and (3.9). A second iteration is required between μ_w and $k_{v,f}$ and the wall temperature when heat flux is the independent variable. If wall temperature is the independent variable then this iteration is not needed.

From the data comparison presented in section (4.4.2) the ability of the correlation to predict both the quality and mass flux dependency on the post critical heat flux is evident. An increase in G for a given set of system variables is readily seen to increase the post critical heat flux. Comparing Figures 37 and 39 demonstrate this. The effect of quality as represented by X_E on the post critical heat flux is rather complicated and its trends

have not been until now wholly correlated. The particular trend that X_E will have on q/A in post dryout is basically dependent on X_{DO} and G. Three possible trends of q/A vs X_E can occur. The first case is that q/A continually decreases after dryout as X_E increases. This occurs at a high value of X_{DO} and a corresponding moderate to low G. Secondly q/A vs X_E can increase to a point, then subsequently decrease as X_E increases. This generally occurs at low values of X_{DO} for any G or at moderate to high values of X_{DO} for high values of G. The final possibility is that q/A initially decreases, increases and finally decreases again as X_E increases. These three trends can be verified by returning to Figures 13-15 containing temperature length plots for various G and X_{DO} combinations. These trends are only partially observed in Figures 34-39 as the X_E variable is not high enough to demonstrate the eventual decrease in heat flux. The post critical heat transfer correlation presented here is capable of producing these trends because it is the sum of two terms which have opposite trends of q/A vs X_E . $q/A_{w,\delta}$ decreases with increasing X_E. $q/A_{w,v}$ increases at a decreasing rate due to vapor super heat. It is possible for this term to go negative if the decrease of the heat transfer due to vapor superheat is greater than the increase in $h_{w,v}$ due to higher vapor velocity.

The sum of the two heat transfer mechanisms can produce the three trends discussed depending on the relative rates of change with X_E . The correlation automatically goes to the all vapor asymtote as X_A goes to 1.

The final system variable affecting the post critical heat flux is the wall superheat defined as $(T_w - T_{sat})$. The heat flux from the wall, q/A, increases as $(T_w - T_{sat})$ increases. The particular shape that this curve takes depends on the quantity $(X_E - X_{DO})$. For $(X_E - X_{DO}) = 0$ the q/A vs $(T_w - T_{sat})$ curve for any G is nearly a straight line with a slope slightly higher than one as $(X_E - X_{DO})$ increases, q/A vs $(T_w - T_{sat})$ deviates from a straight line and looks more like a curve that approaches a straight line. A straight line drawn through this curve would have a slope somewhat higher than one. Figure 38 demonstrates this effect very well.

A very useful property of the post critical heat transfer prediction scheme as presented in this thesis is its ability to give the upper and lower bound to q/A vs $(T_w - T_{sat})$ in post dryout for any given system conditions. The upper bound is obtained immediately upon substituting $\kappa = 1$ into equation (4.15) . The lower bound can be obtained by selecting a value of κ from Figure 22 that is below the data for any given G and $(1-X_{DO})$. Figure 40 demonstrates the ability of $\kappa = 1.$ and $\kappa = .5$ to bound

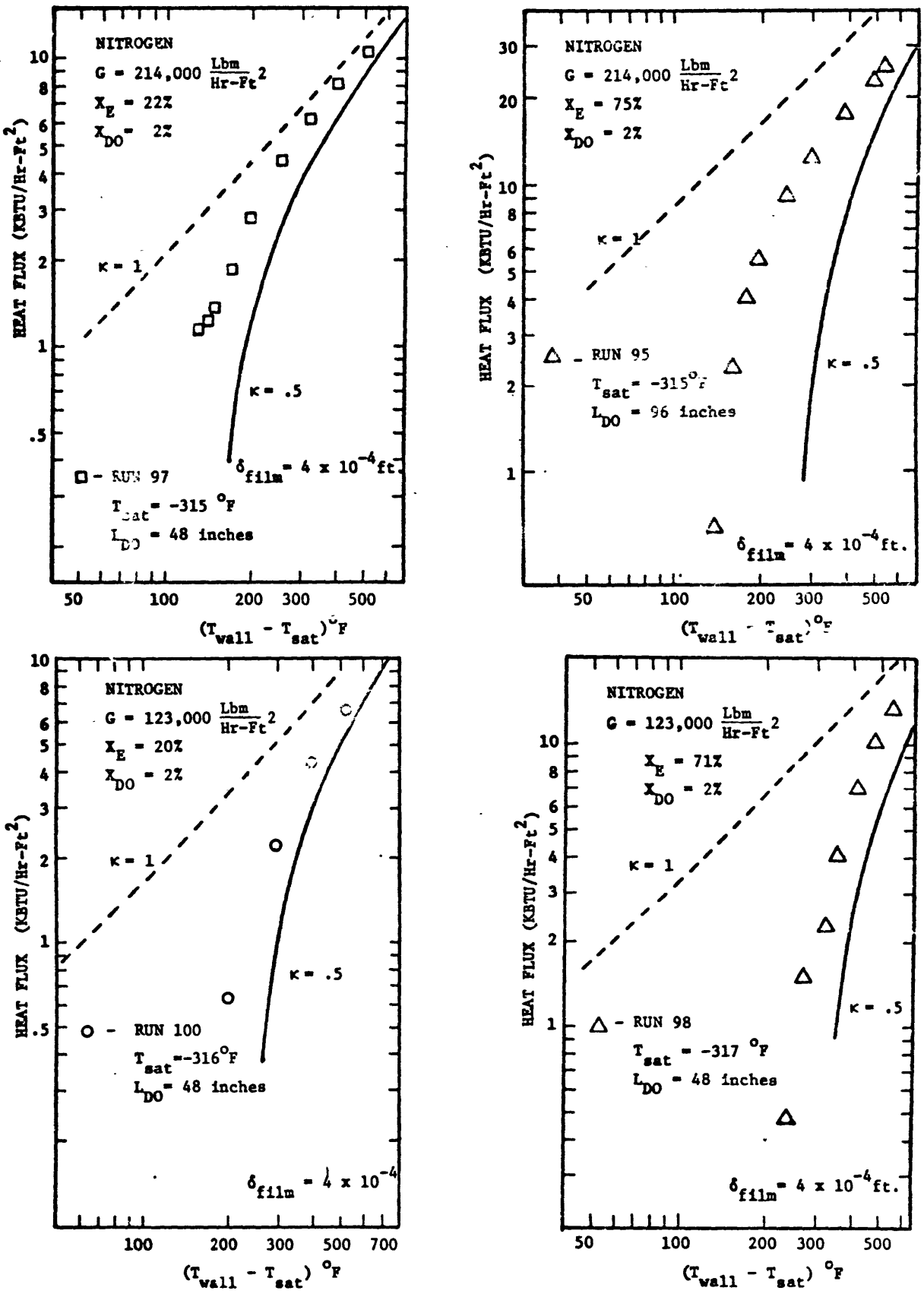

FIGURE 40 COMPARISON OF BOUNDED SOLUTION WITH REPRESENTATIVE TRANSIENT DATA

the transient data given in Runs 95, 97, 98 and 100. One can see that as $(X_E - X_{DO})$ increases, the two bounds grow further apart. At $(X_E - X_{DO}) = 0$ the upper and lower bounds are the same.

It is interesting now to compare the results of this correlating procedure with the Groeneveld post critical heat transfer correlation for tubes as given in Chapter 1 [equation (1.1)]. The constants for the heat flux dependent case were used. This comparison is presented in Figure 41 for the case of G = 250,000 lbm/hr-ft^2, X_{DO} = 20% and X_E = 40, 80%. From Figure 20 a value of κ = .62 was selected given this set of conditions. For X_E = 40% there appears to be very little discrepancy between the two correlations at least at high wall superheats. At low wall superheats the vapor superheat begins to have an affect on the nitrogen correlation whereas no affect is given by the Groeneveld correlation. The Groeneveld correlation shows very little quality effect on the heat flux which is understandable considering that the correlation was based on water data which has a ρ_v/ρ_ℓ ratio almost an order of magnitude higher than nitrogen. This comparison vividly illustrates the inability of this type of post critical heat transfer correlation to predict accurately any data outside the range of data correlated. Just knowing X_E and G is not sufficient to quantify every conceivable post critical situation. The

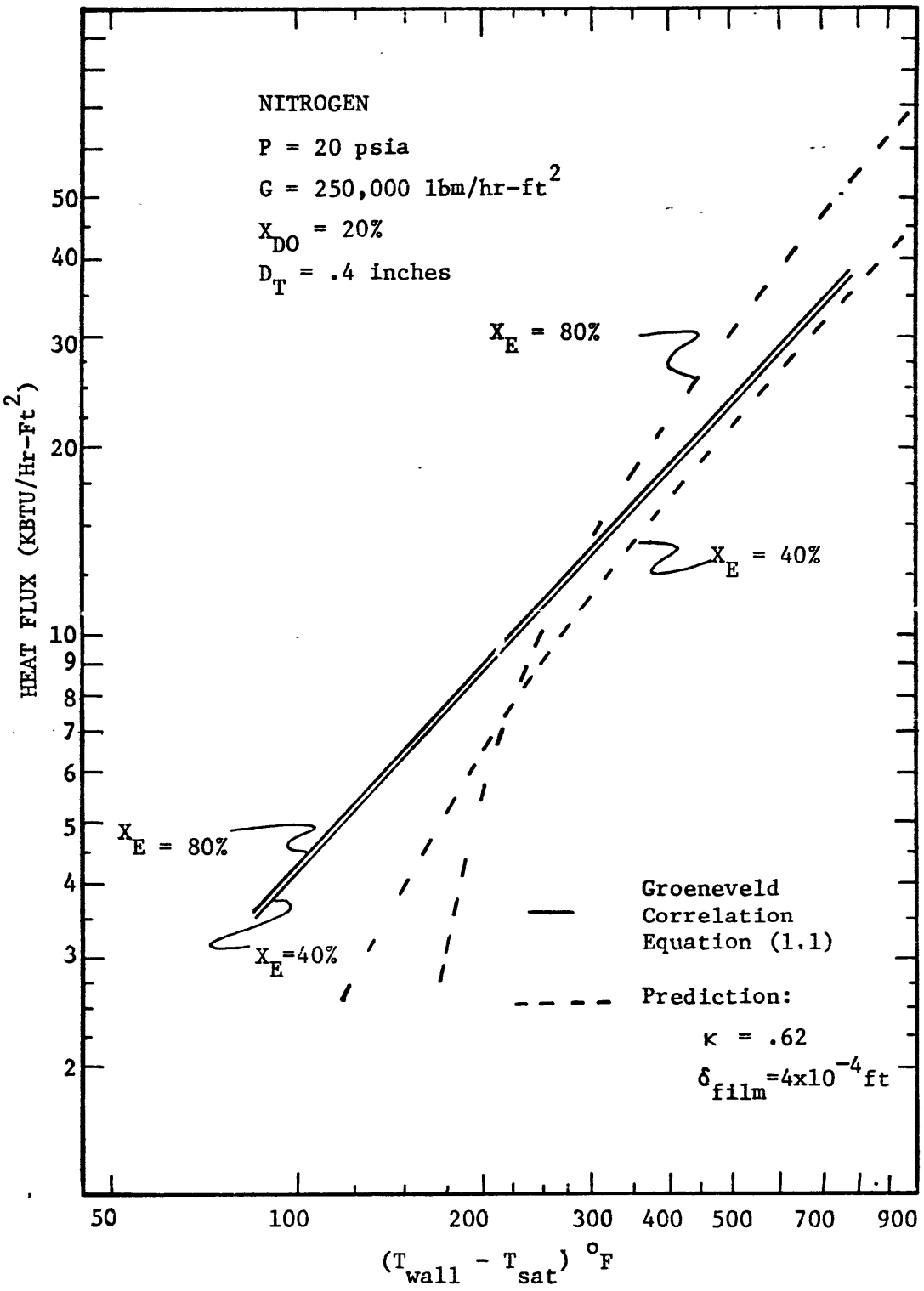

FIGURE 41 COMPARISON OF THE GROENEVELD POST CRITICAL HEAT TRANSFER CORRELATION WITH THE PREDICTION SCHEME OF THIS REPORT

post critical heat transfer prediction scheme presented here for nitrogen does have the necessary variables that will allow it to be extrapolated outside the data on which it was based and as such this correlation should be able to predict data for different fluids. There is a possibility that δ_{film} will have to be modified but this can be taken care of by evaluating the constant with available data for the particular fluid in question. The next section presents a preliminary comparison of the nitrogen correlation with Water and Freon 12 data in the literature.

4.5 Comparison of Nitrogen Prediction Scheme with Other Fluids

Since the κ vs G and $(1 - X_{DO})$ relation and the post dryout α relation for Water and Freon 12 were determined simultaneously with the derivation of the post critical heat transfer correlation for nitrogen, it is a simple matter to apply these quantities to the general prediction scheme for nitrogen as given in equation (4.15) and ascertain its validity in predicting water and Freon 12 post critical heat transfer data. In the following comparison process the value of κ was obtained from Figure 22 instead of using the appropriate correlation equation as specified in Section (4.4.1

4.5.1 Water Comparison

Figures 42, 43, and 44 present the resulting comparison of the post critical heat transfer correlation with water data at 1000 psia for three mass fluxes G = 485,000, 740,000 and 1,000,000 lbm/hr-ft^2 respectively. This data was obtained by Bennett[6] in a uniformly heated tube. The Heineman superheated steam correlation was used instead of the modified McAdams equation for the wall to vapor heat transfer coefficient.

The prediction scheme does suprisingly well considering the data is a cross plot of a number of runs having different values of X_{DO} . Figure 42 indicates an under-

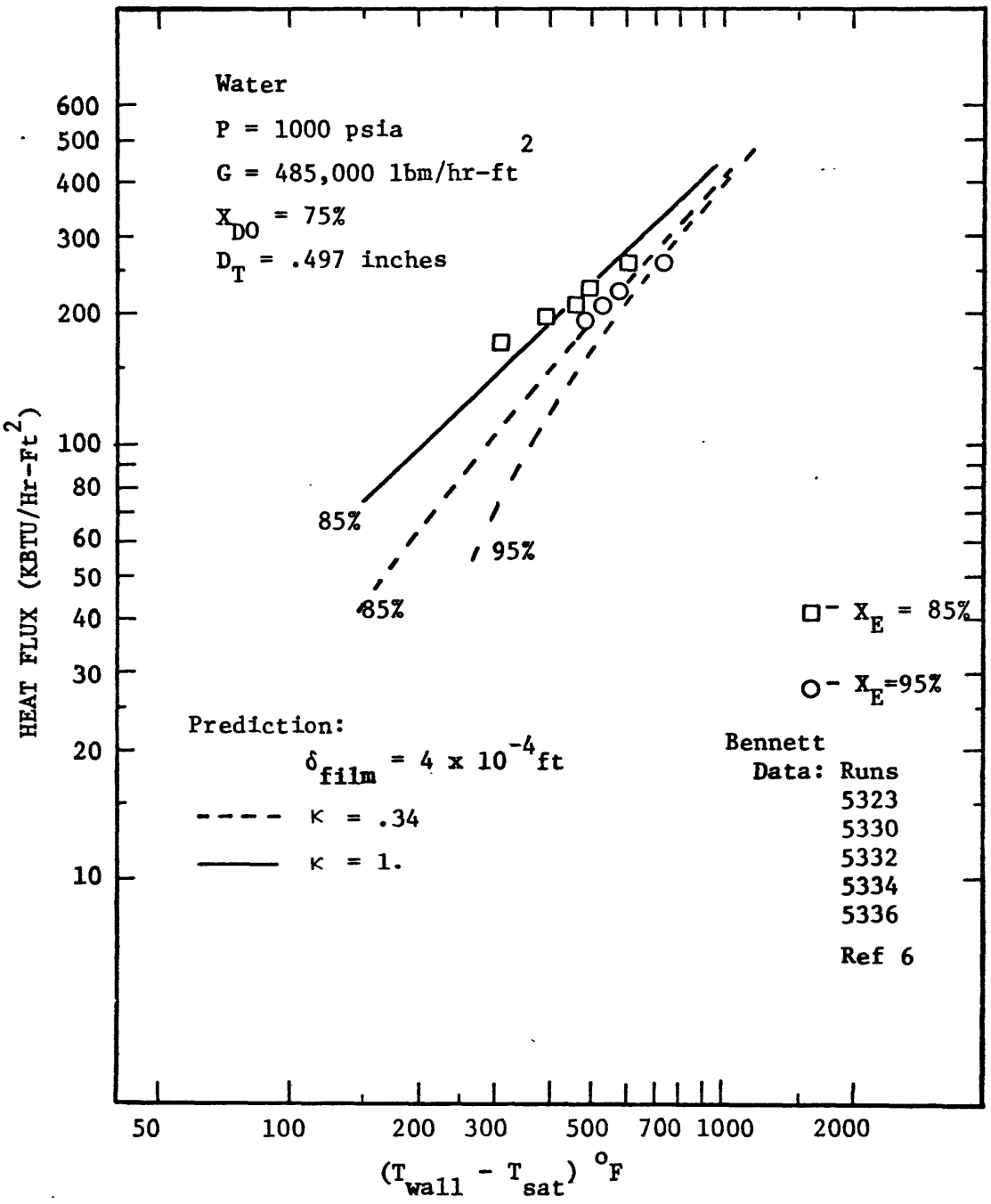

FIGURE 42 COMPARISON OF POST CRITICAL HEAT TRANSFER CORRELATION WITH UNIFORMLY HEAT TUBE WATER DATA - G = 485,000 lbm/hr-ft²

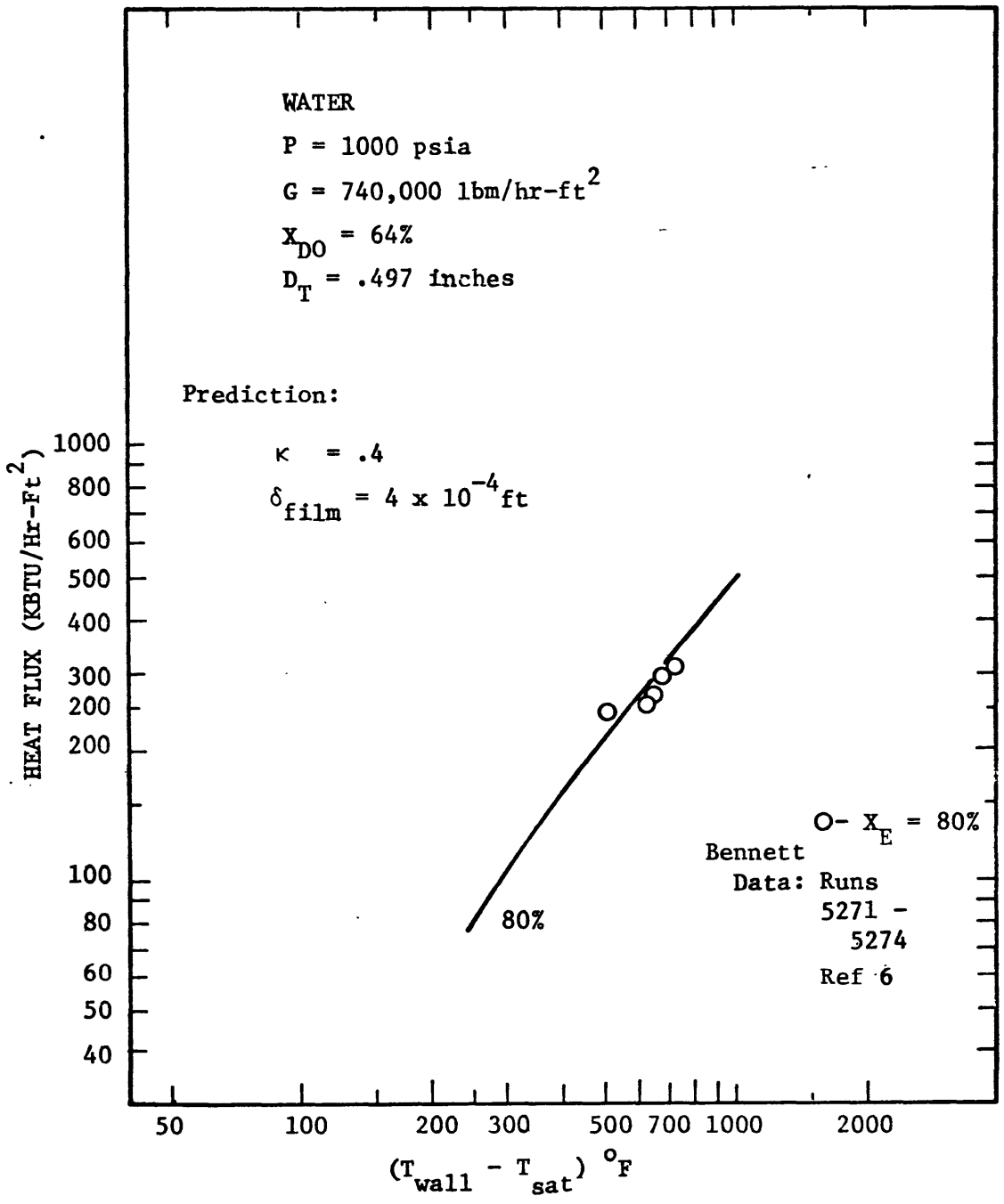

FIGURE 43 COMPARISON OF POST CRITICAL HEAT TRANSFER CORRELATION WITH UNIFORMLY HEATED TUBE WATER DATA - G = 740, 000 lbm/hr-ft^2

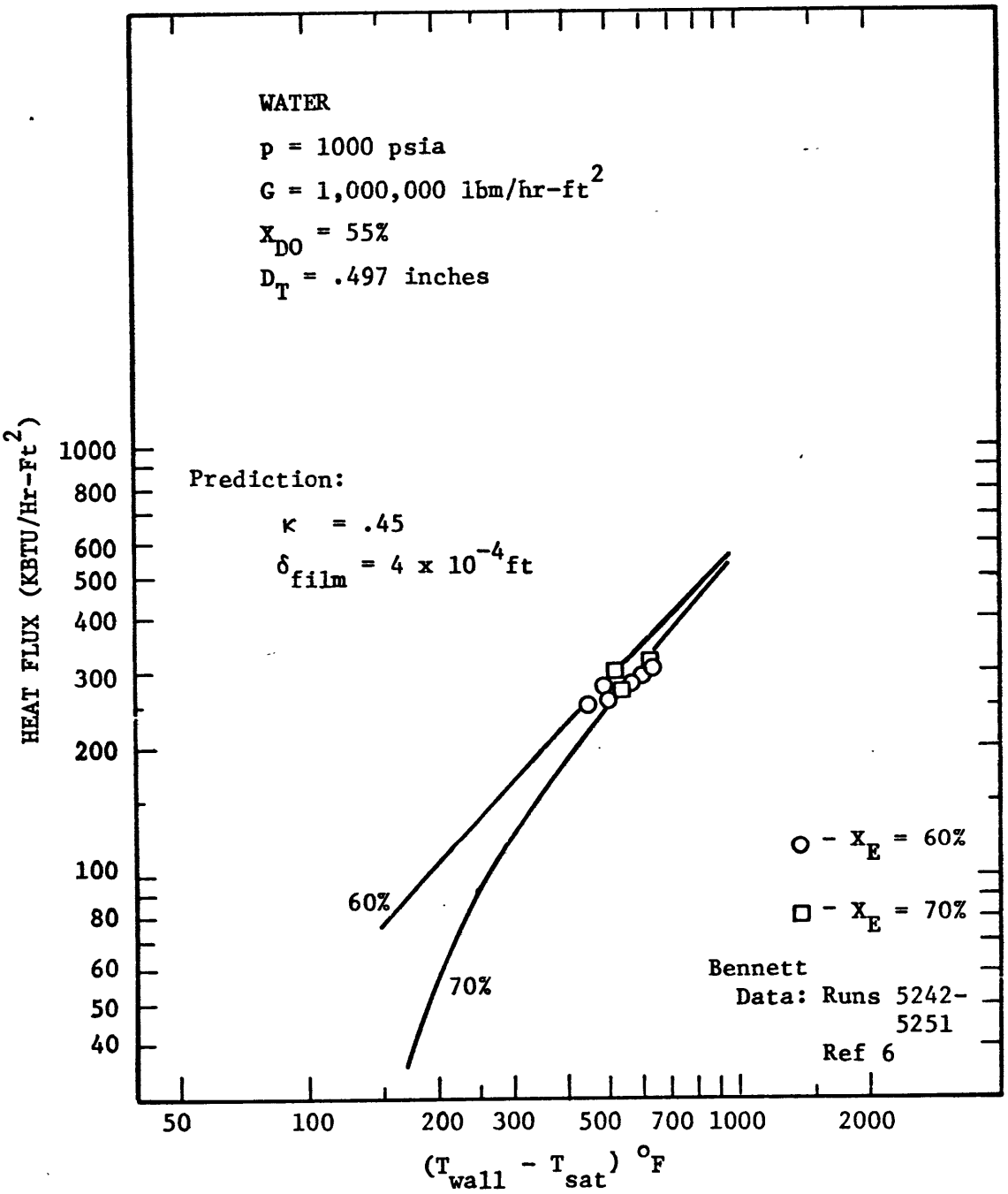

FIGURE 44 COMPARISON OF POST CRITICAL HEAT TRANSFER CORRELATION WITH UNIFORMLY HEATED TUBE WATER DATA - G = 1,000,000 LBM/HR-FT^2

prediction of the data. The correct trend of the quality is observed in the prediction though. It appears that a δ_{film} somewhat smaller than 4×10^{-4} feet is needed. However, by reason of the high void decreasing δ_{film} will not appreciably affect the resulting prediction. Also plotted on Figure 42 is the prediction for the 85% quality case using $\kappa = 1$. This does a reasonable job in predicting the data. The comparisons for the two higher mass fluxes are quite good with less than 15% deviation between the prediction and data.

4.5.2 Freon 12 Comparison

The Freon 12 data for this comparison is again taken from Groeneveld[7]. It has been replotted in a q/A vs $(T_w - T_{sat})$ coordinates. Figures 45 and 46 present the resulting comparisons for G = 250,000 and 1.5×10^6 lbm/hr-ft^2 $\delta_{film} = 4 \times 10^{-4}$ ft appears to correlate this data fairly well. The McAdams equation was used for the wall to vapor heat transfer term. Figure 45 indicates that some superheating of the vapor has occurred as seen by the comparison of the $\kappa = 1$ prediction with that of $\kappa = .4$. X_E has not significantly increased above X_{DO} in Figure 46 with the result that any value of κ will give the same prediction for this case.

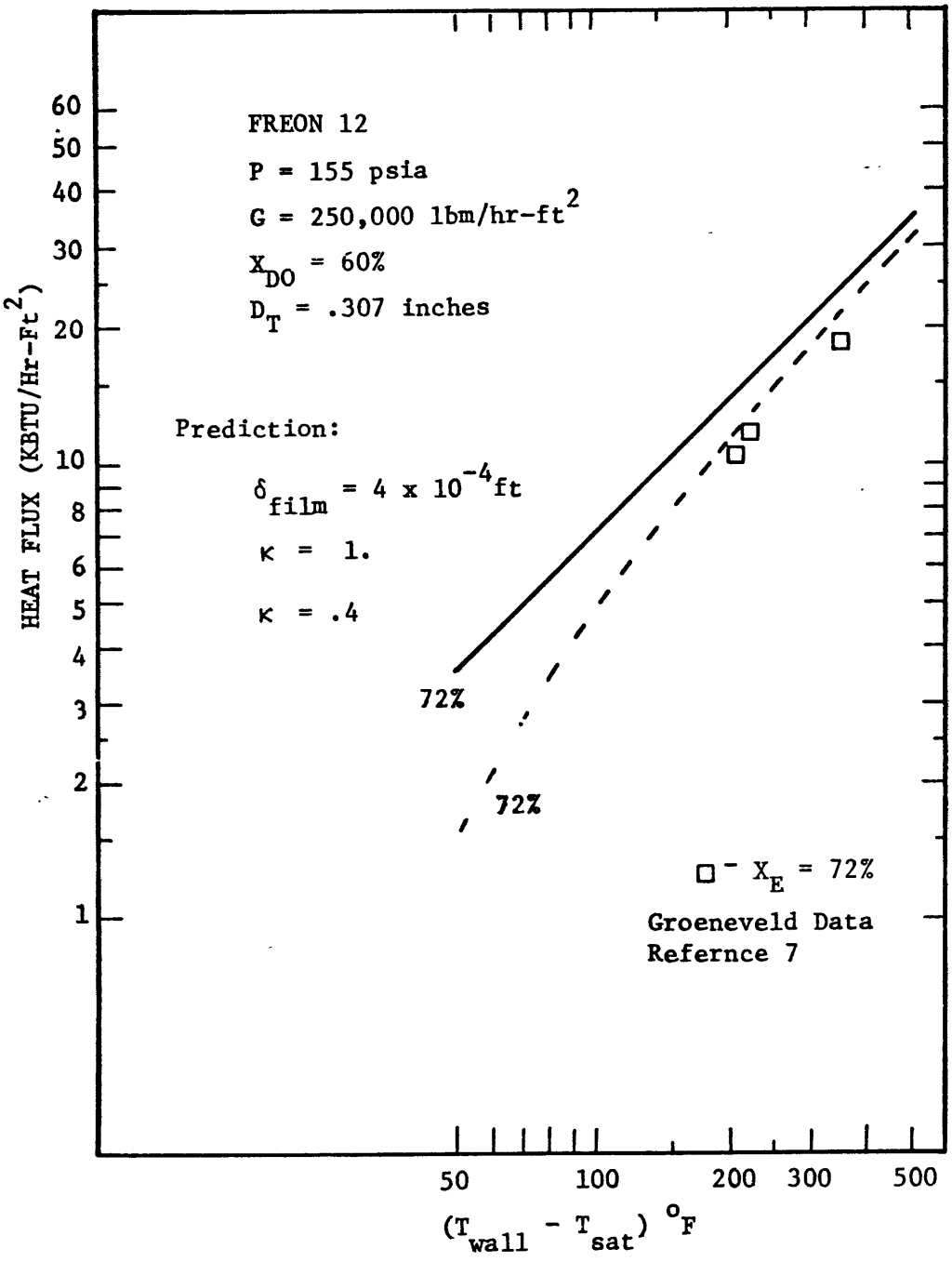

FIGURE 45 COMPARISON OF POST CRITICAL HEAT TRANSFER CORRELATION WITH UNIFORMLY HEATED TUBE FREON 12 DATA - G = 250,000 LBM/HR-FT^2

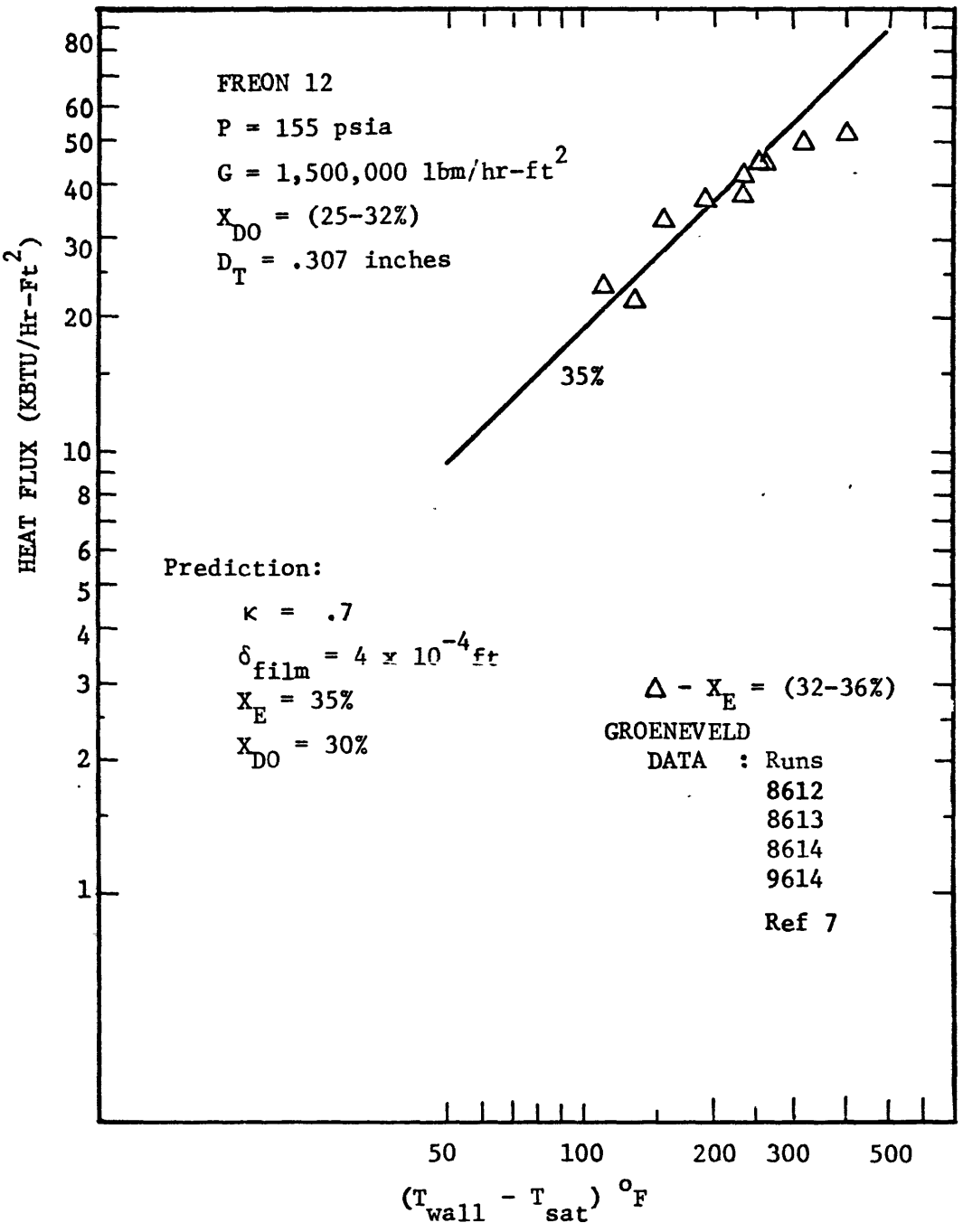

FIGURE 46 COMPARISON OF POST CRITICAL HEAT TRANSFER CORRELATION WITH UNIFORMLY HEATED TUBE FREON 12 DATA - G = 1,500,000 LBM/HR-FT^2

V. SUMMARY AND CONCLUSIONS

5.1 Summary

1. An experimental investigation of post critical heat transfer in forced vertical flow for a tube geometry was undertaken. A novel transient experimental technique was devised and implemented. The extreme versatility of this technique was demonstrated by its ability to generate, in one operation, post critical heat transfer data at one particular G and X_E combination for various dryout lengths up to eight feet. The flexibility of the transient experiment was further increased with the ability to interchange transient test pieces for determining material, roughening and oxide effects on post critical heat transfer. Forced convection dry wall film boiling data was obtained using this experimental technique for the following range of parameters.

For a 0.4 inch inside diameter tube:

G variation: 30,000 - 220,000 lbm/hr-ft^2

X_E variation: 0 - 90%

L_{DO} variation: 2 - 96 inches

Test material: Copper, Inconel 600, Aluminum 100

Surface Conditions : Smooth (10 - 50 microinches)

Roughened (approx. 400 microinches)

Oxidized (film approx. 10^{-5} inch thick)

q/A variation: 1,000 - 25,000 btu/hr - ft^2

($T_{wall} - T_{sat}$) variation: 50 - 550°F

This apparatus was capable of investigating dry wall film boiling heat transfer at such close proximity to the dryout point without axial conduction effects because of the careful insulation procedure used to isolate the transient test section from the preheater.

2. An extensive comparison of the Hynek and Groeneveld dispersed flow film boiling models with data in the post critical heat transfer regime was carried out. The original Hynek computer code was modified to include the Groeneveld droplet breakup mechanism. This code was compared with a large range of post critical heat transfer data for nitrogen, water and Freon 12.

3. A generalized post critical heat flux prediction scheme was developed upon application of the assumption that the X_A vs X_E curve can be approximated by the linear function $X_A - X_{D_0} = \kappa(X_E - X_{DO})$ to a modified form of the differential two-step dispersed flow model used by Hynek. Considering, therefore, that heat is transferred in post dryout from the wall to superheated vapor and from the wall to drops via dry collisions, expressions for T_v and α were

obtained in terms of κ. T_v was obtained from direct application of the above assumption to the post dryout energy balance. The void fraction was obtained using a post dryout slip correlation based on computer generated slip ratios obtained from the solution of the momentum, energy and critical weber number equations. T_v and α were subsequently substituted into the McAdams vapor heat transfer and Groeneveld droplet heat transfer to provide the total solution in terms of κ. κ was evaluated using a visual best fit procedure to X_A vs X_E curves generated from modified Hynek computer code of the differential two-step dispersed flux mode. The final procedure in the development of the post critical heat transfer prediction scheme consisted of correlating κ vs G and X_{DO} using the following nondimensional parameter

$$G\sqrt{D_T/\rho_v\sigma}\,(1-X_{DO})^5$$

The resulting post critical heat flux correlation given in Equation (4.15) was compared with the transient data obtained in this study as well as nitrogen, water and Freon 12 data found in the literature.

5.2 Conclusions

From the above investigation the following conclusions were made.

1. A transient boiling experiment will give the correct

representation of the post critical heat transfer as evidenced by the positive comparison between the transient data in this study and steady state data found in the literature.

2. No consistant trend for the effect of material on drywall film boiling heat transfer was observed.

3. Increasing the roughness of the heater surface increases its heat transfer capability. This results from increasing the wall-to-vapor heat transfer coefficient as demonstrated by the Colburn analogy. This effect is more pronounced as the vapor Reynolds number increases.

4. The addition of oxide to the heating surface increases the heat transfer characteristics of the surface. The reason for this effect is linked with the evidence that actual liquid contact can occur in dry wall film boiling even if the surface temperature is above the maximum liquid temperature. The increased wettability and porosity of the oxide allows the attached liquid to spread and adhere to the surface for a longer period of time than if the surface were clean. The combination of increased area of liquid contact, increase in time of contact and vigorous evaporation at the liquid-solid interface has the effect of increasing the heat transfer over and above any thermal resistance that the oxide might have. It is noted that the

augmentation of the heat transfer with oxide is more pronounced at low quality, high mass flux combinations where the liquid fraction is higher.

5. No major differences were noted in the ability of Hynek's and Groeneveld's models to predict data in post dryout conditions. The computer code, FILMBOIL, using a value of $\delta_{film} = 1. \times 10^{-4}$ feet for the correlating constant in Groeneveld's wall-to-droplet heat transfer coefficient predicts nitrogen, water and Freon 12 post dryout temperatures profiles with an accuracy of 10 - 20%.

6. The ability of the post critical heat transfer prediction scheme to correlate nitrogen data has been demonstrated. The effects of G, X_E, X_{DO} and T_{sat} on the post critical heat flux are properly accounted for through the implicit inclusion of nonequilibrium effects resulting from vapor superheating in post dryout. The only restrictions to the use of the post critical heat transfer correlation as presented in this thesis is that G be greater than that required for liquid carryover.

5.3 Recommendations

1. It is recommended that a quantitative study of the effects of roughness and oxide on the post dryout heat transfer initiated. Included in this study should be a detailed analysis of liquid-solid contact at surface

temperatures above the maximum liquid temperature to more clearly understand the process.

2. The generalized post critical heat transfer correlation presented in this research can be further improved by reexamining the linear approximation to the X_A vs X_E curve with the possibility of using instead a polynomial curve fitting procedure. It was noted that the approximate vapor temperature was quite sensitive to how well the approximation resembled the actual curve. Luckily, this sensitivity was not wholly transferred to the predicted heat flux.

APPENDIX A

Estimation of Heat Losses for Transient Test Section (Design 1 and 2)

From Fig 5 heat interactions between the test specimen and its environment can occur via three means: first, conduction radially through the cup, across the air cap to the exposed area of the test piece; second, conduction at contact points between the specimen and the cover assembly and third, at the contact point of the specimen and textolite spacer separating the specimen from the brass base. The following presents idealized models to estimate the heat flow resistance for the three cases.

A.1 Heat Interactions common to transient Design 1 and 2

radial heat interaction:

Figure A1 presents the model used to calculate this interaction. The model assumes heat can be transferred to the copper wall from outside through the insulation and through direct contact with the brass base which has a high heat capacity. The heat that reaches the copper wall is then transferred across the air gap to the test specimen. The gap is broken into two resistances: a conduction resistance and a convection resistance to account for the natural circulation.

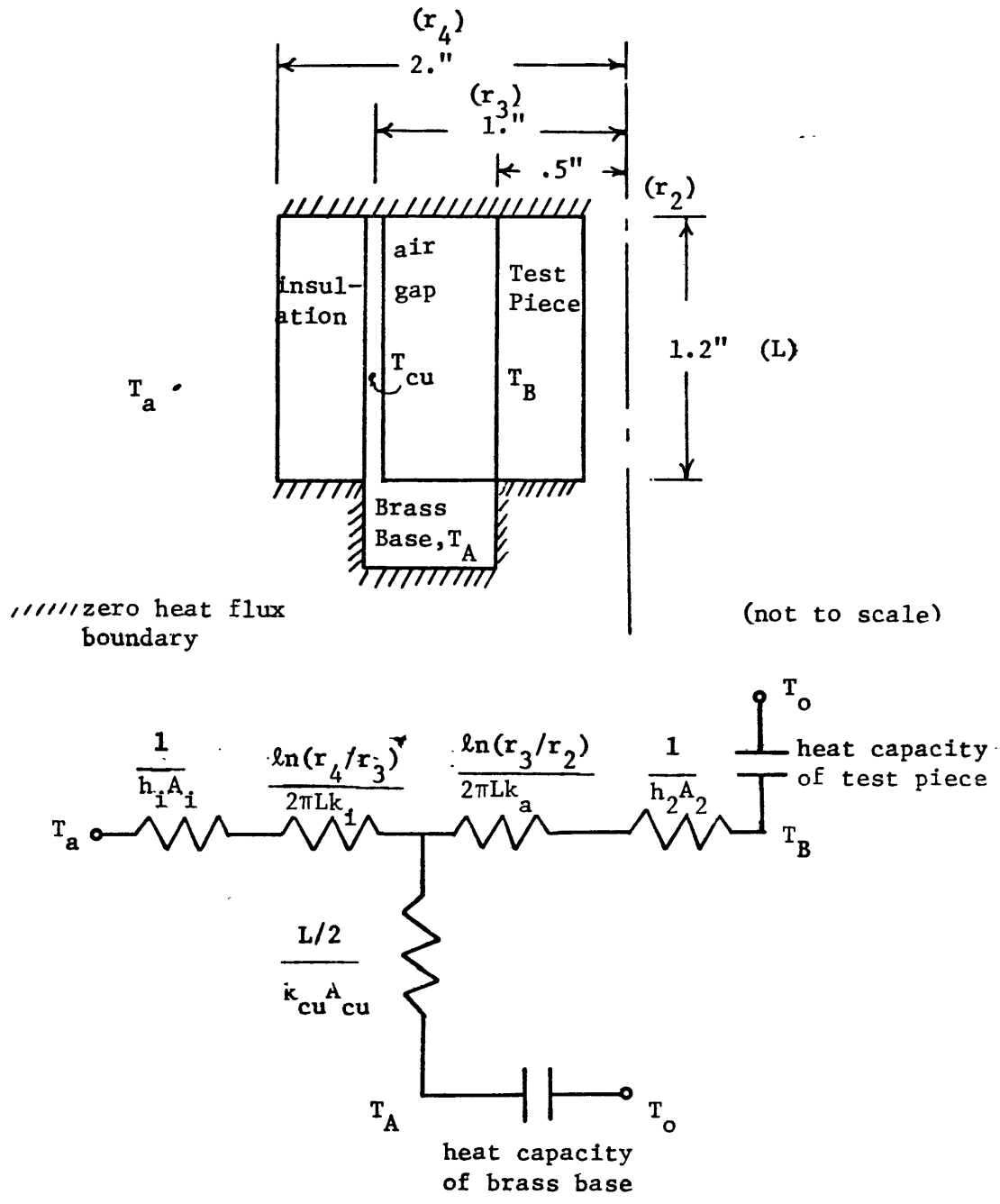

FIGURE A1 PICTORAL REPRESENTAION AND RESISTANCE NETWORK MODEL OF RADIAL HEAT INTERACTION WITH TEST PIECE AND ENVIRONMENT

Substituting in the values for each resistance gives

$$a)\ \frac{1}{h_1 A_1} \simeq 5\ \frac{^oF - Hr}{Btu}$$

$$b)\ \frac{\Delta X}{k_{cu} A_{cu}} \simeq .09\ \frac{^oF - Hr}{Btu}$$

$$c)\ \frac{\ell n\ (D_4/D_3)}{2\pi\ L\ k_i} \simeq 22\ \frac{^oF - Hr}{Btu} \qquad (A.1)$$

$$d)\ \frac{\ell n\ (D_3/D_2)}{2\pi\ L\ k_a} \simeq 41\ \frac{^oF - Hr}{Btu}$$

$$e)\ \frac{1}{h_2 A_2} \simeq 20\ \frac{^oF - Hr}{Btu}$$

As the resistance from T_a to T_{cu} is so much larger than the resistance from T_A to T_{cu} we can neglect it. Furthermore we can assume that $T_A = T_{cu}$. The radial heat transfer becomes

$$q_{Rad} = (T_A - T_B)/61\ [Btu/hr] \qquad (A.2)$$

Cover-Specimen Interaction:

The cover-specimen interaction is very difficult to estimate as there are a number of forces at play which could result in either heat gain or loss depending on the dominant force. The problem centers on whether the micarta-cap assembly quenches before the test specimen after the steam is shut off. This translates to a heat gain if the cover

assembly remains higher than the specimens or a heat loss if the cover assembly is always lower in temperature than the test piece. There is also a distinct possibility of continuous liquid contact of the micarta spacing even during the heat up period because the low conductivity causes the micarta area exposed to the nitrogen flow to act like a cold spot. This would cause a heat loss even during the initial portion of the transient where normally one would expect no heat losses or gains due to the uniformity of all temperatures. Figure A2 presents a conceptual model of the entire cover-specimen interaction which gives a clearer picture of the processes described.

Figure A2a indicates that the heat loss or gain is dependant on T_m, some average temperature inside the micarta spacing. This temperature is influenced by the surface temperature of the micarta exposed to the flowing nitrogen indicated as $T_{coldspot}$ as well as the average temperature of the brass cap, T_A. In order to estimate the behavior of this system it is assumed that only two mutually exclusive processes can occur. Either $T_{coldspot} = T_m$ resulting in the conduction path being brass cap to micarta to rubber O-ring to specimen or $T_{coldspot} = T_{sat}$ resulting in conduction path being from $T_{coldspot}$ through short length of micarta, through rubber O-ring to specimen. The first of these two cases is given in Figure A2b. The resistances

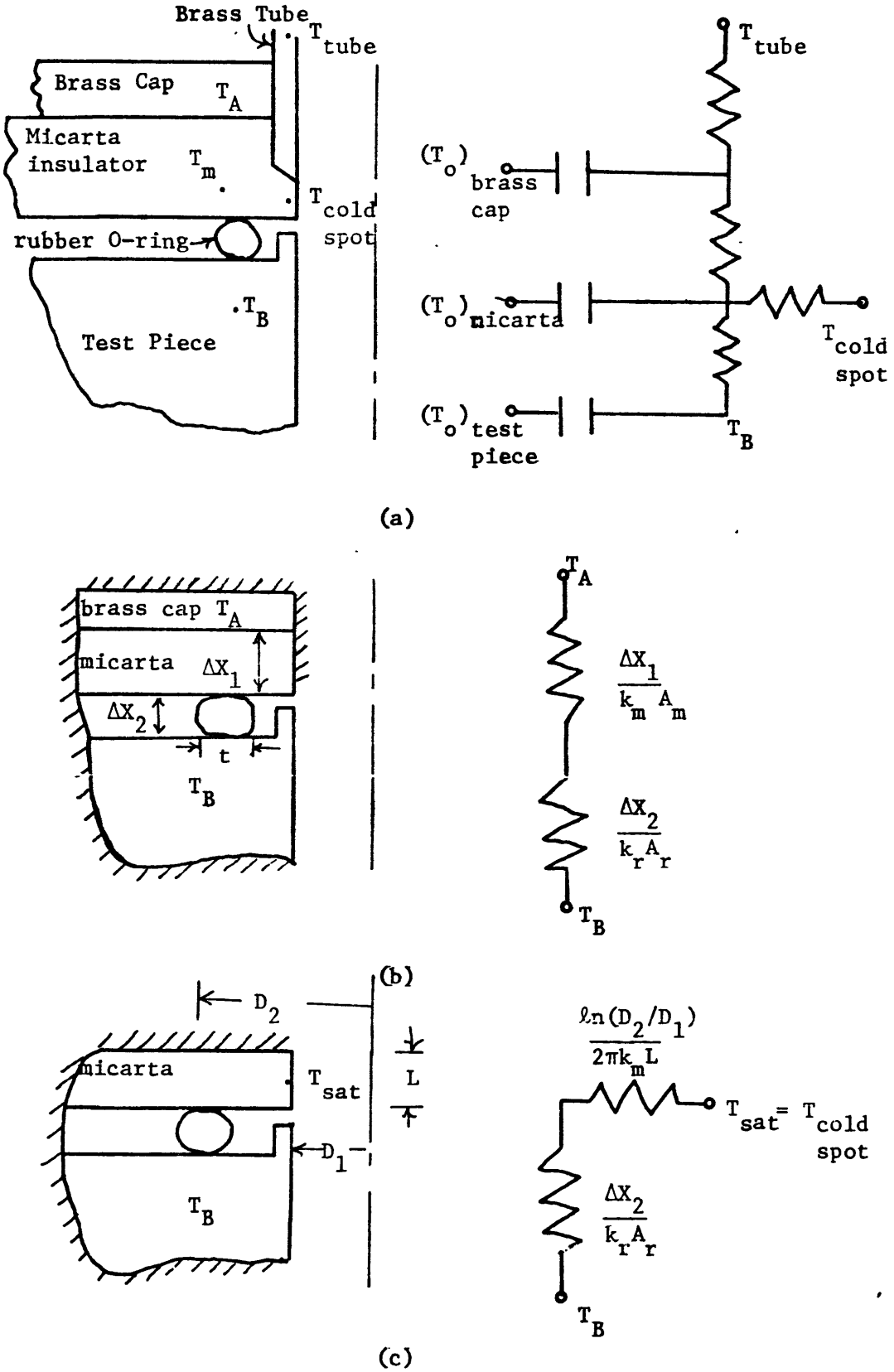

FIGURE A2 BRASS CAP - TEST SPECIMEN HEAT TRANSFER INTERACTION FOR DESIGN 1 and 2

are simply

$$a)\ \frac{\Delta X_1}{k_m A_m} = \frac{\Delta X_1}{k_m \pi (r_2^2 - r_2^2)} = 18\ \frac{hr\text{-}^oF}{Btu} \qquad (A.3)$$

$$b)\ \frac{\Delta X_2}{k_r A_r} = \frac{\Delta X_2}{k_r \pi D_3 t} = 24\ \frac{hr\text{-}^oF}{Btu}$$

This gives the heat gain for Case 1 as

$$q_{cup_1} = \frac{(T_A - T_B)}{42}\ [Btu/hr.] \qquad (A.4)$$

Figure A2c gives the circuit diagram for the second case where $T_{coldspot}$ is assumed equal to T_{sat}.

The resistances are

$$\frac{\ell n(D_2/D_1)}{2\pi k_m L} = 9\ \frac{hr^oF}{Btu}$$

$$\frac{\Delta X_2}{k_r A_r} = 24\ \frac{hr^oF}{Btu} \quad \text{from (A.3.a)}$$

This gives the heat loss for case 2 as

$$q_{cup_2} = -\frac{(T_B - T_{sat})}{57} \qquad (A.5)$$

A.2 Heat interactions of test piece to base

A.2.1 Design 1

Figure A3a indicates how we tried to cut the heat losses down through the fin protruding from the base of the test specimen with a micarta sleeve.

An upper bound of the heat loss can be found by assuming that the two surfaces of the micarta contacting the inconel is at the temperature of the brass base, T_A, and that the two surfaces touching the fin are at the test piece temperature. Figure A3b indicates the geometry.

The upper bound on the heat transfer from the base is approximately

$$q_{\substack{\text{upper}\\ \text{limit}}} = (A_1 + A_2) \frac{k_m (T_A - T_B)}{\delta} \qquad (A.7)$$

where $A_1 = \pi D_1 L$

$$A_2 = \pi (r_1^2 - r_2^2)$$

Substituting in the appropriate dimensions gives the upper limit as

$$q_{\substack{\text{upper}\\ \text{limit}}} = .3(T_A - T_B) \qquad (A.8)$$

Figure A3c gives an approximation for the calculation of the lower bound on the heat transfer up through the base. The lower bound becomes

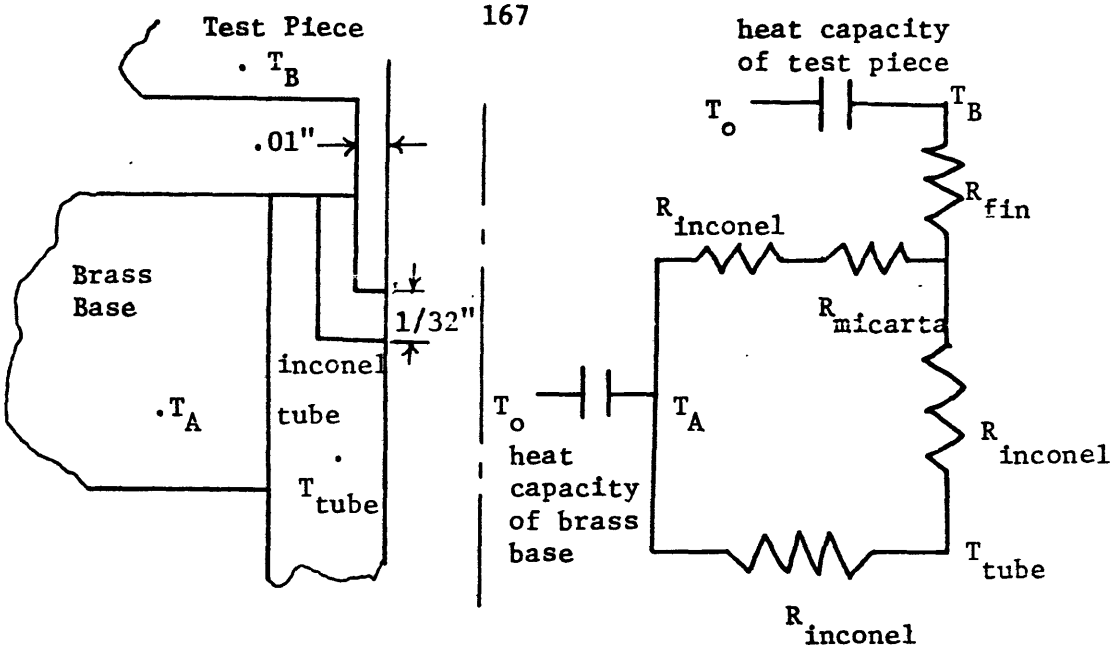

(a)

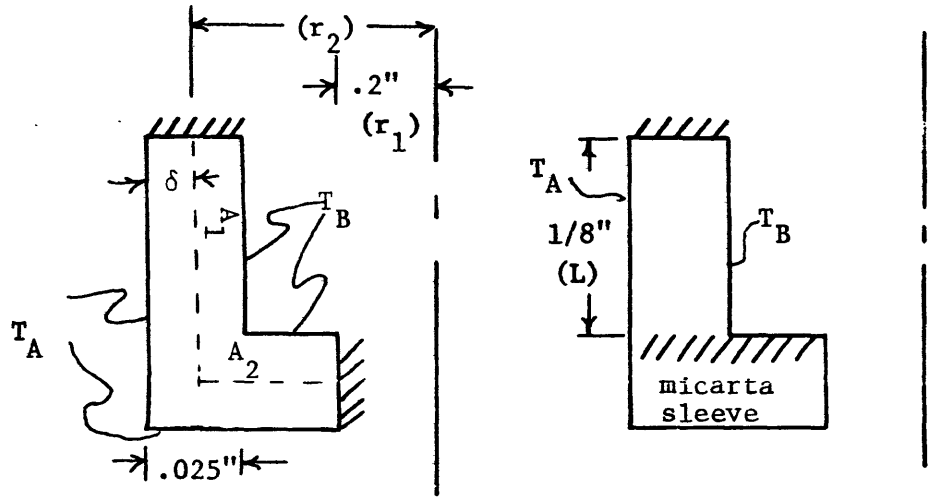

Upper Limit

(b)

Lower Limit

(c)

/////// zero heat flux boundary

(not to scale)

FIGURE A3 INTERACTION OF TEST PIECE WITH BRASS BASE FOR TRANSIENT DESIGN 1

$$q_{\substack{\text{lower}\\ \text{limit}}} = \frac{(T_A - T_B)}{\frac{\ln(r_2/r_1)}{2\pi L k_m}} \qquad (A.9)$$

substituting in the appropriate values gives

$$q_{\substack{\text{lower}\\ \text{limit}}} = .05\ (T_A - T_B) \qquad (A.10)$$

A.2.2 Design 2

The only difficulty involved in estimating the heat interaction between the base and test piece for this design is the section where the copper sleeve, textolite and test piece come together as shown in Figure A4. Here it is assumed that the copper sleeve is at the temperature of the brass base and the conduction length separating it from the test piece is 1/3 of that used for each of the other two resistances. These resistances are

$$\text{a)}\ \frac{\Delta x_1}{k_m A_1} = \frac{.25}{.2\pi D_1 t} = 95\ \frac{^oF\text{-Hr}}{Btu} \qquad (A.11)$$

$$\text{b)}\ \frac{\Delta x_1}{k_m A_2} = \frac{.25}{.2\pi D_2 t} = 110\ \frac{^oF\text{-Hr}}{Btu}$$

$$\text{c)}\ \frac{\Delta x_2}{k_m A_3} = \frac{.25/_3}{.2\pi D_3 t} = 70\ \frac{^oF\text{-Hr}}{Btu}$$

The heat gain up through the base becomes

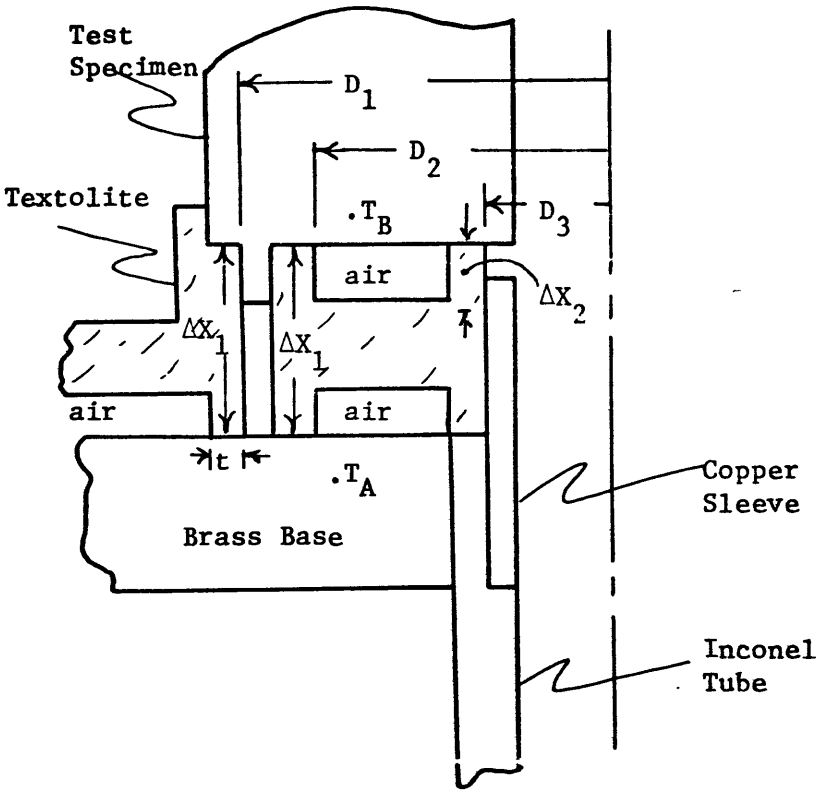

(Not to Scale)

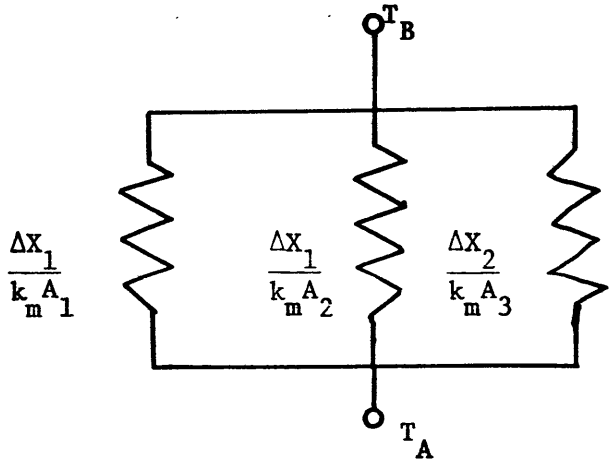

FIGURE A4 INTERACTION OF TEST PIECE WITH BRASS BASE FOR TRANSIENT DESIGN 2

$$q_{Base} = (T_A - T_B) \left[\frac{1}{95} + \frac{1}{110} + \frac{1}{70} \right]$$

$$q_{Base} = .023 \, [T_A - T_B] \qquad (A.12)$$

A.3 Summary of heat interactions

A.3.1 Design 1

The results are separated into two catagories. The first catagory includes the assumption that the brass cover and base quench down at the same rate so that their temperatures are equal and that the liquid does not attach itself to the micarta. The summation of heat gains calculated by (A.2), (A.4) and 1.5 times the heat transfer given by (A.10) results in the total heat gain as a function of the temperature difference between the test piece and brass base for the case of no liquid attachment to be

$$(q_{gain\ 1})_{N.L.A.} = .106 \, (T_{brass\ base} - T_{specimen}) \qquad (A.13)$$

Equation (A.13) is probably valid for all data runs except those of high mass flux and moderate to low quality.

The second catagory which takes care of the high mass flux and moderate to low quality runs contains the assumption

that the complete cover assembly is at T_{sat}. The summation of heat gains calculated by (A.2) and 1.5 times (A.10) with (A.6) results in equation (A.14) for the case of liquid attachment.

$$(q_{gain\ 1})_{L.A.} = (.09)\ (T_{brass\ base} - T_{specimen}) - .04(T_{specimen} - T_{sat}) \qquad (A.14)$$

These results indicate that the data from Design 1 transient section will be accurate at the initial portions of each transient where $(T_{brassbase} - T_{specimen})$ is low if no rewetting of the micarta takes place. In most of the runs of this type the specimen quenched faster than the brass base with the difference never exceeding $200^{o}F$. The maximum initial error for the case where rewetting of the micarta is assumed is 20 Btu/hr obtained by substituting $T_{specimen} = T_{Brassbase} = 212^{o}F$ and $T_{sat} = -320^{o}F$ into equation (A.14). A general value for the film boiling heat transfer for this case is 200 Btu/hr. The error is 10%.

A.3.2 Design 2

This design cut the heat gains in through the test specimen by at least a factor of 3. The respective equations for the two cases described in Section A. 3.1 for design 2 are

$$(q_{gain\ 2})_{N.L.A.} = .063\ (T_{brassbase} - T_{specimen}) \qquad (A.15)$$

$$(q_{gain\ 2})_{L.A.} = .039\ (T_{brassbase} - T_{specimen}) - .04\ (T_{specimen} - T_{sat}) \quad (A.16)$$

We are not able to quantify the heat losses very well from these equations as the brass base temperatures was not recorded during the data runs. The closest indication we have of the behavior of the brass base is from the thermocouples placed on the preheater at the exit as shown in Figure 5. The thermocouple was influenced to a much greater extent by the tube than by the brass base. It did show, however, a gradual decrease after steam was shut off.

A maximum value of the heat gains for design 1 and 2 can be estimated by substituting a value of 200 ^{o}F for ($T_{brass\ base} - T_{specimen}$) into equations (A.13) and (A.15). This gives a maximum heat gain for design 1 of 20 Btu/hr and a maximum heat gain for design 2 of 12 Btu/hr. These values of heat gain are present near the end of each transient quench test. The film boiling heat fluxes in this range (ΔT_{sat} on the order of 50 - 100 ^{o}F) is 1000 Btu/hr-Ft^{2}. The respective errors for the two designs are, therefore, 200 and 100%. These errors drop off sharply for higher wall superheat data where ($T_{brass\ base} - T_{specimen}$) is small. It is concluded that all transient data with wall superheats above 200 ^{o}F will be free from heat gains.

APPENDIX B

Determination of System Variables and Experimental Errors

B.1 System Variables

The important system variables calculated in the experimental program are mass flux, equilibrium quality to the transient section and the saturation temperature of liquid nitrogen at the transent section. The uncertainties in these are related to the independant quantities which go into their evaluation. This section presents the equation used in the determination of the quantities described above and tabulates the estimated errors for each. This is achieved using the principle of superposition of errors (Topping[25]).

Mass Flux:

The mass flux is obtained by measuring the flow rate of the evaporated nitrogen via two rotometers in parallel. The rotometers were calibrated with water over the entire scale of each meter. The following equation resulted.

$$G = 1.143 \times 10^{3} \{ -1.0806 + .07796 (R_{\text{scale } 1})] + [.1116 + .199 (R_{\text{scale } 2})] \cdot [(500 - \rho_{n_2})\rho_{n_2}]^{1/2} \quad (B.1)$$

where the scale range for each rotometer is

Rotometer	Range	Increment
1	0-250	2
2	0-100	1

The density of gaseous nitrogen, ρ_{n_2} is obtained from the perfect gas relationship.

$$\rho_{n_2} = 2.61 \frac{P_{n_2}}{T_{n_2}} \qquad (B.2)$$

The estimated uncertainties for the independant quantities for G are given in Table B.1

Variable	Uncertainty
P_{n_2}	6%
T_{n_2}	1%
Scale reading 1	2%
Scale reading 2	2%

Table B.1

From Topping[24] the error in G due to the errors in its independant variables can be determined from

$$\delta G = \left|\frac{\partial G}{\partial P_{n_2}} \delta P_{n_2}\right| + \left|\frac{\partial G}{\partial T_{n_2}} \delta T_{n_2}\right| + |\cdots| \text{ etc} \qquad (B.3)$$

taking representative values for P_{n_2}, T_{n_2}, Scale reading 1 and 2 and performing the operations indicated by (B.3) gives

$$\frac{\delta G}{G} = .09 \qquad \text{(B.4)}$$

Preheater Exit Quality:

Preheater exit quality is calculated thermodynamically knowing the inlet subcool, preheater heat and unheated lengths, insulation losses, preheater power, and mass flux. The preheater exit quality is assumed to be the quality of the transient section. This quality is determined from (B.5).

$$X = \frac{120}{84\ G}\left[(QIN + DLOSS)\ (L_{heated} - DLENT) + 2.73\ L_{unheated}\right] \qquad \text{(B.5)}$$

where

$$QIN = \frac{2607.34\ (Volt)(Amp)}{L_{heated}} \quad \text{[power to preheater]}$$

$$DLOSS = \frac{1.23\ (75 - T_{wall\ average})}{1.65} \quad \text{[insulation gains]}$$

$$DLENT = .5(\Delta T_{s.c})\ /120\ (QIN + DLOSS) \quad \text{[position of zero quality]}$$

The estimated uncertainties for the independant quantities for X are given in Table B.2

Variable	Uncertainty
Volt	1/2%
Amp	1/2%
L_{heated}	1/2%

$\Delta T_{s.c.}$	1/2%
G	9%

Table B.2

Using the method of superposition of errors gives

$$\frac{\delta X}{X} = .01 \qquad \text{(B.6)}$$

B.2 Heat transfer data.

All heat transfer data is obtained from the transient section and consists of the surface heat flux vs. surface wall super heat. This is obtained from the temperature - time transient assuming lumped heat capacity. The heat flux and wall superheat assuming no losses are given by (B.7) and (B.8)

$$q/A = \frac{V}{A}\,\rho(a + bT(i + n/2))\,\left[\frac{T(i) - T(i + n)}{\Delta t}\right]$$

$$(T_w - T_{sat}) = T(i + n/2) - T_{sar} \qquad \text{(B.7)}$$

where i = 1,2,3 +

n = number of points over which the slope is averaged.

a,b = coefficients for a linear temperature dependance of

C_p vs T(i)

Δt = time interval

The assumption of no heat losses has been shown in Appendix A to be extremely bad in certain instances which has been discussed. For the data considered to be free of heat losses, thermocouple errors and measurement errors are the major sources of error. Table B.3 gives the thermocouple calibration check for the three thermocouples used in the measurement of transient thermal history.

The therocouples deviate from the standard thermocouples tables only near the saturation temperatures of liquid nitrogen. Thermocouples 1 & 2 are recorded on a Leeds & Northrup Speedomax W strip chart recorder which can be read to .05 millivolts or $5^{\circ}F$ at liquid nitrogen temperatures ($-300^{\circ}F$) and $2^{\circ}F$ at steam temperatures ($200^{\circ}F$). The data thermocouple (#2) is amplified, recorded on FM tape and subsequently digitized and converted to temperatures on the computer. Although there is no human interpolalian errors, the resolution of the digitizing process is only .01 millivolts. This is 1/5 of the error inherent in the strip chart recorder. From this discussion the errors associated with q/A and $(T_w - T_{sat})$ within the assumption of no heat losses is on the order of 3%. This includes errors of non uniformity of temperature resulting from the high Biot number associated with the Inconel-600 piece.

Temperature Source	Thermocouple (See Fig. 5)	Thermocouple Reading (Mv)	Temperature (^{o}F) (Ref 26)
liquid nitrogen (-320.6^{o}F)			
	1	-5.51	-325.
	2 (data)	-5.51	-325
	3	-5.52	-326
ice (32.2^{o}F)			
	1	0.0	32.2
	2 (data)	0.0	32.2
	3	0.0	32.2
steam (212^{o}F)			
	1	4.285	212.2
	2 (data)	4.288	212.5
	3	4.285	212.2

Thermocouple Calibration

TABLE B.3

APPENDIX C

Tabulation of Transient Data

Explanatory remarks:

G .....mass flux at entrance to transient section

X .....X_E at entrance to transient section

TSAT .....T_{sat} at entrance to transient section

LDO .....L_{DO}, length of dryout in preheater

PREHEATER Q/A .heat flux in preheater that generated X

(TW -TSAT).....($T_{wall} - T_{sat}$) recorded during quench by thermocouple 2

TIME .....Time from start of quench

Q/A .....Corresponding q/A calculated from Equation (B.7)

Warning: Consider heat flux data at wall superheats of 250 ^{o}F and less as faulty due to heat gains for Runs with an LDO less than 5 inches. (see Appendix A)

RUN 73

G: 217592. LBM/HR-SQ.FT. TSAT: =315.8 (F)
X: 9.4 % LDO: 2. INCHES
PREHEATER Q/A: 1751.9 BTU/HR-SQ.FT.
SPECIMEN MATERIAL: ALUMINUM 1100
FINISH: SMOOTH APP. 50 μ INCH

TIME (MINUTES)	(TW - TSAT) (DEGREES F)	Q/A (BTU/HR-SQ.FT.)
0.128	540.8	13538.
0.256	479.3	15409.
0.384	459.2	15875.
0.512	439.0	14263.
0.640	420.7	13036.
0.768	403.5	11980.
0.896	387.8	11093.
1.024	372.8	10329.
1.152	359.0	9484.
1.280	346.4	7504.
1.408	337.8	5744.
1.536	330.1	5792.
1.664	321.3	6954.
1.792	310.2	7992.
1.920	298.3	8947.
2.048	286.9	7725.
2.176	275.8	7474.
2.304	265.0	6992.
2.432	255.2	6652.
2.560	245.2	6349.
2.688	236.3	6817.
2.944	218.8	6875.
3.456	181.2	5930.

RUN 90

G: 213785. LBM/HR-SQ.FT. TSAT: =314.9 (F)
X: 87.7 % LDO: 4. INCHES
PREHEATER Q/A: 10541.8 BTU/HR-SQ.FT.
SPECIMEN MATERIAL: COPPER
FINISH: SMOOTH APP. 50 μ INCH

TIME (MINUTES)	(TW - TSAT) (DEGREES F)	Q/A (BTU/HR-SQ.FT.)
0.213	510.3	21457.
0.427	469.3	25364.
0.640	430.1	23842.
0.853	393.1	21804.
1.067	359.7	18564.
1.280	332.6	15865.
1.493	307.6	14937.
1.707	283.2	14203.
1.920	260.3	12916.
2.133	239.9	11595.
2.347	221.2	10677.
2.560	203.7	9302.
2.773	189.5	7831.
2.987	176.9	7016.
3.200	165.4	6383.
3.413	154.9	5901.
3.627	145.2	4787.
3.840	138.3	4087.
4.053	130.8	3676.
4.267	125.5	3039.
4.480	120.2	2863.
4.907	111.6	2256.
5.760	98.7	1571.
7.467	83.5	878.

RUN 91

G: 214213. LBM/HR-SQ.FT. TSAT: =315.8 (F)
X: 39.5 % LDO: 2. INCHES
PREHEATER Q/A: 7232.1 BTU/HR-SQ.FT.
SPECIMEN MATERIAL: COPPER
FINISH: SMOOTH APP. 50 μ INCH

TIME (MINUTES)	(TW - TSAT) (DEGREES F)	Q/A (BTU/HR-SQ.FT.)
0.213	524.2	24103.
0.427	460.2	27949.
0.640	415.6	26582.
0.853	374.7	23201.
1.067	340.3	19347.
1.280	311.3	17343.
1.493	283.4	16303.
1.707	257.7	14602.
1.920	234.7	12996.
2.133	213.1	11622.
2.347	194.5	10272.
2.560	178.7	8999.
2.773	163.6	7655.
2.987	151.6	6848.
3.200	139.9	6162.
3.413	130.2	5197.
3.627	121.8	4640.
3.840	114.8	4057.
4.053	107.4	3451.
4.267	101.9	3018.
4.480	97.2	2587.
4.907	88.6	2183.
5.760	75.5	1687.

RUN 92

G: 214213. LBM/HR-SQ.FT. TSAT: =314.6 (F)
X: 19.7 % LDO: 2. INCHES
PREHEATER Q/A: 3684.1 BTU/HR-SQ.FT.
SPECIMEN MATERIAL: COPPER
FINISH: SMOOTH APP. 50 μ INCH

TIME (MINUTES)	(TW - TSAT) (DEGREES F)	Q/A (BTU/HR-SQ.FT.)
0.213	499.8	22618.
0.427	461.2	23133.
0.640	426.5	20757.
0.853	394.2	18841.
1.067	365.7	16506.
1.280	341.1	14286.
1.493	318.9	13712.
1.707	295.9	13412.
1.920	274.4	12251.
2.133	255.0	11408.
2.347	236.1	10309.
2.560	220.2	9141.
2.773	205.1	8220.
2.987	192.2	7253.
3.200	180.3	6616.
3.413	169.5	5985.
3.627	159.7	5301.
3.840	151.2	4970.
4.053	142.5	4438.
4.267	135.8	3653.
4.480	129.2	3474.
4.907	118.3	2890.
5.760	102.3	1972.
7.467	80.3	1283.

RUN 93

G: 214213. LBM/HR-SQ.FT. TSAT: =314.8 (F)
X: 9.9 % LDO: 2. INCHES
PREHEATER Q/A: 1815.2 BTU/HR-SQ.FT.
SPECIMEN MATERIAL: COPPER
FINISH: SMOOTH APP. 50 μ INCH

TIME (MINUTES)	(TW - TSAT) (DEGREES F)	Q/A (BTU/HR-SQ.FT.)
0.213	508.7	18814.
0.427	466.5	20526.
0.640	434.1	19150.
0.853	405.7	17314.
1.067	378.7	16130.
1.280	353.7	14386.
1.493	332.8	12401.
1.707	313.2	11117.
1.920	295.5	10698.
2.133	277.9	10765.
2.347	259.8	10829.
2.560	241.8	10236.
2.773	225.5	9297.
2.987	210.5	8429.
3.200	197.0	7689.
3.413	184.4	6897.
3.627	173.5	6290.
3.840	162.9	5833.
4.053	153.5	5323.
4.267	144.6	4815.
4.480	136.9	4283.
4.907	123.2	3690.
5.760	101.4	2627.

RUN 94

G: 213388. LBM/HR-SQ.FT. TSAT: =314.5 (F)
X: 57.5 % LDO: 96. INCHES
PREHEATER Q/A: 10735.9 BTU/HR-SQ.FT.
SPECIMEN MATERIAL: COPPER
FINISH: SMOOTH APP. 50 μ INCH

TIME (MINUTES)	(TW - TSAT) (DEGREES F)	Q/A (BTU/HR-SQ.FT.)
0.267	488.4	19229.
0.533	446.8	19691.
0.800	410.1	17129.
1.067	378.0	15077.
1.333	349.0	12385.
1.600	327.4	10120.
1.867	307.4	9410.
2.133	288.5	8758.
2.400	271.0	7900.
2.667	255.5	7198.
2.933	240.8	6289.
3.200	229.0	5463.
3.467	217.7	4927.
3.733	208.1	4372.
4.000	199.1	3939.
4.267	191.3	3485.
4.533	184.2	3011.
4.800	178.4	2727.
5.067	172.5	2582.
5.333	167.3	2090.
5.600	163.5	1949.
6.133	155.1	1689.
7.200	144.1	1050.
9.333	130.4	704.

RUN 95

G: 214076. LBM/HR-SQ.FT. TSAT: =314.8 (F)
X: 75.6 % LDO: 96. INCHES
PREHEATER Q/A: 14284.3 BTU/HR-SQ.FT.
SPECIMEN MATERIAL: COPPER
FINISH: SMOOTH APP. 50 μ INCH

TIME (MINUTES)	(Tw - TSAT) (DEGREES F)	Q/A (BTU/HR-SQ.FT.)
.267	491.5	20719.
.533	444.6	22744.
.800	401.0	19816.
1.067	364.8	16053.
1.333	335.7	12606.
1.600	313.1	10733.
1.867	291.4	10185.
2.133	270.8	9264.
2.400	252.7	8311.
2.667	235.9	7275.
2.933	222.0	6160.
3.200	209.8	5480.
3.467	198.7	4782.
3.733	189.4	4021.
4.000	181.5	3545.
4.267	174.2	3095.
4.533	168.2	2625.
4.800	162.9	2296.
5.067	158.3	2131.
5.333	153.7	1791.
5.600	150.6	1803.
6.133	142.7	1568.
7.200	133.0	1035.

RUN 96

G: 214672. LBM/HR-SQ.FT. TSAT: =315.5 (F)
X: 40.1 % LDO: 48. INCHES
PREHEATER Q/A: 14795.3 BTU/HR-SQ.FT.
SPECIMEN MATERIAL: COPPER
FINISH: SMOOTH APP. 50 μ INCH

TIME (MINUTES)	(Tw - TSAT) (DEGREES F)	Q/A (BTU/HR-SQ.FT.)
.267	476.4	14396.
.533	447.5	14107.
.800	420.3	12480.
1.067	397.5	10715.
1.333	377.1	9766.
1.600	357.9	8340.
1.867	343.1	6889.
2.133	329.7	6279.
2.400	317.3	5966.
2.667	305.1	5776.
2.933	293.4	5564.
3.200	282.8	5498.
3.467	270.5	5145.
3.733	260.5	4486.
4.000	251.7	4213.
4.267	242.8	4272.
4.533	233.7	3883.
4.800	226.4	3308.
5.067	219.7	3018.
5.333	213.6	3060.
5.600	206.7	2748.
6.133	196.3	2471.
7.200	178.3	1829.

RUN 97

G: 213299. LBM/HR-SQ.FT. TSAT: =314.9 (F)
X: 21.8 % LDO: 48. INCHES
PREHEATER Q/A: 7854.1 BTU/HR-SQ.FT.
SPECIMEN MATERIAL: COPPER
FINISH: SMOOTH APP. 50 μ INCH

TIME (MINUTES)	(Tw - TSAT) (DEGREES F)	Q/A (BTU/HR-SQ.FT.)
.267	508.6	12785.
.533	480.4	13297.
.800	456.2	11748.
1.067	433.8	10599.
1.333	413.9	9494.
1.600	395.7	8777.
1.867	378.5	7773.
2.133	364.2	6833.
2.400	350.7	5974.
2.667	339.8	4833.
2.933	330.9	4480.
3.200	321.4	4808.
3.467	311.1	5012.
3.733	300.7	5215.
4.000	289.5	5294.
4.267	278.7	4774.
4.533	269.6	4403.
4.800	260.9	4295.
5.067	251.6	3924.
5.333	243.9	3491.
5.600	236.9	3532.
6.133	221.1	3386.
7.200	195.7	2664.
9.333	162.2	1577.

RUN 98

G: 123592. LBM/HR-SQ.FT. TSAT: =317.1 (F)
X: 70.8 % LDO: 48. INCHES
PREHEATER Q/A: 15029.7 BTU/HR-SQ.FT.
SPECIMEN MATERIAL: COPPER
FINISH: SMOOTH APP. 50 μ INCH

TIME (MINUTES)	(Tw - TSAT) (DEGREES F)	Q/A (BTU/HR-SQ.FT.)
.405	514.4	10811.
.811	478.2	10989.
1.216	448.5	8750.
1.621	425.3	7117.
2.027	405.2	6162.
2.432	387.6	5270.
2.837	372.8	4471.
3.243	360.0	4003.
3.648	348.2	3169.
4.053	340.3	2392.
4.459	333.1	2323.
4.864	325.8	2446.
5.269	317.8	2568.
5.675	309.7	2482.
6.080	302.2	2128.
6.485	296.9	1952.
6.891	289.7	1843.
7.296	284.4	1611.
7.701	279.5	1436.
8.107	275.3	1339.
8.512	271.2	1259.
9.323	262.9	1123.
10.944	252.3	791.

RUN 99

G: 123592. LBM/HR-SQ.FT. TSAT: =316.5 (F)
X: 40.9 % LDO: 48. INCHES
PREHEATER Q/A: 8572.2 BTU/HR-SQ.FT.
SPECIMEN MATERIAL: COPPER
FINISH: SMOOTH APP. 50 μ INCH

TIME (MINUTES)	(Tw - TSAT) (DEGREES F)	Q/A (BTU/HR-SQ.FT.)
.405	510.6	9775.
.811	480.3	9328.
1.216	454.7	7938.
1.621	432.4	6770.
2.027	413.6	5899.
2.432	396.4	5235.
2.837	381.5	4466.
3.243	368.9	4030.
3.648	356.6	3548.
4.053	346.9	2976.
4.459	338.1	2647.
4.864	330.4	2482.
5.269	322.6	2604.
5.675	314.1	2725.
6.080	305.5	2575.
6.485	297.9	2316.
6.891	290.9	2058.
7.296	284.9	2544.
7.701	277.8	2458.
8.107	269.3	1636.
8.512	264.4	1351.
9.323	257.8	1176.

RUN 100

G: 123592. LBM/HR-SQ.FT. TSAT: =316.3 (F)
X: 20.4 % LDO: 48. INCHES
PREHEATER Q/A: 4138.8 BTU/HR-SQ.FT.
SPECIMEN MATERIAL: COPPER
FINISH: SMOOTH APP. 50 μ INCH

TIME (MINUTES)	(Tw - TSAT) (DEGREES F)	Q/A (BTU/HR-SQ.FT.)
1.067	477.8	6813.
2.133	428.4	5508.
3.200	389.7	4305.
4.267	358.8	3257.
5.333	336.6	2474.
6.400	318.2	2268.
7.467	299.2	2171.
8.533	282.2	1854.
9.600	268.3	1417.
10.667	258.5	1222.
11.733	247.8	1087.
12.800	240.2	949.
13.867	231.8	887.
14.933	225.2	738.
16.000	219.3	825.
17.067	211.2	835.
18.133	205.1	604.
19.200	200.9	692.
20.267	193.3	819.
21.333	186.9	665.
22.400	181.9	542.
24.533	172.5	512.
28.800	156.8	418.

RUN 101

G: 30707. LBM/HR-SQ.FT. TSAT: -320.3 (F)
X: 18.4 % LDO: 3. INCHES
PREHEATER Q/A: 273.2 BTU/HR-SQ.FT.
SPECIMEN MATERIAL: INCONEL 600
FINISH: SMOOTH APP. 10 μ INCH

TIME (MINUTES)	(TW - TSAT) (DEGREES F)	Q/A (BTU/HR-SQ.FT.)
1.493	475.9	4025.
2.987	424.9	4843.
4.480	381.6	3906.
5.973	346.5	3255.
7.467	314.4	2937.
8.960	284.5	2570.
10.453	259.2	2138.
11.947	237.6	1767.
13.440	219.7	1517.
14.933	203.2	1314.
16.427	189.5	1192.
17.920	175.5	1025.
19.413	165.4	831.
20.907	155.8	812.
22.400	146.0	730.
23.893	138.2	614.
25.387	131.1	586.
26.880	123.9	558.
28.373	117.4	534.
29.867	110.7	612.
31.360	102.2	515.
34.347	93.4	299.
40.320	80.7	215.

RUN 102

G: 31677. LBM/HR-SQ.FT. TSAT: -320.3 (F)
X: 28.6 % LDO: 3. INCHES
PREHEATER Q/A: 273.3 BTU/HR-SQ.FT.
SPECIMEN MATERIAL: INCONEL 600
FINISH: SMOOTH APP. 10 μ INCH

TIME (MINUTES)	(TW - TSAT) (DEGREES F)	Q/A (BTU/HR-SQ.FT.)
1.493	450.6	4166.
2.987	398.8	4953.
4.480	352.4	4084.
5.973	315.1	3537.
7.467	277.9	3148.
8.960	246.9	2523.
10.453	221.9	2032.
11.947	200.9	1620.
13.440	184.6	1298.
14.933	170.6	1148.
16.427	157.5	989.
17.920	147.0	814.
19.413	137.9	700.
20.907	130.0	651.
22.400	122.0	585.
23.893	115.6	493.
25.387	109.8	470.
26.880	103.9	444.
28.373	98.7	382.
29.867	94.3	420.
31.360	88.1	457.
34.347	78.1	285.
40.320	69.7	155.

RUN 103

G: 30707. LBM/HR-SQ.FT. TSAT: -320.4 (F)
X: 49.9 % LDO: 3. INCHES
PREHEATER Q/A: 1318.6 BTU/HR-SQ.FT.
SPECIMEN MATERIAL: INCONEL 600
FINISH: SMOOTH APP. 10 μ INCH

TIME (MINUTES)	(TW - TSAT) (DEGREES F)	Q/A (BTU/HR-SQ.FT.)
0.427	478.3	17803.
0.853	432.4	17111.
1.280	383.6	16169.
1.707	339.8	14320.
2.133	299.0	12436.
2.560	264.1	10388.
2.987	234.0	8503.
3.413	209.6	6686.
3.840	190.3	5379.
4.267	173.9	4422.
4.693	160.6	3639.
5.547	139.7	2732.
6.400	122.7	2045.
7.253	111.0	1627.
8.107	99.6	1420.
8.960	90.6	1004.
9.813	85.1	829.
10.667	78.6	839.
11.520	72.8	587.
12.373	69.9	530.
13.227	65.0	465.
14.933	58.0	440.
16.640	51.9	309.

RUN 105

G: 30894. LBM/HR-SQ.FT. TSAT: -320.0 (F)
X: 69.4 % LDO: 3. INCHES
PREHEATER Q/A: 1833.1 BTU/HR-SQ.FT.
SPECIMEN MATERIAL: INCONEL 600
FINISH: SMOOTH APP. 10 μ INCH

TIME (MINUTES)	(TW - TSAT) (DEGREES F)	Q/A (BTU/HR-SQ.FT.)
0.427	496.7	8946.
0.853	471.6	8657.
1.280	450.0	7638.
1.707	429.9	6823.
2.133	412.2	6192.
2.560	395.1	6176.
2.987	377.1	6054.
3.413	360.3	5486.
3.840	345.2	4635.
4.267	333.0	4046.
4.693	321.2	3996.
5.547	296.8	3785.
6.400	275.0	3383.
7.253	254.8	3114.
8.107	235.8	2884.
8.960	217.9	2540.
9.813	202.8	2181.
10.667	189.3	1907.

RUN 109

G: 59526. LBM/HR SQ.FT. TSAT: -319.8 (F)
X: 39.0 % LDO: 3. INCHES
PREHEATER Q/A: 1906.4 BTU/HR-SQ.FT.
SPECIMEN MATERIAL: INCONEL 600
FINISH: SMOOTH APP. 10 μ INCH

TIME (MINUTES)	(TW - TSAT) (DEGREES F)	Q/A (BTU/HR-SQ.FT.)
1.280	459.7	8254.
2.560	394.2	6959.
3.840	341.1	5379.
5.120	299.0	4214.
6.400	264.1	3240.
7.680	238.2	2506.
8.960	216.1	2074.
10.240	197.7	1647.
11.520	183.5	1373.
12.800	170.3	1188.
14.080	159.5	960.
16.640	141.6	786.
19.200	126.9	735.
21.760	110.8	536.
24.320	104.1	458.
26.880	91.1	483.
29.440	83.1	350.
32.000	75.9	356.
34.560	67.8	297.
37.120	62.7	304.
39.680	54.0	375.
47.680	37.6	355.

RUN 107

G: 60917. LBM/HR-SQ.FT. TSAT: -319.8 (F)
X: 12.3 % LDO: 3. INCHES
PREHEATER Q/A: 640.6 BTU/HR-SQ.FT.
SPECIMEN MATERIAL: INCONEL 600
FINISH: SMOOTH APP. 10 μ INCH

TIME (MINUTES)	(TW - TSAT) (DEGREES F)	Q/A (BTU/HR-SQ.FT.)
0.880	460.6	6807.
1.760	420.8	6899.
2.640	384.7	5785.
3.520	352.6	4896.
4.400	325.6	4248.
5.280	300.3	3881.
6.160	276.9	3498.
7.040	255.6	3104.
7.920	236.6	2693.
8.800	220.1	2461.
9.680	203.7	2358.
11.440	174.3	1985.
13.200	148.7	1556.
14.960	130.2	1146.
16.720	115.7	898.
18.480	104.0	811.
20.240	91.8	710.
22.000	82.9	636.
23.760	72.7	617.
25.520	64.2	504.
27.280	57.4	1854.

RUN 110

G: 61341. LBM/HR-SQ.FT. TSAT: -320.8 (F)
X: 49.0 % LDO: 3. INCHES
PREHEATER Q/A: 2571.0 BTU/HR-SQ.FT.
SPECIMEN MATERIAL: INCONEL 600
FINISH: SMOOTH APP. 10 μ INCH

TIME (MINUTES)	(Tw - TSAT) (DEGREES F)	Q/A (BTU/HR-SQ.FT.)
0.960	466.2	8475.
1.920	414.4	7458.
2.880	372.1	6067.
3.840	335.6	4996.
4.800	305.5	4386.
5.760	275.8	3844.
6.720	251.9	3125.
7.680	231.4	2673.
8.640	213.3	2280.
9.600	198.0	2241.
10.560	180.1	1613.
12.480	167.9	907.
14.400	152.5	898.
16.320	140.3	720.
18.240	130.1	736.
20.160	117.1	776.
22.080	105.4	608.
24.000	97.6	460.
25.927	90.6	356.
27.840	86.1	361.
29.760	78.8	421.
35.760	56.7	297.

RUN 111

G: 62158. LBM/HR-SQ.FT. TSAT: -320.8 (F)
X: 68.4 % LDO: 3. INCHES
PREHEATER Q/A: 3636.8 BTU/HR-SQ.FT.
SPECIMEN MATERIAL: INCONEL 600
FINISH: SMOOTH APP. 10 μ INCH

TIME (MINUTES)	(Tw - TSAT) (DEGREES F)	Q/A (BTU/HR-SQ.FT.)
0.960	451.2	8890.
1.920	397.5	7818.
2.880	351.5	6421.
3.840	312.9	5062.
4.800	282.8	4397.
5.760	251.9	3598.
6.720	231.7	2827.
7.680	211.4	2372.
8.640	196.9	1938.
9.602	184.1	1689.
10.560	171.6	1436.
12.480	154.3	1098.
14.400	137.8	1005.

RUN 115

G: 60478. LBM/HR-SQ.FT. TSAT: -319.8 (F)
X: 90.3 % LDO: 3. INCHES
PREHEATER Q/A: 1669.7 BTU/HR-SQ.FT.
SPECIMEN MATERIAL: INCONEL 600
FINISH: SMOOTH APP. 10 μ INCH

TIME (MINUTES)	(Tw - TSAT) (DEGREES F)	Q/A (BTU/HR-SQ.FT.)
2.853	452.8	10678.
1.787	397.0	9233.
2.560	348.1	7378.
3.413	310.4	6187.
4.267	273.4	5452.
5.120	242.7	4408.
5.973	217.3	3383.
6.827	198.8	2973.
7.680	178.2	2827.
8.533	160.9	2200.
9.387	148.3	1931.
11.093	123.3	1418.
12.800	108.4	974.
14.507	95.5	915.
16.213	82.1	714.
17.920	74.7	575.
19.627	65.2	518.
21.333	59.4	498.
23.040	50.4	823.

RUN 117

G: 122799. LBM/HR-SQ.FT. TSAT: -319.1 (F)
X: 16.9 % LDO: 3. INCHES
PREHEATER Q/A: 1771.9 BTU/HR-SQ.FT.
SPECIMEN MATERIAL: INCONEL 600
FINISH: SMOOTH APP. 10 μ INCH

TIME (MINUTES)	(Tw - TSAT) (DEGREES F)	Q/A (BTU/HR-SQ.FT.)
0.160	504.2	5346.
0.320	498.9	9178.
0.480	486.0	12981.
0.640	472.9	11229.
0.800	463.4	8581.
0.960	455.5	7026.
1.122	449.0	5909.
1.282	443.4	5695.
1.440	437.3	5930.
1.600	431.2	5818.
1.760	426.9	3651.
2.080	419.3	4126.
2.400	409.6	4843.
2.720	398.9	4634.
3.040	389.9	4315.
3.360	380.4	4098.
3.680	372.9	3647.
4.000	364.7	4142.
4.320	354.3	4994.
4.640	342.8	5991.
4.960	327.8	6887.
6.460	243.9	6991.
7.900	171.8	5370.
9.460	116.8	5962.

RUN 118

G: 126478. LBM/HR-SQ.FT. TSAT: -318.8 (F)
X: 38.8 % LDO: 3. INCHES
PREHEATER Q/A: 3332.8 BTU/HR-SQ.FT.
SPECIMEN MATERIAL: INCONEL 600
FINISH: SMOOTH APP. 10 μ INCH

TIME (MINUTES)	(Tw - TSAT) (DEGREES F)	Q/A (BTU/HR-SQ.FT.)
0.160	503.4	14241.
0.320	486.1	17161.
0.480	469.0	17528.
0.640	450.7	17864.
0.800	432.5	17031.
0.960	415.4	16001.
1.120	398.9	15471.
1.280	382.6	14435.
1.440	367.9	13626.
1.600	353.0	12770.
1.760	339.9	11682.
2.080	315.2	10795.
2.400	291.2	10124.
2.720	268.7	9174.
3.040	248.4	8207.
3.360	229.8	7599.
3.680	211.8	6943.
4.000	195.9	5980.
4.320	182.2	5406.
4.640	168.8	5231.
4.960	155.7	5052.
5.960	117.8	8844.

RUN 119

G: 127269. LBM/HR-SQ.FT. TSAT: -318.5 (F)
X: 52.3 % LDO: 3. INCHES
PREHEATER Q/A: 6686.7 BTU/HR-SQ.FT.
SPECIMEN MATERIAL: INCONEL 600
FINISH: SMOOTH APP. 10 μ INCH

TIME (MINUTES)	(Tw - TSAT) (DEGREES F)	Q/A (BTU/HR-SQ.FT.)
0.160	500.8	13773.
0.320	482.7	18928.
0.480	462.9	19517.
0.640	443.0	19431.
0.800	422.9	18622.
0.960	404.2	17426.
1.120	386.0	16689.
1.280	368.5	15910.
1.440	351.5	14386.
1.600	336.9	13093.
1.760	322.5	12504.
2.080	295.0	11654.
2.400	269.2	10385.
2.720	246.5	8822.
3.040	227.3	7722.
3.360	209.2	7277.
3.680	192.6	6396.
4.000	177.5	5837.
4.320	163.3	5248.
4.640	150.8	4635.
4.960	139.5	4284.
5.960	107.6	6661.
6.960	30.2	6022.

RUN 120

G: 126851. LBM/HR-SQ.FT. TSAT: -318.4 (F)
X: 71.6 % LDO: 4. INCHES
PREHEATER Q/A: 7718.1 BTU/HR-SQ.FT.
SPECIMEN MATERIAL: INCONEL 600
FINISH: SMOOTH APP. 10 μ INCH

TIME (MINUTES)	(Tb - TSAT) (DEGREES F)	Q/A (BTU/HR-SQ.FT.)
0.160	521.6	13821.
0.320	483.4	19447.
0.480	462.7	20260.
0.640	442.3	19497.
0.800	422.5	18701.
0.960	403.3	17959.
1.120	384.5	16998.
1.280	366.9	15741.
1.440	350.4	14454.
1.600	335.1	13632.
1.760	320.1	12562.
2.080	294.6	11098.
2.400	269.3	10430.
2.720	245.9	9384.
3.040	224.7	8425.
3.360	205.2	7255.
3.680	189.1	6173.
4.000	174.5	5025.
4.320	163.8	4277.
4.640	152.8	4205.
4.960	142.2	3681.
6.242	111.3	2424.
7.520	90.7	1703.
8.800	74.4	1346.

RUN 122

G: 205430. LBM/HR-SQ.FT. TSAT: -316.6 (F)
X: 30.7 % LDO: 3. INCHES
PREHEATER Q/A: 5397.1 BTU/HR-SQ.FT.
SPECIMEN MATERIAL: INCONEL 600
FINISH: SMOOTH APP. 10 μ INCH

TIME (MINUTES)	(TW - TSAT) (DEGREES F)	Q/A (BTU/HR-SQ.FT.)
0.299	471.5	19864.
0.597	439.7	20871.
0.896	398.7	18695.
1.195	355.3	16354.
1.493	324.0	14304.
1.792	295.6	12949.
2.091	268.8	11784.
2.389	244.3	10595.
2.688	221.8	9198.
2.987	202.8	8305.
3.285	183.7	8514.
3.883	114.6	18367.
4.480	2.3	10473.

RUN 123

G: 204939. LBM/HR-SQ.FT. TSAT: -316.2 (F)
X: 19.2 % LDO: 3. INCHES
PREHEATER Q/A: 8612.6 BTU/HR-SQ.FT.
SPECIMEN MATERIAL: INCONEL 600
FINISH: SMOOTH APP. 10 μ INCH

TIME (MINUTES)	(TW - TSAT) (DEGREES F)	Q/A (BTU/HR-SQ.FT.)
0.299	468.7	28427.
0.597	422.8	22748.
0.896	380.3	20010.
1.195	342.6	17208.
1.493	309.5	14923.
1.792	279.7	13464.
2.091	251.4	12329.
2.389	225.3	10732.
2.688	203.1	9183.
2.987	183.2	8411.
3.285	163.9	7897.
3.883	128.5	11282.
4.480	53.9	12095.

RUN 125

G: 200980. LBM/HR-SQ.FT. TSAT: -316.8 (F)
X: 72.7 % LDO: 3. INCHES
PREHEATER Q/A: 12488.8 BTU/HR-SQ.FT.
SPECIMEN MATERIAL: INCONEL 600
FINISH: SMOOTH APP. 10 μ INCH

TIME (MINUTES)	(TW - TSAT) (DEGREES F)	Q/A (BTU/HR-SQ.FT.)
0.299	457.7	19498.
0.597	415.7	20397.
0.896	378.0	17739.
1.195	344.6	15221.
1.493	315.5	13261.
1.792	288.9	12127.
2.091	263.5	11191.
2.389	240.2	10106.
2.688	218.6	8968.
2.987	199.4	7753.
3.285	183.2	6767.
3.883	154.5	5302.
4.480	132.4	4032.
5.077	115.3	3123.
5.675	101.6	2388.
6.272	91.5	1860.
6.869	82.8	1461.
7.467	76.7	1135.
8.064	71.3	969.
8.661	66.7	801.
9.259	63.0	811.
11.648	45.7	980.

RUN 126

G: 200980. LBM/HR-SQ.FT. TSAT: -317.7 (F)
X: 10.5 % LDO: 3. INCHES
PREHEATER Q/A: 1868.4 BTU/HR-SQ.FT.
SPECIMEN MATERIAL: INCONEL 600
FINISH: SMOOTH APP. 10 μ INCH

TIME (MINUTES)	(TW - TSAT) (DEGREES F)	Q/A (BTU/HR-SQ.FT.)
0.299	482.4	15454.
0.597	449.3	16496.
0.896	419.3	14767.
1.195	391.7	13516.
1.493	365.5	11967.
1.792	343.2	10633.
2.091	321.7	10157.
2.389	300.7	9803.
2.688	280.1	9161.
2.987	261.1	8251.
3.285	243.9	7451.
3.883	212.9	6733.
4.480	182.6	6330.
5.077	153.9	6008.
5.675	125.2	14149.

RUN 131

G: 80691. LBM/HR-SQ.FT. TSAT: -319.8 (F)
X: 91.7 % LDO: 3. INCHES
PREHEATER Q/A: 4759.6 BTU/HR-SQ.FT.
SPECIMEN MATERIAL: ALUMINUM 1100
FINISH: SMOOTH APP. 30 μ INCH

TIME (MINUTES)	(TW - TSAT) (DEGREES F)	Q/A (BTU/HR-SQ.FT.)
0.533	408.8	7181.
1.067	369.8	5816.
1.600	341.0	5013.
2.133	310.5	4951.
2.667	281.5	4448.
3.200	256.2	3976.
3.733	232.4	3517.
4.267	212.2	3028.
4.800	194.1	2605.
5.333	178.9	2159.
5.867	166.2	1802.
6.933	146.1	1355.
8.000	130.7	1025.
9.067	118.9	797.
10.133	109.4	653.
11.200	101.4	567.
12.267	94.2	441.
13.333	89.5	379.
14.400	83.9	383.
15.467	79.1	389.
16.533	73.3	320.
21.533	57.2	214.
26.533	46.6	174.

RUN 132

G: 61872. LBM/HR-SQ.FT. TSAT: 319.6 (F)
X: 69.6 % LDO: 3. INCHES
PREHEATER Q/A: 3634.8 BTU/HR-SQ.FT.
SPECIMEN MATERIAL: ALUMINUM 1100
FINISH: SMOOTH APP. 30 μ INCH

TIME (MINUTES)	(TW - TSAT) (DEGREES F)	Q/A (BTU/HR-SQ.FT.)
0.533	47.9	868.
1.067	42.5	804.
1.600	37.2	677.
2.133	33.3	549.
2.667	29.5	555.
3.200	25.7	560.
3.733	21.8	423.
4.267	19.8	429.
4.800	15.9	431.
5.333	13.9	290.
5.867	11.9	366.
6.933	15.7	402.
8.000	10.5	418.
9.067	34.1	1396.

RUN 133

G: 59742. LBM/HR-SQ.FT. TSAT: 319.7 (F)
X: 51.6 % LDO: 2. INCHES
PREHEATER Q/A: 2637.8 BTU/HR-SQ.FT.
SPECIMEN MATERIAL: ALUMINUM 1100
FINISH: SMOOTH APP. 30 μ INCH

TIME (MINUTES)	(TW - TSAT) (DEGREES F)	Q/A (BTU/HR-SQ.FT.)
0.800	458.7	9392.
1.300	408.2	8147.
1.800	363.3	7315.
2.300	327.9	5961.
2.800	296.8	5224.
3.300	271.2	4449.
3.800	245.6	3574.
4.800	208.5	3385.
5.800	165.2	2657.

RUN 134

G: 61324. LBM/HR-SQ.FT. TSAT: 319.6 (F)
X: 19.8 % LDO: 2. INCHES
PREHEATER Q/A: 1036.6 BTU/HR-SQ.FT.
SPECIMEN MATERIAL: ALUMINUM 1100
FINISH: SMOOTH APP. 30 μ INCH

TIME (MINUTES)	(TW - TSAT) (DEGREES F)	Q/A (BTU/HR-SQ.FT.)
0.533	392.2	6098.
1.067	358.6	5102.
1.600	332.4	4397.
2.133	306.4	4066.
2.667	283.5	3677.
3.200	261.6	3520.
3.733	240.1	3197.
4.267	221.7	2753.
4.800	205.5	2662.
5.333	187.9	2440.
5.867	174.2	2049.
6.933	149.9	1628.
8.000	131.5	1261.
9.067	116.5	1117.
10.133	101.7	990.
11.200	89.9	922.
12.267	76.7	913.
13.333	65.0	872.
14.400	52.8	825.
15.467	42.1	1826.

RUN 135

G: 61968. LBM/HR-SQ.FT. TSAT: 319.6 (F)
X: 67.6 % LDO: 2. INCHES
PREHEATER Q/A: 3588.6 BTU/HR-SQ.FT.
SPECIMEN MATERIAL: INCONEL 600
FINISH: OXIDE COATING

TIME (MINUTES)	(TW - TSAT) (DEGREES F)	Q/A (BTU/HR-SQ.FT.)
0.533	417.1	11776.
1.067	378.2	10186.
1.600	343.9	8678.
2.133	314.3	7657.
2.667	286.3	7129.
3.200	259.5	6331.
3.733	236.6	5522.
4.267	215.4	4902.
4.800	196.8	4245.
5.333	180.4	3732.
5.867	165.6	3190.
6.933	141.6	2528.
8.000	122.0	2097.
9.067	104.8	1880.
10.133	88.4	1743.
11.200	73.2	1867.
12.267	54.2	3324.

RUN 136

G: 61329. LBM/HR-SQ.FT. TSAT: 319.7 (F)
X: 50.3 % LDO: 2. INCHES
PREHEATER Q/A: 2637.2 BTU/HR-SQ.FT.
SPECIMEN MATERIAL: INCONEL 600
FINISH: OXIDE COATING

TIME (MINUTES)	(TW - TSAT) (DEGREES F)	Q/A (BTU/HR-SQ.FT.)
0.533	405.1	11074.
1.067	368.2	9538.
1.600	336.2	8225.
2.133	307.3	7486.
2.667	279.6	6863.
3.200	254.3	6065.
3.733	231.8	5401.
4.267	211.0	4770.
4.800	192.9	4104.
5.333	177.1	3674.
5.867	162.1	3308.
6.933	137.0	2794.
8.000	113.7	2581.
9.067	91.3	2561.
10.133	67.4	3885.

RUN 137

G: 61329. LBM/HR-SQ.FT. TSAT: 319.9 (F)
X: 19.3 % LDO: 3. INCHES
PREHEATER Q/A: 1011.3 BTU/HR-SQ.FT.
SPECIMEN MATERIAL: INCONEL 600
FINISH: OXIDE COATING

TIME (MINUTES)	(TW - TSAT) (DEGREES F)	Q/A (BTU/HR-SQ.FT.)
0.533	421.5	9492.
1.067	390.5	8415.
1.600	361.5	7360.
2.133	337.2	6588.
2.667	312.8	6003.
3.200	291.8	5735.
3.733	268.9	5508.
4.267	248.9	4902.
4.800	230.1	4427.
5.333	213.3	3928.
5.867	198.1	3398.
6.933	172.2	2902.
8.000	149.3	2508.
9.067	129.1	2220.
10.133	110.5	2059.
11.200	92.6	2098.
12.267	72.7	2948.
13.333	38.5	3761.

RUN 138

G: 62432. LBM/HR-SQ.FT. TSAT: 319.9 (F)
X: 89.1 % LDO: 3. INCHES
PREHEATER Q/A: 4754.3 BTU/HR-SQ.FT.
SPECIMEN MATERIAL: INCONEL 600
FINISH: OXIDE COATING

TIME (MINUTES)	(TW - TSAT) (DEGREES F)	Q/A (BTU/HR-SQ.FT.)
0.533	432.9	9464.
1.067	401.8	8442.
1.600	373.2	7551.
2.133	347.4	6461.
2.667	325.8	5748.
3.200	304.6	5524.
3.733	285.9	5057.
4.267	265.6	4510.
4.800	248.7	4103.
5.333	233.1	3682.
5.867	219.2	3243.
6.933	196.4	2645.
8.000	175.5	2460.
9.067	155.1	2073.
10.133	140.1	1624.
11.200	127.0	1326.
12.267	116.9	1063.
13.333	108.3	786.
14.400	102.9	600.
15.467	97.5	504.
16.533	93.9	468.
21.533	74.0	382.
26.533	61.1	341.

RUN 139

G: 31866. LBM/HR-SQ.FT. TSAT: 320.1 (F)
X: 66.1 % LDO: 3. INCHES
PREHEATER Q/A: 1756.9 BTU/HR-SQ.FT.
SPECIMEN MATERIAL: INCONEL 600
FINISH: OXIDE COATING

TIME (MINUTES)	(TW - TSAT) (DEGREES F)	Q/A (BTU/HR-SQ.FT.)
0.533	423.5	6580.
1.067	401.1	6140.
1.600	380.1	5710.
2.133	360.1	5183.
2.667	342.4	4722.
3.200	325.3	4402.
3.733	309.5	4158.
4.267	293.9	3973.
4.800	279.1	3710.
5.333	265.2	3443.
5.867	252.2	3333.
6.933	227.9	2759.
8.000	207.8	2243.
9.067	191.2	1910.

RUN 140

G: 38641. LBM/HR-SQ.FT. TSAT: 320.1 (F)
X: 48.3 % LDO: 3. INCHES
PREHEATER Q/A: 1266.5 BTU/HR-SQ.FT.
SPECIMEN MATERIAL: INCONEL 600
FINISH: OXIDE COATING

TIME (MINUTES)	(TW - TSAT) (DEGREES F)	Q/A (BTU/HR-SQ.FT.)
0.533	441.6	7711.
1.067	416.8	7872.
1.600	392.1	6515.
2.133	369.6	5858.
2.667	349.8	5183.
3.200	331.6	4719.
3.733	314.7	4557.
4.267	297.3	4388.
4.800	281.3	4126.
5.333	265.5	3783.
5.867	251.8	3359.
6.933	227.2	2828.
8.000	206.3	2394.
9.067	188.8	2017.
10.133	172.7	1622.
11.200	160.7	1389.
12.267	149.1	1277.
13.333	138.8	1114.
14.400	129.8	998.
15.467	121.5	818.
16.533	115.6	727.
20.800	89.7	635.
25.867	69.7	506.

RUN 141

G: 30292. LBM/HR-SQ.FT. TSAT: 320.1 (F)
X: 28.9 % LDO: 3. INCHES
PREHEATER Q/A: 748.1 BTU/HR-SQ.FT.
SPECIMEN MATERIAL: INCONEL 600
FINISH: OXIDE COATING

TIME (MINUTES)	(TW - TSAT) (DEGREES F)	Q/A (BTU/HR-SQ.FT.)
0.533	440.5	6658.
1.067	418.1	6198.
1.600	397.2	5835.
2.133	376.7	5531.
2.667	357.4	4912.
3.200	340.9	4361.
3.733	325.2	4183.
4.267	309.7	4159.
4.800	293.8	3967.
5.333	279.4	3701.
5.867	265.2	3425.
6.933	241.0	2855.
8.000	219.7	2465.
9.067	201.1	2046.
10.133	186.1	1741.
11.200	172.1	1587.
12.267	160.7	1312.
13.333	149.8	1149.
14.400	141.0	981.
15.467	132.8	900.
16.533	125.3	766.
21.533	96.4	626.
26.533	72.6	550.

RUN 142

G: 29722. LBM/HR-SQ.FT. TSAT: 320.2 (F)
X: 18.0 % LDO: 3. INCHES
PREHEATER Q/A: 254.2 BTU/HR-SQ.FT.
SPECIMEN MATERIAL: INCONEL 600
FINISH: OXIDE COATING

TIME (MINUTES)	(TW - TSAT) (DEGREES F)	Q/A (BTU/HR-SQ.FT.)
0.533	142.9	648.
1.067	139.7	744.
1.600	136.5	568.
2.133	134.9	564.
2.667	131.6	754.
3.200	128.3	663.
3.733	125.8	571.
4.267	123.3	669.
4.800	119.9	574.
5.333	118.2	385.
5.867	116.5	581.
6.933	110.5	638.
8.000	105.2	546.
9.067	100.8	502.
10.133	96.2	508.
11.200	91.6	564.
12.267	86.0	779.
13.333	77.5	733.
14.400	72.6	587.
15.467	66.7	538.
16.533	62.7	491.

RUN 143

G: 120311. LBM/HR-SQ.FT. TSAT: 318.7 (F)
X: 74.5 % LDO: 3. INCHES
PREHEATER Q/A: 7658.6 BTU/HR-SQ.FT.
SPECIMEN MATERIAL: COPPER
FINISH: SMOOTH APP. 20 μ INCH

TIME (MINUTES)	(TW - TSAT) (DEGREES F)	Q/A (BTU/HR-SQ.FT.)
0.500	468.3	17813.
1.000	423.2	16807.
1.500	341.3	13127.
2.000	302.3	10858.
2.500	256.9	10043.
3.000	223.3	7721.
3.500	195.5	5931.
4.000	175.7	5320.
4.500	152.6	4949.
5.000	135.5	4060.
5.500	119.5	2853.
6.000	112.2	1810.
6.500	104.6	1661.
7.000	98.5	1550.

RUN 144

G: 12224. LBM/HR-SQ.FT. TSAT: -319.2 (F)
X: 53.7 % LDO: 3. INCHES
PREHEATER Q/A: 5512.8 BTU/HR-SQ.FT.
SPECIMEN MATERIAL: COPPER
FINISH: SMOOTH APP. 20 μ INCH

TIME (MINUTES)	(TW - TSAT) (DEGREES F)	Q/A (BTU/HR-SQ.FT.)
0.400	470.8	19042.
0.900	407.7	15848.
1.400	351.2	12860.
1.900	329.1	10748.
2.400	267.8	9704.
2.900	242.9	8070.
3.400	223.8	6926.
3.900	177.8	6292.
4.400	153.1	5324.
5.400	112.7	3871.
6.400	89.5	2641.

RUN 145

G: 114447. LBM/HR-SQ.FT. TSAT: -319.2 (F)
X: 33.8 % LDO: 3. INCHES
PREHEATER Q/A: 3388.5 BTU/HR-SQ.FT.
SPECIMEN MATERIAL: COPPER
FINISH: SMOOTH APP. 20 μ INCH

TIME (MINUTES)	(TW - TSAT) (DEGREES F)	Q/A (BTU/HR-SQ.FT.)
0.400	484.9	16769.
0.900	424.0	15889.
1.400	365.6	12649.
1.900	327.4	9770.
2.400	290.2	9292.
2.900	255.0	7559.
3.900	200.8	6467.
4.900	151.5	5429.
5.900	112.7	4111.
6.900	83.9	3051.

RUN 146

G: 125648. LBM/HR-SQ.FT. TSAT: -318.9 (F)
X: 15.9 % LDO: 3. INCHES
PREHEATER Q/A: 1782.8 BTU/HR-SQ.FT.
SPECIMEN MATERIAL: COPPER
FINISH: SMOOTH APP. 20 μ INCH

TIME (MINUTES)	(TW - TSAT) (DEGREES F)	Q/A (BTU/HR-SQ.FT.)
0.500	461.5	17441.
1.000	405.2	14338.
1.500	353.2	11775.
2.000	315.0	9847.
2.500	277.0	9099.
3.000	243.7	9773.
4.000	161.1	8112.
5.000	112.4	5627.

RUN 147

G: 54609. LBM/HR-SQ.FT. TSAT: -319.6 (F)
X: 77.5 % LDO: 3. INCHES
PREHEATER Q/A: 3616.3 BTU/HR-SQ.FT.
SPECIMEN MATERIAL: COPPER
FINISH: SMOOTH APP. 20 μ INCH

TIME (MINUTES)	(TW - TSAT) (DEGREES F)	Q/A (BTU/HR-SQ.FT.)
0.500	491.3	12888.
1.000	444.3	11988.
1.500	402.4	10303.
2.000	366.4	8256.
2.500	339.3	7244.
3.000	310.7	6949.
3.500	285.4	6052.
4.000	263.4	5924.
4.500	238.9	5107.
5.000	223.0	3814.
6.000	193.4	3611.
7.000	165.1	2988.
8.000	145.1	2214.
9.000	129.0	1958.

RUN 148

G: 54945. LBM/HR-SQ.FT. TSAT: -319.6 (F)
X: 55.1 % LDO: 3. INCHES
PREHEATER Q/A: 2587.1 BTU/HR-SQ.FT.
SPECIMEN MATERIAL: COPPER
FINISH: SMOOTH APP. 20 μ INCH

TIME (MINUTES)	(TW - TSAT) (DEGREES F)	Q/A (BTU/HR-SQ.FT.)
0.300	510.3	12718.
0.800	465.5	11880.
1.300	422.3	10579.
1.800	385.9	9318.
2.300	351.6	7579.
2.800	327.8	6268.
3.300	303.2	6455.
3.800	277.7	5837.
4.300	257.5	5141.
4.800	237.2	4286.
5.800	206.6	3712.
6.800	177.9	3190.
7.800	155.2	2361.

RUN 149

G: 53661. LBM/HR-SQ.FT. TSAT: -319.6 (F)
X: 48.4 % LDO: 3. INCHES
PREHEATER Q/A: 1945.1 BTU/HR-SQ.FT.
SPECIMEN MATERIAL: COPPER
FINISH: SMOOTH APP. 20 μ INCH

TIME (MINUTES)	(TW - TSAT) (DEGREES F)	Q/A (BTU/HR-SQ.FT.)
0.550	481.3	12634.
1.050	440.1	10673.
1.550	401.5	10171.
2.050	363.2	8698.
2.550	335.1	7148.
3.050	308.2	6724.
3.550	282.9	6416.
4.050	258.1	5872.
4.550	236.6	5527.
5.050	214.3	5044.
5.550	196.4	4893.
6.550	165.1	3173.
7.550	145.1	2522.

RUN 150

GI 53749. LBM/HR-SQ.FT. TSAT: -319.6 (F)
XI 21.6 % LDO: 3. INCHES
PREHEATER Q/A: 994.2 BTU/HR-SQ.FT.
SPECIMEN MATERIAL: COPPER
FINISH: SMOOTH APP. 20 μ INCH

TIME (MINUTES)	(TW - TSAT) (DEGREES F)	Q/A (BTU/HR-SQ.FT.)
0.750	485.3	8818.
1.750	426.1	7750.
2.750	369.8	6441.
3.750	327.8	5078.
4.750	290.4	4577.
5.750	256.	3926.
6.750	228.7	3364.
7.750	203.8	2787.
8.750	184.1	2360.
9.750	165.1	1892.
10.750	153.5	1742.
11.750	136.8	1808.

RUN 151

GI 25813. LBM/HR-SQ.FT. TSAT: -328.3 (F)
XI 81.6 % LDO: 3. INCHES
PREHEATER Q/A: 1881.9 BTU/HR-SQ.FT.
SPECIMEN MATERIAL: COPPER
FINISH: SMOOTH APP. 20 μ INCH

TIME (MINUTES)	(TW - TSAT) (DEGREES F)	Q/A (BTU/HR-SQ.FT.)
1.000	492.0	5728.
2.000	448.8	5579.
3.000	408.8	4864.
4.000	375.4	4200.
5.000	344.8	3520.
6.000	321.3	3196.
7.000	295.4	3022.
8.000	274.2	2402.
9.000	257.7	2304.
10.000	237.9	2146.
11.000	223.7	1774.
12.000	219.7	1475.
13.000	210.1	1474.
14.000	196.1	1341.
15.000	178.6	1111.
17.000	159.2	1012.
19.000	145.8	848.

RUN 152

GI 25968. LBM/HR-SQ.FT. TSAT: -328.2 (F)
XI 57.5 % LDO: 3. INCHES
PREHEATER Q/A: 1273.3 BTU/HR-SQ.FT.
SPECIMEN MATERIAL: COPPER
FINISH: SMOOTH APP. 20 μ INCH

TIME (MINUTES)	(TW - TSAT) (DEGREES F)	Q/A (BTU/HR-SQ.FT.)
0.830	473.8	8318.
1.830	419.5	6556.
2.830	375.3	5190.
3.830	342.4	4644.
4.830	323.2	3998.
5.830	278.3	3334.
6.830	251.6	3030.
7.830	230.5	2536.
8.830	211.4	2286.
9.830	194.2	1737.
11.830	169.6	1859.
13.830	153.9	1654.

RUN 153

GI 24774. LBM/HR-SQ.FT. TSAT: -328.2 (F)
XI 35.7 % LDO: 3. INCHES
PREHEATER Q/A: 755.3 BTU/HR-SQ.FT.
SPECIMEN MATERIAL: COPPER
FINISH: SMOOTH APP. 20 μ INCH

TIME (MINUTES)	(TW - TSAT) (DEGREES F)	Q/A (BTU/HR-SQ.FT.)
1.000	471.8	7232.
2.000	425.0	5674.
3.000	386.5	5572.
4.000	340.4	4171.
5.000	322.4	3086.
6.000	292.7	3503.
7.000	267.8	2965.
8.000	246.1	2355.
10.000	212.0	1972.
12.000	183.2	1539.
14.000	162.4	1169.
16.000	145.3	1050.

RUN 154

GI 23174. LBM/HR-SQ.FT. TSAT: -328.2 (F)
XI 11.8 % LDO: 3. INCHES
PREHEATER Q/A: 233.1 BTU/HR-SQ.FT.
SPECIMEN MATERIAL: COPPER
FINISH: SMOOTH APP. 20 μ INCH

TIME (MINUTES)	(TW - TSAT) (DEGREES F)	Q/A (BTU/HR-SQ.FT.)
1.000	491.9	4796.
2.000	461.5	3984.
3.000	432.7	3528.
4.000	408.7	3429.
5.000	380.9	3313.
6.000	358.3	2647.
7.000	340.4	2359.
9.000	303.8	2337.
11.000	267.8	2049.
13.000	239.5	1541.
15.000	219.0	1238.
17.000	200.0	1225.
19.000	179.7	1107.

RUN 156

GI 26457. LBM/HR-SQ.FT. TSAT: -328.3 (F)
XI 79.5 % LDO: 3. INCHES
PREHEATER Q/A: 1797.8 BTU/HR-SQ.FT.
SPECIMEN MATERIAL: INCONEL 600
FINISH: ARTIFICIALLY ROUGHENED

TIME (MINUTES)	(TW - TSAT) (DEGREES F)	Q/A (BTU/HR-SQ.FT.)
1.000	482.0	6532.
2.000	435.7	6509.
3.000	397.8	5406.
4.000	363.9	4645.
5.000	334.6	4314.
6.000	323.9	3403.
7.000	296.1	3253.
9.000	237.9	2773.
11.000	203.1	1927.
13.000	178.6	1547.
15.000	154.6	1304.
17.000	136.8	807.
19.000	128.3	657.
21.000	115.2	805.

RUN 157

G: 25959. LBM/HR-SQ.FT. TSAT: -320.2 (F)
X: 58.0 % LDO: 3. INCHES
PREHEATER Q/A: 1284.6 BTU/HR-SQ.FT.
SPECIMEN MATERIAL: INCONEL 600
FINISH: ARTIFICIALLY ROUGHENED

TIME (MINUTES)	(TW - TSAT) (DEGREES F)	Q/A (BTU/HR-SQ.FT.)
1.000	475.9	7084.
2.000	432.2	6437.
3.000	392.4	5548.
4.000	358.3	4246.
6.000	325.3	3561.
8.000	257.1	2968.
10.000	21[illegible]	2316.
12.000	186.6	1526.
14.000	170.2	1144.
16.000	150.4	1042.
18.000	136.7	949.

RUN 158

G: 25330. LBM/HR-SQ.FT. TSAT: -320.2 (F)
X: 34.4 % LDO: 3. INCHES
PREHEATER Q/A: 744.4 BTU/HR-SQ.FT.
SPECIMEN MATERIAL: INCONEL 600
FINISH: ARTIFICIALLY ROUGHENED

TIME (MINUTES)	(TW - TSAT) (DEGREES F)	Q/A (BTU/HR-SQ.FT.)
0.800	477.5	7618.
1.800	435.2	5824.
2.800	402.1	5112.
3.800	367.5	4578.
4.800	339.9	3797.
6.800	288.6	3317.
8.800	244.5	2417.
10.800	216.6	1921.
12.800	186.2	1737.
14.800	162.4	1282.
16.800	147.7	863.

RUN 159

G: 25818. LBM/HR-SQ.FT. TSAT: -320.2 (F)
X: 11.5 % LDO: 3. INCHES
PREHEATER Q/A: 249.8 BTU/HR-SQ.FT.
SPECIMEN MATERIAL: INCONEL 600
FINISH: ARTIFICIALLY ROUGHENED

TIME (MINUTES)	(TW - TSAT) (DEGREES F)	Q/A (BTU/HR-SQ.FT.)
1.000	486.7	5422.
2.000	453.7	4995.
3.000	422.9	4629.
4.000	393.2	3984.
5.000	369.8	3409.
6.000	347.0	2582.
7.000	334.2	2426.
8.000	313.3	2651.
9.000	296.8	2371.
11.000	262.4	2142.
13.000	233.9	1564.
15.000	215.5	1309.
17.000	194.0	1336.
19.000	174.0	1106.

APPENDIX D

Computer Listing of FILMBOIL

INPUT:

QONA.....Heat Flux [btu/hr-ft^2]

G.....Mass Flux [lbm/hr-ft^2]

XIN.....Dryout Quality

FILMZ.....δ_{film}[feet]

DT.....Tube Diameter[feet]

MUL.....μ_ℓ[lbm/ft-hr]

GAM.....γ[Coefficient of isentropic expansion]

GAS.....R[Universal Gas Constant]

SIGMA.....σ[lbm/hr^2]

HFG.....h_{fg}[btu/lbm]

TSAT.....T_{sat}[^oF]

RHOL.....ρ_ℓ[lbm/ft^3]

RHOGS.....$(\rho_v)_{sat}$[lbm/ft^3]

CPGS.....$(C_{pv})_{sat}$[btu/lbm-^oF]

KGS.....$(k_v)_{sat}$[btu/hr-ft-^oF]

MUGS.....$(\mu_v)_{sat}$[lbm/hr-ft]

CPG1, CPG2, CPG3, CPG4...Curve Fit coefficients, C_{pv} vs T_v

KG1, KG2, KG3.....Curve Fit Coefficients, k_v vs T_v

MUG1, MUG2, MUG3.....Curve Fit Coefficients, μ_v vs T_v

NODRP = 2 LOM = 5

NOIT = 2 NOREP = 3

NOSTP = 250 NQUIT = 5

ERHOG.....Curve Fit Coefficient, ρ_v vs T_v

```
C
C       PROGRAM FILMBOIL
C
C       DISPERSED FLOW FILM BOILING MODEL
C
        REAL MUGS,KGS,KGF,MUG,MUGW,MUG1,MUG2,MUG3,KG1,KG2,KG3,KG,MUL
        DIMENSION XA(2 ),XE(2 ),TV(2 ),WE(2 ),DD(2 ),DELV(2 )
        DIMENSION VG(2 ),VL(2 ),Z(2 ),TW(2 )
        DIMENSION PLUM(3,200)
        DIMENSION DAV(2,200)
        READ(8,1) GCNA,G,XIN,FILMZ,WEC,MUL ,ERHOG
        READ(8,1) DT,DZ,GAM,GAS,SIGMA,HFG,TSAT
        READ(8,1) RHOL, RHOGS, CPGS, KGS, MUGS
        READ(8,10)  CPG1, CPG2, CPG3, CPG4
        READ(8,10)  KG1, KG2, KG3
        READ(8,10)  MUG1, MUG2, MUG3
        READ(8,5) NODRP,NOIT,NOSTP,LOM
        READ(8,15)   NOREP,NQUIT, ISELT,INIT
1       FORMAT(7F10.2)
5       FORMAT(2I2,1I3,1I2)
10      FORMAT(4E15.0)
15      FORMAT(4I5)
        NOSTP=30000
        XOO = XIN
C
C       ** ISELT **
C                   (1)---GROENEVELD VAPOR HEAT TRANSFER COEF.
C                   (2)---BENNETT VAPOR HEAT TRANSFER COEF.
C
C
C       ** INIT **
C                 (1)---GROENEVELD INITIALIZATION PROCEDURE
C                 (2)---HYNEK INITIALIZATION PROCEDURE
C
        GRAV=32.16*3600.*3600.
        TSAT1=TSAT+459.75
```

```
      NOITS=NOIT+2
      PI=3.14159
      LM=0
      IW=5
C     SET UP THE INITIAL VALUES
      I=1
      JX=0
      XA(I)=XIN
      XE(I)=XIN
      TV(I)=TSAT
      WE(I)=WEC
      CD=.45
      GO TO (20,25),INIT
20    SLIP=(RHOL/RHOGS)**.205/(G*DT/MUL )**.016
      SLIP=(SLIP-1.)/2.+1.
      VOID=XIN/(XIN+RHOGS*SLIP*(1.-XIN)/RHOL)
      VL(1)=(1.-XIN)*G/(RHOL*(1.-VOID))
      VG(1)=XIN*G/(RHOGS*VOID)
      GO TO 30
25    CALL DOCAL(G,GONA,XDO,RHOL,RHOGS,SIGMA,HFG,MUGS,DT,WEC,VGDO,VLDO,
     1 DDO,CD)
      VG(1)=VGDO
      VL(1)=VLDO
      SLIP=VG(1)/VL(1)
      VOID=XIN/(XIN+RHOGS*SLIP*(1.-XIN)/RHOL)
30    DELV(1)=VG(1)-VL(1)
      DD(1)=SIGMA*WEC/(RHOGS*DELV(1)**2)
      DFLUX=6.*G*(1.-XIN    )/(PI*DD(I)**3*RHOL)
      WRITE(5,35  )  G, GONA, FILMZ
35    FORMAT('1',25X,'*** GROENEVELD MODEL ***'//5X,'G =  ',F10.0,
     1 ' LBM/HR-SQ.FT.',5X,'Q/A = ',F10.0,' BTU/HR-SQ.FT.',5X,
     2'FILMZ = ',E9.3,' FEET'//)
      WRITE(5,40)
40    FORMAT(    20X,'CONDITIONS AT DRYOUT'/4X,'SLIP',5X,'VOID',10X,'VG'
     1,10X,'VL',10X,'DELV',10X,'DROP DIA.',5X,'CD',5X,'TWALL')
C     SET UP THIRD ITERATION FOR TW, FILM PROPERTIES
```

```
      TW(I)=TSAT+100.
      DO 45 IND=1,NOITS
      MUGW = MUGS+MUG1+MUG2*TW(I)+MUG3*TW(I)**2
      UN=.023*(VG(I)*RHOGS*DT/MUGS)**.8*(CPGS*MUGS/KGS)**.4
     1   *(MUGS/MUGW)**.14*(10.68)
45    TW(I)=(QONA+UN*TV(I)*KGS/DT)/(UN*KGS/DT)
      WRITE(IW,50)SLIP,VOID,VG(1),VL(1),DELV(1),DD(1),CD,TW(1)
50    FORMAT(3X,F6.3,3X,F6.3,4X,2E12.5,1X,E12.5,4X,E12.5,2X,F5.2,4X,
     1F7.1//20X,'POST DRYOUT RESULTS')
      WRITE(IW,55)
55    FORMAT(    4X'Z N',5X'DXADZ',5X'DTVDZ',3X'DDM',5X'DVLDZ',4X'XA',4X
     1,'XE    TV',8X,'VL',8X,'VG',6X,'DELV',4X,'WE    CD    TW'//)
      Z(I)=0.0
      KOP = 0
C     BEGINNING OF STEPWISE ITERATION
      I=I+1
60    IF(I-21)75,75,65
65    IF(23  -I) 75,75,70
70    DZ=10.*DZ
75    CONTINUE
      CALL DATSW(2,JM)
      GO TO (80,85),JM
80    DIP = 1.
      KOP = KOP + 1
      IF(KOP.EQ.1) DIP = 3.
      DZ = DIP*DZ
85    CONTINUE
      IF(JM.EQ.2) KOP = 0
      Z(2)=Z( 1 )+DZ
      DO 215 IRIP = 1,NOREP
      TRANK=TV(1)+459.75
      RHOG= RHOGS*(TSAT1/TRANK)**ERHOG
      CPG = CPGS+CPG1+CPG2*(TV(1)      )+CPG3*(TV(1)      )**2
     1  + CPG4*(TV(1)      )**3
      KG  =  KGS+KG1+KG2*TV(1)+KG3*TV(1)**2
      MUG  =  MUGS+MUG1+MUG2*TV(1)+MUG3*TV(1)**2
```

```
      HDC=(2.*KG/DD(1))*(1.+.276*SQRT(RHOG*DELV(1)*DD(1)/MUG)
     1  *(MUGS*GAS/(KGS*(GAM-1.)))**.333)
      KGF=KGS+KG1+KG2*.5*(TW(1)+TSAT )+KG3*(.5*(TW(1)+TSAT ))**2
      SLIP = VG(1)/VL(1)
      VOID = XA(1)/(XA(1)+RHOG*SLIP*(1.-XA(1))/RHOL)
      IF(I-NQUIT)90, 90, 95
90    QADE = 0.
      GO TO 100
95    QADE = KGF*(1.-VOID)*(TW(1)-TSAT) /(FILMZ*EXP(2.*DT/Z(2)))
100   QADT = QADE*2.*DD(1)/(3.*DT) + HDC*(TV(1)-TSAT)
      QVD=HDC*(TV(1)-TSAT)
      DDDDZ=-2.*QADT/(HFG*RHOL          *VL( 1 ))
      DXADZ=-DFLUX*PI*DD(1)**2*RHOL*DDDDZ/(2.*G)
      NSH=-1
      HFGP=HFG+CPG*(TV( 1 )-TSAT)
      DXEDZ=4.*QDNA/(G*HFG*DT)
      DTVDZ=(HFG*DXEDZ-HFGP*DXADZ)/(XA( 1 )*CPG)
      DD(2)=DD( 1 )+DDDDZ*DZ
105   IF(I-2) 110,110, 115
110   DVLDZ=4.*QDNA*XIN/(HFG*DT*RHOGS)
      GO TO 120
115   DVLDZ=3.*CD*RHOG*DELV( 1 )**2/(VL( 1 )*4.*RHOL*DD(2))
     1  -(1.-RHOG/RHOL)*GRAV/VL(1)
120   CONTINUE
      NSH=NSH+1
      XA(2)=XA( 1 )+DXADZ*DZ
      XE(2)=XE( 1 )+DXEDZ*DZ
      TV(2)=TV( 1 )+DTVDZ*DZ
      VL(2)=VL( 1 )+DVLDZ*DZ
      VG(2)=G*XA(2)/(RHOG*(1.-G*(1.-XA(2))/(RHOL*VL(2))))
      DELV(2)=VG(2)-VL(2)
      WE(2)=RHOG*DELV(2)**2*DD(2)/SIGMA
C     TEST FOR SHATTERING
      IF(WE(2)-WEC) 145, 125, 125
125   IF(NSH-3) 130, 135, 135
130   DD(2)=WEC*SIGMA/(RHOG *DELV(2)**2)
```

```
      GO TO 140
135   DD(2) = DD(2)-.01*DD(2)
140   DFLUX=6.*G*(1.-XA(2))/(PI*DD(2)**3*RHOL)
      GO TO 105
145   CONTINUE
      RED=RHOG*DELV(2)*DD(2)/MUG
      IF(RED-2000.) 150, 155, 155
150   CD=(24./RED)*(1.+0.142*RED**0.698)
      GO TO 160
155   CD=0.45
160   CONTINUE
      TW(2)=TW( 1 )
      DO 210 IND=1, NOIT
      TRANK=TV(2)+459.75
      BRHOG=RHOGS*(TSAT1/TRANK)**ERHOG
      BCPG= CPGS+CPG1+CPG2*(TV(2)      )+CPG3*(TV(2)      )**2
     1   + CPG4*(TV(2)      )**3
      BKG = KGS+KG1+KG2*(TV(2)      )+KG3*(TV(2)      )**2
      BMUG= MUGS+MUG1+MUG2*(TV(2)      )+MUG3*(TV(2)      )**2
      MUGW = MUGS+MUG1+MUG2*TW(2)+MUG3*TW(2)**2
      KGF=KGS+KG1+KG2*.5*(TW(2)+TSAT )+KG3*(.5*(TW(2)+TSAT ))**2
      SLIP = VG(2)/VL(2)
      VOID = XA(2)/(XA(2)+RHOG*SLIP*(1.-XA(2))/RHOL)
      IF(I-NQUIT) 165, 165, 170
165   HWD = 0.
      GO TO 175
170   HWD=KGF*(1.-VOID)/(FILMZ*EXP(2.*DT/Z(2)))
175   GO TO (180,185),ISELT
180   UN=.023*(VG(2)*BRHOG*DT/BMUG)**.8*(BCPG*BMUG/BKG)**.4
     1    *(BMUG/MUGW)**.14*(1.+.3*(DT/(Z(2)+.01*DT))**.7)
      GO TO 205
185   TOPI =.5*(TV(2)+TW(2))
      BCPG   =CPGS+CPG1+CPG2*TOPI +CPG3*TOPI **2+CPG4*TOPI **3
      BMUG   =MUGS+MUG1+MUG2*TOPI + MUG3*TOPI **2
      BKG    =KGS+KG1+KG2*TOPI +KG3*TOPI **2
      RHOG=BRHOG
```

```
      RAT = Z(2)/DT
      IF(RAT-60.) 190, 195, 195
190   UN=.0157*(VG(2)*RHOG*DT/BMUG)**.84*(BCPG*BMUG/BKG)**.333*(1./RAT)
     1  **.04
      GO TO 200
195   UN=.0133*(VG(2)*RHOG*DT/BMUG)**.84*(BCPG*BMUG/BKG)**.333
200   CONTINUE
205   QWD=HWD*(TW(2)-TSAT)
      QWV=UN*BKG*(TW(2)-TV(2))/DT
      TW(2)=(QDNA+UN*TV(2)*BKG/DT + HWD*TSAT    )/(UN*BKG/DT  +HWD    )
210   CONTINUE
215   TW(1)=TW(2)
      DDM=DD(2)*12.*25.4E3
      IF(I-LM) 240, 220, 220
220   IF(JX-200) 225, 240, 240
225   LM=LM+LOM
      JX=JX+1
      PLUM(1,JX)=QVD
      PLUM(2,JX)=QWV
      PLUM(3,JX)=QWD
C     LENGTH NOW IN INCHES
      FEET=Z(2)*12.
      WRITE(6,230)   XE(2)
230   FORMAT(////////// 15X, 5('*'),3X,'DISPERSED FLOW FILM BOILING MODE
     1L',3X,5('*')///5X,'DATASWITCH (1): TERMINATE PROGRAM'//5X,
     2'DATASWITCH (2): ON --- DZ*3.'/21X,'OFF --- RESET'///////5X,
     3'XE = ',F8.4////////)
      WRITE(IW,235)FEET,NSH,DXADZ,DTVDZ,DDM,DVLDZ,XA(2),XE(2),TV(2),
     1   VL(2),VG(2),DELV(2),WE(2),CD,TW(2)
235   FORMAT(F7.1,I2,2E10.3,F6.0,E10.3,2F6.3,F6.0,3E10.3,2F6.3,F6.0)
      DAV(1,JX)=Z(1)
      DAV(2,JX)=TW(1)
240   XA(1)=XA(2)
      XE(1)=XE(2)
      TV(1)=TV(2)
      VL(1)=VL(2)
```

```
      VG(1)=VG(2)
      DELV(1)=DELV(2)
      WE(1)=WE(2)
      TW(1)=TW(2)
      Z(1)=Z(2)
      DD(1)=DD(2)
      IF(XA(1)-.97) 245, 245, 260
245   CALL DATSW(1,MM)
      GO TO (260,250),MM
250   IF(NOSTP-I) 265, 255, 255
255   I=I+1
      GO TO 60
260   NOSTP=JX
265   CONTINUE
      WRITE(5,270) QONA
270   FORMAT(///20X,'TEST SECTION HEAT FLUX IS ',E10.3/10X,'QVD',10X,
     1  'QWV',10X,'QWD'//)
      WRITE(5,275) (PLUM(1,I),PLUM(2,I),PLUM(3,I),I=1,JX)
275   FORMAT(4X,E12.5,3X,E12.5,3X,E12.5)
      CALL PICTR(DAV,2,XLAB,XSCL,2,NOSTP,1,0,2,1,FTIME,1)
      CALL EXIT
      END
```

```
      SUBROUTINE DOCAL(G,QONA,XDO,RHOL,RHOGS,SIGMA,HFG,MUGS,DT,WEC,VGDO,
     1 VLDO,DDO, CD)
C
C     CALCULATION OF CONDITIONS AT DRYOUT USING HYNEK'S METHOD
C
      REAL MUGS
      XIN=XDO
      GRAV=32.16*3600.*3600.
      CD=.45
      IJ=0
  111 IJ=IJ+1
      IIF=1
      VVL=10.+G*(1.-XIN)/RHOL
  100 VGA=G*XIN/(RHOGS*(1.-G*(1.-XIN)/(RHOL*VVL)))
      VGB=VVL+SQRT(SQRT(RHOL*WEC*SIGMA*(GRAV+4.*QONA*XIN*VVL/(HFG*DT*
     1   RHOGS))/(0.75*CD*RHOGS**2)))
      GO TO      (102,103),IIF
  102 IF(VGB-VGA) 106,110,107
  106 VVL=VVL+1.E2
      GO TO 100
  107 IIF=2
      VVL=VVL-1.E1
      GO TO 100
  103 IF(VGB-VGA)110,110,108
  108 VVL=VVL-1.E1
      GO TO 100
  110 CONTINUE
      VLDO=VVL
      VGDO=0.5*(VGA+VGB)
      DELVO=VGDO-VLDO
      DDO=  SIGMA*WEC/(RHOGS*DELVO  **2)
      RED=RHOGS*DELVO  *DDO  /MUGS
      IF(RED-2000.) 24,25,25
   24 CD=(24./RED)*(1.+0.142*RED**0.698)
      IF(IJ-5)111,25,25
25    RETURN
```

END

APPENDIX E

Derivation of Criterion to Determine Droplet Carryover

In order that the dispersed flow model as well as the generalized post critical heat transfer prediction scheme function properly, one must be certain that the evaporating vapor at dryout is sufficient to carry the droplets out the tube. If the vapor velocity is below this value the liquid will collect at some level in the tube with the result that the models presented in this work for predicting post critical heat transfer will be invalid. In order to estimate this quantity, it is assumed that at dryout the liquid is in the form of spherical droplets and that the Weber number is critical. Figure E1 gives a physical representation of the problem. The momentum equation for a drop at the dryout point is

$$V_\ell \frac{dV_\ell}{dZ} = \frac{3\rho_v (V_g - V_\ell)^2 C_D}{4\rho_\ell \delta} - g\left[\frac{\rho_\ell - \rho_v}{\rho_\ell}\right] \qquad (E.1)$$

Assuming the Weber number is critical allows one to obtain an expression for drop diameter, δ, to be

$$\delta = \frac{(W_e)_{crit}\,\sigma}{\rho_v (V_g - V_\ell)^2} \qquad (E.2)$$

We can look at two cases where the accleration term in Equation (E.1) is zero; that of a drop standing still just

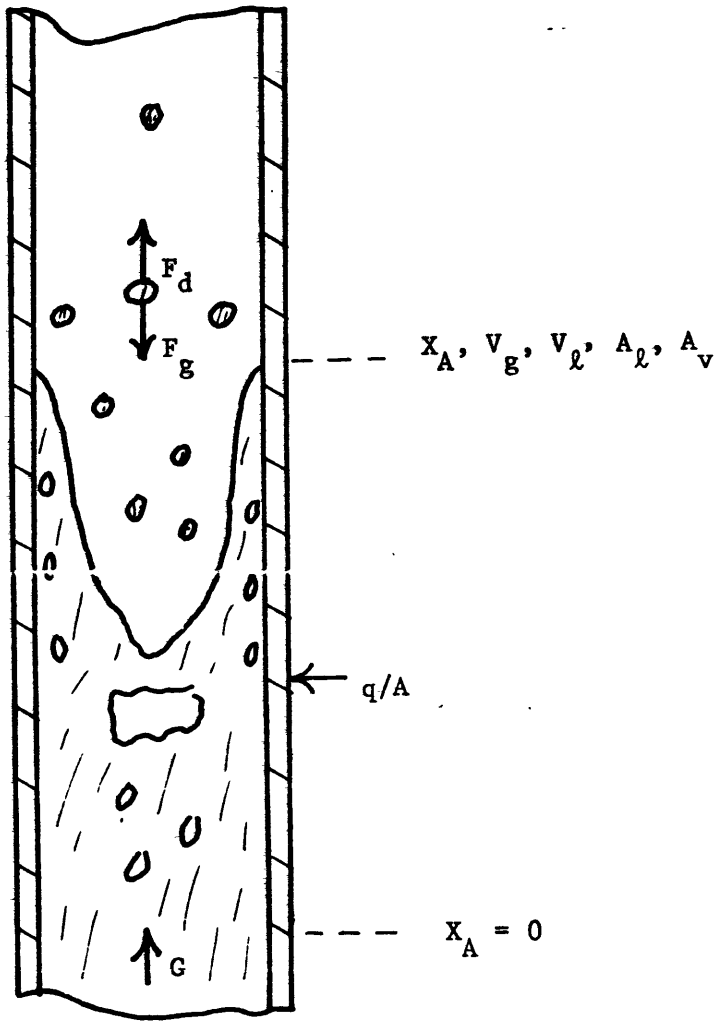

FIGURE E1 PICTORAL REPRESENTATION OF FLOW REGIME FOR DETERMINING G_{crit}

ready to fall back down the tube represented by the equation

$$V_\ell = 0 \tag{E.3}$$

and that of a drop moving at some constant velocity just ready to begin deaccelerating represented by the equation

$$\frac{dV_\ell}{dz} = 0 \tag{E.4}$$

It is felt that Equation (E.3) forces the droplet to be too close to falling back down the tube to be a good cut off point for the determination of the criterion. Therefore, substituting Equation (E.4) and (E.2) into Equation(E.1) gives the minimum criterion for the velocity difference necessary for the droplet to remain at a constant velocity to be

$$(V_g - V_\ell) = \left[\frac{4(W_e)_{crit}}{3C_D}\right]^{1/4} \left[\frac{\sigma(\rho_\ell - \rho_v)g}{\rho_v^2}\right]^{1/4} \tag{E.5}$$

The liquid velocity is chosen such that it will not fall below its inlet velocity defined by

$$V_\ell \geq \frac{G}{\rho_\ell} \tag{E.6}$$

which is obtained by assuming that the inlet void is zero. Substituting Equation (E.6) into Equation (E.5) gives the critical vapor velocity necessary to allow the liquid to continue moving at a constant velocity of G/ρ_ℓ as

$$V_g > \frac{G}{\rho_\ell} + \left[\frac{4(W_e)_{crit}}{3C_D}\right]^{1/4} \left[\frac{\sigma(\rho_\ell - \rho_v)g}{\rho_v^2}\right]^{1/4} \qquad (E.7)$$

Equation (E.7) is not very useful as it stands because V_g is a dependant variable. From the continuity equation given as

$$V_g = \frac{G\ X_A}{\rho_v\left[1 - \frac{G(1-X_A)}{\rho_\ell V_\ell}\right]} \qquad (E.8)$$

one can obtain a second equation for V_g in terms of independent variables from substituting Equation (E.6) into Equation (E.8). This results in

$$V_g = \frac{G}{\rho_v} \qquad (E.9)$$

Substituting Equation (E.9) into Equation (E.7) provides us with a criterion on G alone as

$$G > G_{crit} = \left[\frac{\rho_\ell \rho_v}{\rho_\ell - \rho_v}\right] \left[\frac{4(W_e)_{crit}}{3C_D}\right]^{1/4} \sqrt[4]{\frac{\sigma(\rho_\ell - \rho_v)g}{\rho_v^2}} \qquad (E.10)$$

which must be satisfied in order that V_ℓ after dryout be greater than or equal to G/ρ_ℓ. Assuming that $C_D = .45$ and $(W_e)_{crit} = 7.5$ this criterion for the three fluids considered in this work becomes

Fluid	G_{crit} (lbm/hr-ft^2)
Nitrogen	11500
Water	33700
Freon 12	39000

APPENDIX F

Fluid Properties

This appendix presents the polynomial curve fit equations for μ_v, C_{pv}, k_v, and ρ_v as a function of T_v. The coefficients to these equations and all other fluid properties used in this thesis are tabulated in Table F.1. The computer notation used in FILMBOIL for denoting the various polynomial curve fit coefficients is retained. The equations are as follows.

C_{pv} vs T_v

$$C_{pv} - C_{pg} = CPG1 + CPG2*T_v + CPG3*T_v^2 + CPG4*T_v^3$$

k_v vs T_v

$$k_v - k_g = KG1 + KG2*T_v + KG3*T_v^2$$

μ_v vs T_v

$$\mu_v - \mu_g = MUG1 + MUG2*T_v + MUG3*T_v^2$$

ρ_v vs T_v

$$\rho_v = \rho_g(T_{sat}/T_v)^{ERHOG} \quad \text{where temperatures are absolute}$$

These equations are also used to evaluate the above properties at the wall temperature and film temperature.

TABLE F.1

List of Fluid Properties

Fluid Property		Nitrogen	Water	Freon 12
P	psia	20	1000	155
T_{sat}	^{o}F	-316.	544.	112.
h_{fg}	Btu/lbm	84.13	650.	53.98
σ	lbm/hr^2	$2.34x10^5$	$5.17x10^5$	$1.87x10^5$
μ_ℓ	lbm/hr-ft	.339	.23	.387
ρ_ℓ	lbm/ft^3	49.6	46.3	77.1
ρ_v	lbm/ft^3	.381	2.24	3.84
k_g	Btu/hr-ft-^{o}F	.00435	.0325	.00635
μ_g	lbm/hr-ft	.0145	.0475	.0349
C_{pg}	Btu/lbm-^{o}F	.253	1.25	.1925
γ		1.4	1.366	1.31
R	Btu/lbm-^{o}R	.0709	1.31	.01642
CPG1		0.	1.274	$4.43x10^{-2}$
CPG2		0.	$-4.68x10^{-3}$	$-5.96x10^{-4}$
CPG3		0.	$3.61 x10^{-6}$	$1.78 x10^{-6}$
CPG4		0.	$-8.99x10^{-10}$	$-1.68x10^{-9}$
MUG1		$2.29x10^{-2}$	$-3.6x10^{-2}$	$-5.78x10^{-3}$
MUG2		$6.5x10^{-5}$	$7.25x10^{-5}$	$5.16x10^{-5}$
MUG3		$-1.81x10^{-8}$	$-9.42x10^{-9}$	0.
KG1		$8.99x10^{-3}$	$-4.78x10^{-3}$	$-1.73x10^{-3}$
KG2		$2.47x10^{-5}$	$-3.32x10^{-6}$	$1.54x10^{-5}$
KG3		$-5.47x10^{-9}$	$2.1x10^{-8}$	0.
ERHOG		1.07	1.6	1.7

REFERENCES

1. B.C. Slifer and J.E. Hench, "Loss-of-Coolant Accident and Emergency Core Cooling Models for General Electric Boiling Water Reactors" Licencing Topical Report NEDO-10329 (April 1971).

2. D.C. Groeneveld, "Post-Dryout Heat Transfer at Reactor Operating Conditions," Invited paper presented at National Topical Meeting on Water Reactor Safety, American Nuclear Society, Salt Lake City, Utah, March 26-28, 1973.

3. D.C. Slaughterbeck, L.J. Ybarrondo, and C.F. Obenchain, "Flow Film Boiling Heat Transfer Correlations: A Parametric Study with Data Comparisons," ASME 73-HT-50 (1973).

4. D.C. Slaughterbeck, W.E. Vesely, L.J. Ybarrondo, K.G. Condie, and R.J. Mattson, "Statistical Regression Analysis of Experimental Data for Flow Film Boiling Heat Transfer," ASME 73-HT-20 (1973).

5. R.P. Forslund, and W.M. Rohsenow, "Thermal Non-Equilibrium in Dispersed Flow Film Boiling in a Vertical Tube," MIT Report 75312-44 (1966).

6. A.W. Bennett, G.F. Hewitt, H.A. Kearsey, and R.K.F. Keeys, "Heat Transfer to Steam Water Mixtures Flowing in Uniformly Heated Tubes in Which the Critical Heat Flux has been Exceeded," AERE-R5373 (1967).

7. D.C. Groeneveld, "The Thermal Behaviour of a Heated Surface at and Beyond Dryout," AECL-4309 (1972).

8. S.J. Hynek, W.M. Rohsenow, and A.E. Bergles, "Forced Convection Dispersed Flow Film Boiling," MIT Report DSR-70586-63 (1969).

9. W.F. Laverty, and W.M. Rohsenow, "Film Boiling of Saturated Liquid Nitrogen Flowing in a Vertical Tube," J. of Heat Transfer, 89, pp. 90-98 (1967).

10. O.C. Iloeje, D.N. Plummer and W.M. Rohsenow, "Transition from Film Boiling to Nucleate Boiling in Forced Convection Vertical Flow," MIT Report 72718-78 (1972).

12. A.E. Bergles and W.G. Thompson, "The Relationship of Quench Data to Steady-State Pool Boiling Data," Int. J. of Heat & Mass Transfer, 13, p 55-68 (1970).

13. W.M. Rohsenow and H.Y. Choi, "Heat, Mass and Momentum Transfer," Prentice-Hall, Englewood Cliffs (1961).

14. L.F. Moody, "Friction Factors for Pipe Flow," Trans. ASME Vol. 66, No. 8, pg 671 (1944).

15. R.S. Dougall, "Film Boiling on the Inside of Vertical Tubes with Upward Flow of the Fluid at Low Qualities," MIT Report 9079-26 (1963).

16. D.N. Plummer, O.C. Iloeje, P. Griffith and W. M. Rohsenow, "A Study of Post Critical Heat Flux Heat Transfer in a Forced Convection System," MIT Report 73645-80 (1973).

17. W.S. Bradfield, "Liquid Solid Contact in Stable Film Boiling," Industrial & Engineering Chemistry Fundamentals, 5, (No. 2), p 200-204 (1966).

18. L.H.J. Wachters, and N.A.J. Westerling, "The Heat Transfer from a Hot Wa-l to Impinging Water Drops in the Spheroidal State," Chem. Eng. Science, 21, pp. 1047-1056 (1966).

19. L.H.J. Wachters, L. Smulders, J.R. Vermeulen, and H.C. Kleiweg, "The heat Transfer from a Hot Wall to Impinging Droplets in the Spheroidal State," Chem. Eng. Science, 21, pp. 1231-1238 (1966).

20. S.Y. Ahmad, "Axial Distribution of Bulk Temperature and Void Fraction in a Heated Channel with Inlet Subcooling," J. of Heat Transfer, 92, p 595-609 (1970).

21. N. Isshiki, "Theoretical and Experimental Study on Atomization of Liquid Drop in High Speed Gas Stream," report No. 35, Transportation Technical Research Institute, Tokyo, Japan.

22. J.B. Heineman, "An Experimental Investigation of Heat Transfer to Superheated Steam in Round and Rectangular Channels, "ANL 6213 (1960).

23. W.H. McAdams, "Heat Transmission," 3rd ed. McGraw - Hill (1954).

24. G. Hadaller and S. Banerjee, "Heat Transfer to Superheated Steam in Round Tubes," AECL Internal Report WDI-147 (1969).

25. J. Topping, "Errors of Observation and Their Treatment," Reinhold Publishing Corp., N.Y. p. 20.

26. Anonymous, Conversion Tables for Thermocouples 077989 Issue 4, Leeds & Northrup.

27. J.B. McDonough, W. Milich, and E.C. King, "An Experimental Study of Partial Film Boiling Region with Water at Elevated Pressures in a Round Vertical Tube," Chem. Engrg. Progress Symposium Series, 57, No. 32, pp 197-208.

28. O.C. Iloeje, "A Study of Wall Rewet and Heat Transfer in Dispersed Vertical Flow," Ph.D. thesis in Mech. Eng.,M.I.T. to be completed June 1974.

29. M. Volmer, "Kinetik der Phasenbildung," Theodor Steinkopf, Dresden und Leipzig (1939).

30 K. J. Baumeister, T. D. Hamill, and G.J. Schoessow, "A Generalized Correlation of Vaporization Times of Drops in Film Boiling on a Flat Plate," US-A.I.Ch.E.- No. 120, Third International Heat Transfer Conference and Exhibit, August 7 - 12, 1966.